A titanosaurian sauropod with Gondwanan affinities in the latest Cretaceous of Europe

Bernat Vila, Albert Sellés, Miguel Moreno-Azanza, Novella L. Razzolini, Alejandro Gil-Delgado, José Ignacio Canudo, Àngel Galobart

Supplementary Information

This file includes:

4. Supplementary Data 1–4
5. References for Supplementary Information

1. Materials and methods

1.1 Institutional abbreviations

MCD, Museu de la Conca Dellà, Isona i Conca Dellà, Spain; MNCN, Museo Nacional de Ciencias Naturales, Madrid, Spain.

1.2 Systematic palaeontology

DINOSAURIA Owen, 1842

SAURISCHIA Seeley, 1887

SAUROPODA Marsh, 1878

TITANOSAURIA Bonaparte and Coria, 1993

SALTASAURIDAE Bonaparte and Powell, 1980

SALTASAURINAE Bonaparte and Powell, 1980

Abditosaurus kuehnei, gen. et sp. nov.

List of material (holotype):

1956 *Hypselosaurus* nov. sp.[78], p. 151

2017 Titanosauriformes indet. MNCN 59295 (middle caudal chevron), MNCN 59539 and MNCN 62760 (two anterior caudal chevrons)[79], p. 222, Figures 5a–e and 5f–h.

Titanosauria indet. MNCN 79834 (proximal half of left humerus)[79], p. 224, Figure 5i.

Present study Fragments of isolated teeth (MCD-6749, MCD-6751); 12 (3rd to 14th) articulated and partially preserved cervical and anterior dorsal vertebrae (MCD-9882); 3rd dorsal vertebra (MCD-6718); partial 4th dorsal vertebra (MCD-6729); partial 5th dorsal vertebra (MCD-6730); articulated fragments of ?6th and ?7th dorsal centra (MCD-6744); fragment of ?6th dorsal centrum (MCD-6745); 1st (MCD-6719), 2nd (MCD-6720), and 3rd (MCD-6986) complete left dorsal ribs; 4th (MCD-6722), 5th (MCD-6735), and 6th (MCD-6738) nearly complete left dorsal ribs; proximal half of 1st right dorsal rib; rib shaft fragments (MCD-6717, MCD-6721, MCD-6725, MCD-6728, MCD-6732, MCD-6733, MCD-6734, MCD-6736, MCD-6746, MCD-6750, MCD-6985, MNCN59301); right scapula (MCD-6724); posterior end of the left scapular blade (MCD-6715); right coracoid (MCD-6742); left sternal plate (MCD-6716); sternal rib (MCD-6747); distal half of right humerus (MCD-6988); right radius (MCD-6748); fragment of left ilium (MCD-6731); proximal third of right femur (MCD-6987); right tibia (MNCN79837-79838-79848); right fibula (MCD-6723); distal half of left fibula with adhered calcaneum (MNCN-79847).

1.3 Anatomical nomenclature

We follow the Romerian terminology[80] and the directional terms (anterior, posterior, ventral, and dorsal) employed by Wilson[81]. We also follow Wilson[82] and Wilson et al.[83] for nomenclature of vertebral laminae and fossae and the definitions of positional terms for vertebrae proposed by Tschopp et al.[84].

1.4 Osteohistology methods

With the aim to search for evidence of insular adaptations in the large-bodied *Abditosaurus kuehnei*, the new taxon was histologically analysed. Six histological

samples were taken from the mid-shaft of both anterior and posterior sides of the humerus, femur, and tibia. All histological samples were prepared as thin sections (30 microns) at the “Laboratori de làmines Primes” of the Universitat Autònoma de Barcelona. The resulting sections were studied using a Leica® DM2700 petrographic microscope and photographed with a Leica® EC3 digital camera at the Optics Laboratory of the Institut Català de Paleontologia. Images were acquired with a Nikon® DS-Fi3 camera attached to a Nikon® Eclipse E4000 POL microscope housed at the Geology Department of the UAB and analysed with Image-J software 1.8.0_172[85].

1.5 Body mass and length estimates

Based on the literature, we compiled a dataset of limb bone measurements for the Ibero-Armorican titanosaur species (*Abditosaurus kuehnei*, *Ampelosaurus atacis*, *Atsinganosaurus velauciensis*, *Garrigatitan meridionalis, Lirainosaurus astibiae*, *Lohuecotitan pandafilandi*; Supplementary Table 1) for use in body mass (BM) estimation with the formula of Campione and Evans[69]:

$$\text{Body Mass (BM)} = 10^{a}/1000, \text{ where } a = 2.749 * \log_{10}(FC + HC) - 1.104$$

FC and HC are the femoral (FC) and humeral (HC) circumferences.

When only one of these measurements (FC or HC) was available from the literature, we estimated the other using the allometric equation relating these dimensions, generated by González Riga et al.[70].

$$\text{Log } FC = 1.0459 \log HC - 0.0475$$

In some specimens only mediolateral (D_{ml}) or anteroposterior (D_{ap}) diameters were provided in the literature. In these cases we calculated the FC and HC by using the

Ramanujan approximation formula[86], assuming that the bone shaft has an oval cross-section:

$$C_{oval} = pi * ((3 * (D_{ml} /2 + D_{ap} /2)) - (((3 * D_{ml} /2 + D_{ap} /2) * (D_{ml} /2 + 3 * D_{ap} /2))^{0.5}))$$

We argue that the error in the body mass estimations is minimized when using the allometric equation of González Riga et al.[70] as the linear regression of these authors is based on source measurements from "articulated or definitively associated titanosaurian skeletons that preserve both of these elements [femur and humerus] in their entirety". Alternatively, some authors (e.g., Díez Díaz et al.[6,11]) calculated BM by using midshaft circumferences from different specimens from a sample of scattered limb bones. That is, estimating a range of BM by using the minimum FC and HC values from the smallest and largest specimens, respectively, from a sample of disarticulated limb bones. This latter estimation is biased by the fact that calculations based on the smallest and largest specimens include elements of various individuals that might represent different ontogenetic stages or even different species.

In order to estimate maximum body size of the Ibero-Armorican taxa it is of particular importance to assess their ontogenetic stages[6,9-11] (Supplementary Table 1), as this ensures that individuals had reached the somatic maturity and were fully-grown adults. In this regard, we underscore that the more reliable BM values in Supplementary Table 1 are those from individuals with high histologic ontogenetic stages (HOS). Nevertheless, we provide estimates based on specimens without ontogenetic information or that might represent the smallest and largest individuals of a particular species sample.

We estimate body length with the formula of Seebacher[71]:

$$BM=214.44BL^{1.46}$$

where BM and BL are body mass (kg) and body length (m), respectively.

1.6 Phylogenetic methods

Maximum parsimony analyses

To test the phylogenetic relations of *Abditosaurus kuehnei* gen. et sp. nov., we included the new taxon in the dataset of Gorscak and O'Connor[29]. In addition to the inclusion of the *Abditosaurus*, the following character scores were changed: *Overosaurus*, character 104 was changed from ? to 0, as per the description provided by the authors[26], probably representing a typo in the original study. *Nemegtosaurus* was detected as a wildcard taxon in previous analyses and was *a priori* removed from the dataset. The resulting dataset included in 55 taxa scored for 272 independent characters that were treated as unordered in all analyses.

Due to the size of the dataset, we used new technology search strategies to search for most parsimonious trees (MPTs). The settings for all heuristic searchers were the same: 100 rounds of sectorial searchers, with both random sectorial searchers (rss) and consensus sectorial searches (css) set to a minimal sector size of five taxa; 100 rounds of drift, allowing a fit difference of five and a relative fit difference of 0.1, 100 rounds of ratchet and ten rounds of tree fusing. For each search, ten replications, retaining ten hits per replication were carried out. The resulting MPTs where subjected to an additional round of TBR, to further sample the tree space. A script is provided in the Supplementary Information files that adjusts the analysis settings and runs all analyses carried out, providing a series of outputs for each tree search, including a parenthetical tree file with the starting trees obtained after the new technology search, and an additional tree file with all most parsimonious trees, a

vector file containing the consensus tree, a vector file containing the optimization of synapomorphies shared by all MPTs, and a log file that reports the analysis.

Bayesian analyses

The complete Bayesian dataset of Gorscak and O'Connor[29], including the original 55 taxa plus *Abditosaurus kuehnei* gen. et sp. nov., coded for a total of 272 variable characters plus 260 autapomorphic, invariable characters was updated with the above mentioned rescore of *Overosaurus*, plus all taxa scored for 12 additional autapomorphies identified for *Abditosaurus kuehnei* gen. et sp. nov. *Nemegtosaurus* was removed from the dataset because it is only represented by skull characters that hinders comparison and renders it a wildcard taxon. Although exploring evolutionary rates was not the aim of our research, and invariant characters are of no consequence towards establishing sister group relationships, we decided to include these additional data to make them available for future studies.

Nonclock analysis - A first non-clock analysis was carried out using MrBayes 3.2.6, running in the CIPRES Science Gateway, using a model of variable rates of character state change, sampled from a lognormal-distribution, setting an exponential hyperprior of 1.0 for the rate of variation among characters. Four independent runs of the Markov chain Monte Carlo (MCMC) ran for ten million generations with one hot and three cold chains. The chains sampled tree-space every 1,000 generations and the first 25% of the posterior distribution was discarded to eliminate the initial climbing phase. Convergence of independent runs was assessed in Tracer 1.7 using effective sample size (ESS) for each parameter greater than 200. A script for MrBayes is provided in the Supplementary Information files.

Tip date analysis - We followed Gorscak and O'Connor[29] in performing a tip-dating Bayesian phylogenetic analysis to estimate divergence dates and branch lengths based on the additional data consisting of stratigraphic information. Eric Gorscak provided the XML files for BEAST 2.1.3[87] used in the original publication, which were edited to include *Abditosaurus kuehnei* gen. et sp. nov. and to make the aforementioned changes to the matrix (Supplementary Information files). The assumed tree model for this set of analyses was the birth-death-skyline-serial-sampling[77]. A relaxed clock was assumed under a lognormal distribution of sampled rates. Rates of character change were tested under variable (with an assumed gamma-distribution) assumptions. Four independent runs of the MCMC persisted for 50 million generations with sampling of tree-space occurring every 1,000 generations and the first 25% of the sample was discarded. Stratigraphic ranges of each taxon were sampled under a uniform distribution to account for stratigraphic uncertainty. The initial ranges were the same as those used by Gorscak and O'Connor[29], with the following updates based on recent literature or on the readjustment of stages and substages provided by the primary literature to the Ogg and Hinnov[59] time scale (Suppl. Table 2): *Normanniasaurus* is considered early to middle Albian in age (113–107.7 Ma)[89]; *Ligabuesaurus* is considered late Aptian to Albian in age (123.4–100.5 Ma)[89]; *Rukwatitan* is considered late Campanian to early Maastrichtian in age (75–71.4 Ma)[90]; *Andesaurus* is considered Albian to early Cenomanian in age (113–96.4 Ma)[91]; *Epachthosaurus* is considered late Cenomanian to early Turonian in age (95.4–92.9 Ma)[92]; *Angolatitan* is considered late Turonian in age (91.4–88.8 Ma)[93]; *Mendozasaurus* is considered middle to late Coniacian in age (88.8–86.3 Ma)[94]; *Muyelensaurus* is considered late Turonian to early Coniacian in age (91.4–88.8 Ma)

[27]; *Rinconsaurus* is considered late Turonian to Coniacian in age (91.4–86.3 Ma)[95]; *Gondwanatitan* is considered Turonian to Santonian in age (93.9–83.6 Ma)[96]; *Maxakalisaurus* is considered Turonian to Santonian in age (93.9–83.6 Ma)[97]; *Neuquensaurus* is considered early Campanian in age (83.6–80.7 Ma)[98]; *Panamericansaurus* is considered late Campanian to early Maastrichtian in age (76.4–69.9 Ma)[99]; *Alamosaurus* is considered Maastrichtian in age (72.1–66 Ma)[45]; *Saltasaurus* is considered late Campanian to early Maastrichtian in age (76.4–69.9 Ma)[100]; *Opisthocoelicaudia* is considered early Maastrichtian in age (72.1–69.9 Ma)[42]; *Paluditi*tan is considered early Maastrichtian in age (72.1–69.9 Ma)[101]; *Trigonosaurus* is considered Maastrichtian in age (72.1–66 Ma)[102]; *Pellegrinisaurus* is considered Campanian to early Maastrichtian in age (83.6–69.9 Ma)[103]; *Tastavinsaurus* is considered early Aptian in age (126.3–123.3 Ma)[104]; *Malarguesaurus* is considered late Turonian to early Coniacian in age (91.4-–88.8 Ma)[105]; *Bonitasaura* is considered Santonian in age (86.3–83.6 Ma)[106]; *Shingopana* is considered late Campanian to early Maastrichtian in age (75–71.4 Ma)[90]; *Notocolossus* is considered late Coniacian to early Santonian in age (87.9–85.6 Ma)[71]; *Patagotitan* is considered late Albian in age (107.7–100.5 Ma)[107]; *Lirainosaurus* is considered latest Campanian in age, within the magnetochron C32n (73.5–72 Ma)[108]; *Ampelosaurus* is considered earliest Maastrichtian in age, close to the C32n.1n-C31r magnetochron transition (73–71 Ma)[109]; *Atsinganosaurus* is considered latest Campanian to earliest Maastrichtian in age, within the C32n.1n, C32n.2n, or C32r.1n magnetochrons (74.0–71.6 Ma)[110]; and *Lohuecotitan* is considered late Campanian to early Maastrichtian in age (76.4–69.9 Ma)[7]. Convergence of independent runs was assessed in Tracer 1.7 using effective sample size (ESS) for each parameter greater than 200. Details of additional

parameter values can be found in the Supplementary Information files, which contains the modified script. Synapomorphies for *Abditosaurus* and Saltasaurinae were obtained by optimization of the characters under maximum parsimony on the topology obtained with the tip-date analyses.

1.7 Paleobiogeographic methods

A paleobiogeographic analysis following the methodology of Sallam et al.[16] was conducted using the R script BioGeoBEARS[77] over the tip dating maximum clade credibility tree. Two different palaeobiogeographical scenarios of the three proposed by Sallam et al.[16] and Poropat et al.[111] were tested: the starting model, where partial connections between land masses were scored with a 0.5 multiplier of happening, versus the 1 multiplier for certain connections between areas; and the harsh model, where connections were severed by means of adding a very low multiplier (0.00001) to minimise the dispersions between continents separated by significant water bodies.

Three palaeobiogeographical models (DEC, DIVALIKE, and BAYAREALIKE) were tested. Additionally, alternative models with the additional +J parameter to facilitate long-distance dispersal events alongside the assumptions of each model were evaluated, although the + J parameter has been recently criticised[112]. The major criticisms by these authors, on top of several conceptual flaws of the DEC and DEC+J models, is that long distance dispersion is not modelled in a way that correctly accounts for anagenesis, thus comparing the likelihood of +J and models without long distance dispersion is meaningless. These critiques have been recently answered, but in any case, the DEC models are regarded as problematic when single area ranges are the rule in the dataset[113], as the case in most or all fossil

analyses. Thus, we chose the BAYAREALIKE model as the most likely to represent the palaeobiogeographical history of Titanosauria, based in its lower model log-likelihood (Lnl) score among the remaining models, although no statistically significant differences are found when comparing models under 'starting' distribution multipliers (Suppl. Fig. 54–65; Suppl. Table 3).

1.8 Photogrammetric models

In order to visualize and document the skeletal morphology of *Abditosaurus kuehnei* we produced high-resolution, 3D models of 16 fossil specimens (including 27 holotypic elements) by using photogrammetric 3D techniques. The models were produced to ensure an accurate documentation and to deliver precise and reproducible measurements following the protocols of Mallison and Wings[72], Matthew et al.[73], and Falkingham et al.[74]. Digital photogrammetric models were created with Agisoft Photoscan Pro (v. 1.2.4, www.agisoft.com), starting from photos taken with Panasonic DMC-TZ80 and DMC-FZ18 cameras with an image resolution of 8.8Mpx. Scaling and alignment were also undertaken in Agisoft Photoscan Pro. Scaling is undertaken through two-point scale bars with a target at each end which codes to be automatically recognized by Agisoft Photoscan Pro. The JPG image coordinates average accuracy of the 3D models is 0.001m and the residual error in 3D space, meaning the distance between the input and the estimated values for scale bar length, is always sub-millimetric (less than 0.0001m). Each model required an average of 315 photos, 237.000 tie points, and more than 3.885.000 faces to be generated, processed, aligned, and reconstructed and scaled correctly. No further retrotopological editing was required and the scaled meshes of the digital skeleton were exported as a series of 16 Stanford PLY files (Supplementary Figures 4, 8, 10,

12–15, 17, 19, 21, 24, 25, 27, 29, 31, 32). All photogrammetric 3D meshes used in this study are freely available in PLY format for download at figshare.com (approximately 1 GB of content has been generated).

2. Results

2.1 History of the discovery, campaigns, and collected material

The Orcau-1 locality was discovered on September 25, 1954, by the German palaeontologist Walter Georg Kühne (1911–1991) after prospecting the outcrops west of the village of Orcau village (Tremp Basin, Catalonia, Spain). The main goal of this early prospecting was to discovery Cretaceous mammals, as Kühne was one of the most renowned specialists on fossil mammals in Europe and worldwide[114,115]. After the unexpected and striking discovery of dinosaurs near Orcau, he wrote “In Spain I ‘encountered’ a titanosaurid from the Upper Cretaceous and brought some specimens to Madrid, the rest – huge – waiting for me until the summer of 1955. Thus, you go out to find rat-sized Cretaceous mammals and bring home a 10-ton beast, and that's just the beginning” (translated from German, personal letter to Professor Schindewolf, December 1954). The excavations performed by Kühne in the following two weeks immediately after the discovery (from September 27th to October 5th) allowed him to identify about ten bones. Some of them (two chevrons, a right tibia, and the distal half of a left femur) were collected, packeted in four boxes, and sent to the Instituto Lucas Mallada in Madrid (ILM, currently Museo Nacional de Ciencias Naturales[116,117]), whereas others (a complete left humerus, the proximal half of a left femur, a “large and flat bone”, two articulated dorsal vertebrae, and various indeterminate bones) were jacketed for the sake of protection and left at the site.

Kühne revisited the site in 1955 (Suppl. Fig. 1), and, assisted by the local Josep Montané and the Professor Emiliano Aguirre (ILM), collected and/or mapped about ten more bones (a complete right femur [Supp. Fig. 2a] and humerus, the distal half of a left fibula, the anterior end of a left scapula, a chevron, an indeterminate “short” bone, a few small fragments of an ilium, a complete dorsal vertebra, and fragments of at least three dorsal ribs) together with almost all the bones left in the previous campaign (except for the dorsal vertebrae and other indeterminate bones).

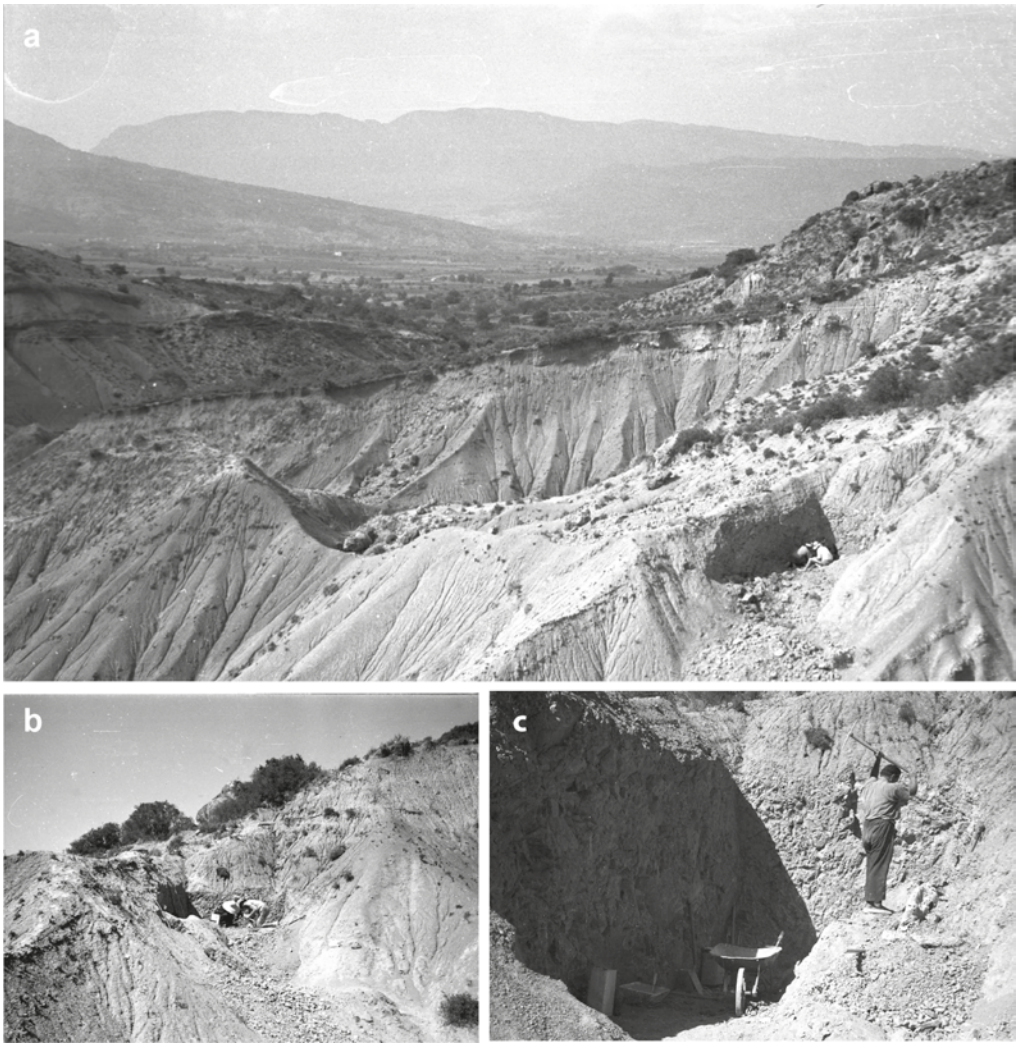

Supplementary Figure 1. Early excavations at the *Abditosaurus kuehnei* gen. et sp. nov. locality. **a**, general view of the locality (bottom right corner) at the Tremp Formation outcrops in the Orcau-Suterranya area (August 29, 1955). **b**, excavation at

the Orcau-1 locality (August 26, 1955) with the explosive technician (Federico Vergés, on the left) and W.G. Kühne placing the shot holes. **c**, Josep Montané excavating the fossiliferous level (August 31, 1955). The jacketed bone to his lower right corresponds to 55/1. Images (Archivo MNCN-CSIC, ACN0738/003/003.10, ACN0738/003/003.15, ACN0738/003/003.6) were taken by Emiliano Aguirre, courtesy of the archive of the Museo Nacional de Ciencias Naturales.

All the material was jacketed, packet in nine boxes, and sent to the ILM in Madrid. As in 1954, Kühne left small parts of mapped bones (most of the ilium fragments, the posterior blade fragment of the left scapula, and three articulated (?middle) dorsal vertebrae) at the site (Suppl. Fig. 2b). By the end of the 1955 season Kühne concluded that the sauropod was complete and articulated from the pelvic girdle onwards, with the body axis oriented north-south, and preserving the neck and the skull (Suppl. Fig. 2c, d). He therefore asked the ILM to undertake an additional excavation at the Orcau-1 locality, but the funding from this institution came to an end, and no more excavations were conducted at the site. In 1956, Lapparent and Aguirre referred part of the collected material to a new species of *Hypselosaurus*[78] but this genus is currently considered as a *nomen dubium*[118].

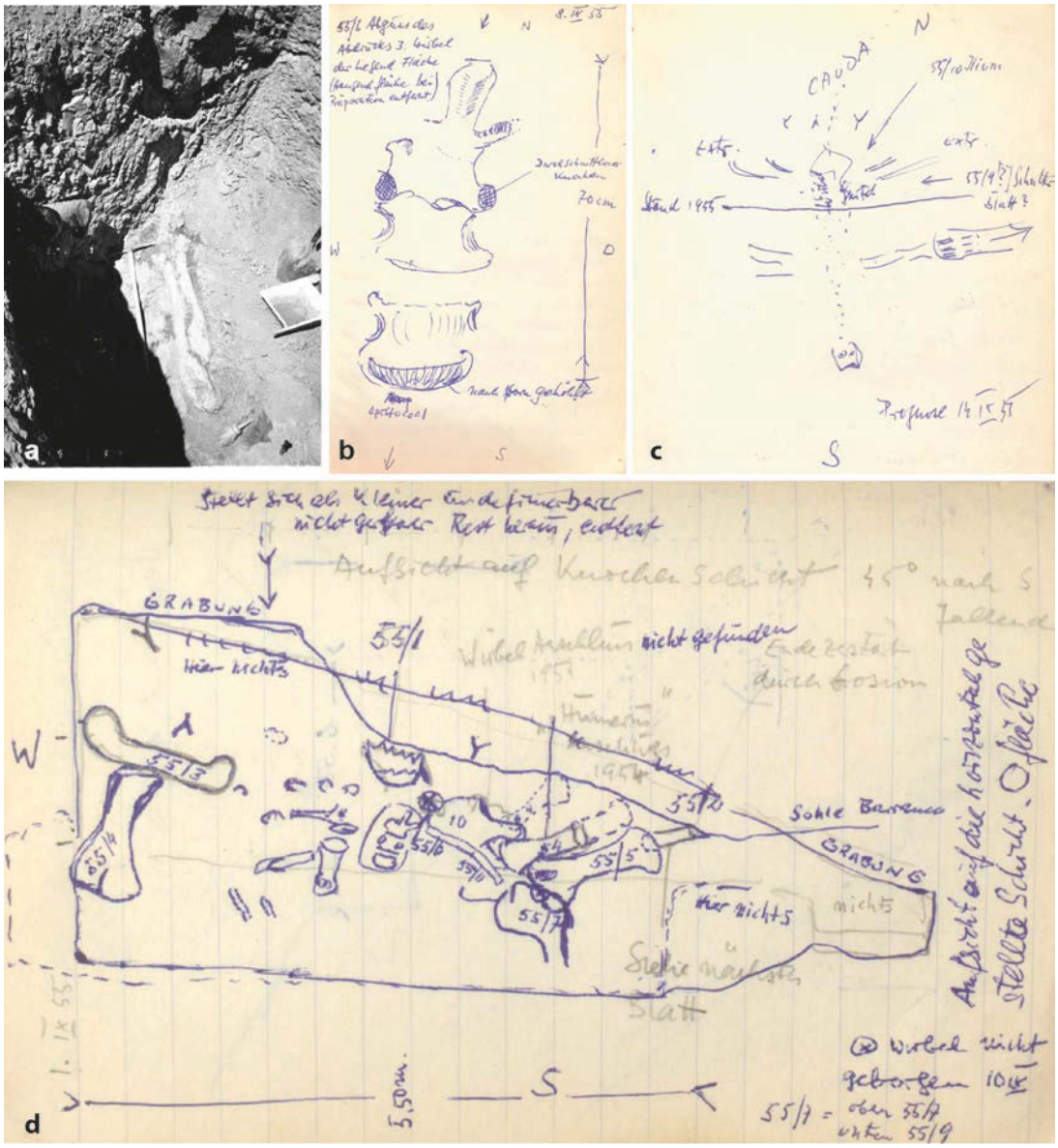

Supplementary Figure 2. Site map and fossil elements of *Abditosaurus kuehnei* gen. et sp. nov. collected during the early (1954–1955) excavations. **a**, right femur (55/3) with an estimated proximodistal length of 130 cm (August 31, 1955). **b**, illustration of three articulated (?middle) dorsal vertebrae (55/6) made by Kühne in his field notebook (September 8, 1955). **c**, scheme depicting the interpretation on how the sauropod skeleton was preserved at the site, made by Kühne in his field notebook (September 14, 1955). **d**, site map made by Kühne, depicting the exposed outcrop with bones at the locality (September 1, 1955). The pick handle in a equals 90 cm. Image a (Archivo MNCN-CSIC, ACN0738/003/003.4) was taken by Emiliano Aguirre,

courtesy of the archive of the Museo Nacional de Ciencias Naturales. Images b to d taken from Kühne's field notebook, courtesy of Urs and Anna Klebe.

In 1984 and 1986 two expeditions led by Josep Vicenç Santafé from the Institut de Paleontologia de Sabadell (Barcelona) and assisted by members of the Institut d'Estudis Ilerdencs (Lleida)[119] revisited the locality. In 1986 and after a very short (five-day) excavation, they identified part of a sternal plate and three dorsal ribs (one of them, MCD-6985, was collected and later housed in the Museu de la Conca Dellà).

Three more decades passed and from 2012 to 2014 a joint team made up of members from the Institut Català de Paleontologia, the Universidad de Zaragoza, and the Museu de la Conca Dellà re-excavated the locality and collected the remaining axial and appendicular elements (see Fig. 1 and list of material in Supplementary Information 1.2), which were deposited at the Museu de la Conca Dellà (Lleida). In six consecutive field campaigns from 2012 to 2014 we recovered all the fossil material that Kühne and Santafé had left on the site in 1955 and 1986, together with a right scapula, coracoid, sternal plate, radius, and fibula, several partial and complete dorsal ribs, one sternal rib, one dorsal vertebra (Fig. 1 and Suppl. Fig. 3a, b), some tooth fragments, and an articulated cervicodorsal series with cervical and dorsal ribs (Suppl. Fig. 3c, d). Recently, Martín Jiménez et al.[79] briefly described some of the specimens housed in the MNCN, originally deposited by Kühne in 1954 and 1955. Finally, after 60 years of oblivion, the sauropod of Orcau discovered by Kühne was completely collected in 2014. Subsequent investigations have made it possible to gather some of the historical (1954 and 1955) material and

reveal previously unknown information on the early excavations and fieldnotes of Kühne.

Supplementary Figure 3. Fossil elements of *Abditosaurus kuehnei* gen. et sp. nov., collected during the recent (2012-2014) excavations. a, general view of the excavation at the Orcau-1 locality (September 19, 2012), with some appendicular, girdle, sternal, and axial elements exposed. **b**, detail of the left sternal plate, the third dorsal vertebra, and the dorsal ribs, as exposed in the field (September 18, 2012). **c**, cervicodorsal transition from the articulated neck during the fieldworks (June 14, 2013). **d**, ventral surface of the cervicodorsal series after the preparation works (November 15, 2019). Scale bar in A equals 25 cm. Images a and b courtesy of Rubén Contreras.

2.2 Extended description

Teeth – The dental elements are limited to two small tooth fragments. The preserved crown fragment has an oval shape and its enamel is wrinkled. No wear facets are preserved.

Cervical vertebrae (Suppl. Fig. 4–6; Suppl. Table 4) – The cervical series includes 12 fragmentary and articulated vertebrae, which have opisthocoelous and anteroposteriorly elongate centra with articular surfaces that are wider than tall (Suppl. Fig. 4 and 5). They are internally pneumatized, with a camellate texture, as in most titanosauriforms[44,46]. The ventral surfaces of the anterior (3rd to 7th) and middle (8th to 12th) cervical vertebrae are flat to slightly concave transversely lacking a ventral keel, ventrolateral ridges, or pneumatic foramina, and differ from the centra of most of titanosaurs, including *Lohuecotitan*[8], *Rapetosaurus*[24], *Saltasaurus*[25], and *Overosaurus*[26]. The concave lateral surfaces are occupied by a lateral fossa, with no evidence of pleurocoels, a character shared with *Atsinganosaurus*[5] and *Maxakalisaurus*[120] and differing from most titanosaurs. The parapophyses are laminar, ventrally flat, and extend half the anteroposterior length of the centrum. They project laterally, unlike in several titanosaurs (e.g., *Rapetosaurus*[24], *Saltasaurus*[25], *Neuquensaurus*[98], *Alamosaurus*[121]), and are located on the anterior margin of the centrum, as in all Ibero-Armorican species with preserved cervical vertebrae and most other titanosaurs. The diapophyses project ventrolaterally and are fused to the dorsal margin of the cervical rib through the tuberculum.

The posterior cervical centra (13th and 14th) have an hourglass shape and are anteroposteriorly less elongate than the middle and anterior elements. On the lateral margins they bear large, deep, oval pleurocoels without internal divisions or septa.

Two elliptical pneumatic foramina are symmetrically placed on the lateral margins of the ventral surface at level with the lateral pleurocoels (Suppl. Fig. 6). These foramina morphologically recall those of the 13th cervical vertebra of *Overosaurus*[26] but in the latter they are more conspicuous and located in a centred and more anterior position, level with the parapophyses. *Alamosaurus* bears foramina on the ventral surfaces of the 12th and 13th cervical vertebrae[121], but they are smaller than those of *Abditosaurus* and located level with the parapophyses. Dorsally, the 14th cervical vertebra has a butterfly-shaped neurocentral junction. The two zygapophyses overhang the anterior and posterior articular surfaces of the condyle and cotyle, respectively, as in *Rapetosaurus*[24], *Overosaurus*[26], *Isisaurus*[28], *Trigonosaurus*[102], and *Uberabatitan*[122]. The anterior centroprezygapophyseal laminae (cprl) are united by a faint intraprezygapophyseal lamina (tprl) that represents the ventral margin of a reduced spinoprezygapophyseal fossa (sprf). The anterior centrodiapophyseal (acdl) and the centroprezygapophyseal (cprl) laminae converge at the dorsal and anteriormost margin of the centrum. The centrodiapophyseal (cdf) and prezygapophyseal centrodiapophyseal (prcdf) fossae are triangular, laterally extended, and deep. The diapophyses are laminar, broad transversely and flattened dorsoventrally, and extend anterolaterally to join the parapophyses ventrally by means of a short and nearly vertical cervical rib. A wide, deep and large spinodiapophyseal fossa (sdf) on the right side of the lateral neural spine differs from the left counterpart where the spinodiapophyseal lamina (spdl) divides the sdf into a small postzygapophyseal spinodiapophyseal fossa (posdf) and a relatively large prezygospinodiapophyseal fossa (prsdf). The epipophyseal prezygapophyseal lamina (eprl) is absent, as in *Atsinganosaurus*[11], *Saltasaurus*[25],

Overosaurus[26], and *Trigonosaurus*[102]. The spine is estimated to be short due as indicated by the confluence of sprl and spol.

Supplementary Figure 4. Cervical and anterior dorsal vertebrae of *Abditosaurus kuehnei* gen. et sp. nov. Downloadable and interactive 3D (PLY file) digital model of the articulated cervical and anterior dorsal vertebrae (MCD-9882) available here: https://doi.org/10.6084/m9.figshare.14865699

Cervical ribs (Suppl. Fig. 4–6; Suppl. Table 4) – The cervical ribs are fused in nine of the 12 cervical vertebrae and well set aside from the centrum, level with its ventral surface (Fig. 2a). The anterior process has a projection that curves medially, resembling a characteristic 'batwing' shape, and extends to the anterior margin of the condyle. Its anterior extent is similar to that of *Overosaurus*[26] but differs from the straight anterior processes that surpass the centrum observed in *Rapetosaurus*[24], *Trigonosaurus*[102], and *Maxakalisaurus*[120], or those of *Alamosaurus*[121] and *Rukwatitan*[123] in which the anterior processes only extend to the posterior margin of the condyle or do not reach it. The posterior process is elongate and thins distally with lengths that overlap 2.5 subsequent centra (Fig. 2a), much more than the

posterior processes of *Isisaurus*[28] (not reaching the subsequent centrum) and *Maxakalisaurus*[120] (overlapping half the subsequent centrum), but less than those of *Rapetosaurus*[24] (overlapping three subsequent centra). The cross-sectional shape of the rib shaft trends from a dorsoventrally compressed plank proximally to rod-like distally, as in *Rukwatitan*[123]. As the authors[120] observed in *Maxakalisaurus*, the length of the cervical ribs in *Abditosaurus* seems to be related with the size of the cervical centra and thus the cervical ribs of anterior (3rd to 7th) and posterior (13th and 14th) vertebrae are shorter than those of the mid-cervical vertebrae (8th to 12th). Ventrally, the cervical ribs of successive vertebrae lie above those of preceding vertebrae, thus forming a bundle of subsequent ribs. Comparisons with cervical ribs of other Ibero-Armorican titanosaur species are not possible since these elements are mostly not preserved in these taxa.

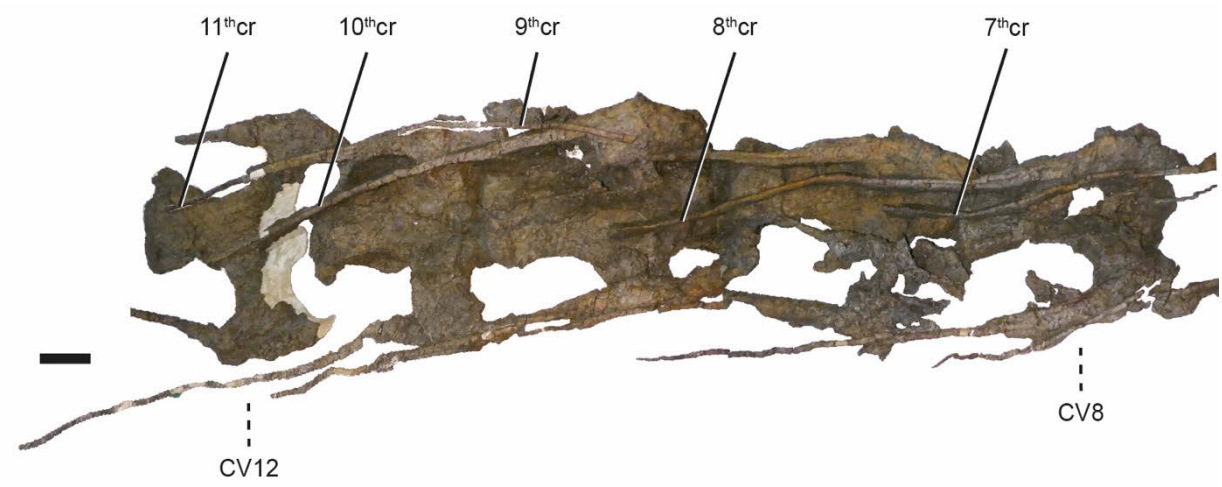

Supplementary Figure 5. Cervical vertebrae and fused ribs of *Abditosaurus kuehnei* gen. et sp. nov. (MCD-9882). Scale bar equals 10 cm. cr, cervical rib; CV, cervical vertebra.

Dorsal vertebrae (Suppl. Fig. 6–10; Suppl. Table 4) – The dorsal vertebrae are described with the neural canal horizontal. They are strongly opisthocoelous, have internal camellate tissue and shorten from the anterior to the middle vertebrae. Their ventral surfaces are flat to shallowly concave in the anterior dorsal vertebrae (DV1 and DV2) and markedly concave in the middle dorsal vertebrae (DV3–DV5), as in most derived titanosaurs and all other European taxa. All the centra lack a central keel, as in *Atsinganosaurus*[5], *Mansourasaurus*[16], *Saltasaurus*[25], *Ampelosaurus*[40], *Barrosasaurus*[124], and the mid-dorsal centra of *Lohuecotitan*[8] but unlike *Lirainosaurus*[125], the anteriormost dorsal centra of *Lohuecotitan*[8], *Opisthocoelicaudia*[41] and *Neuquensaurus australis*[98]. The lateral pleurocoels are oval and undivided.

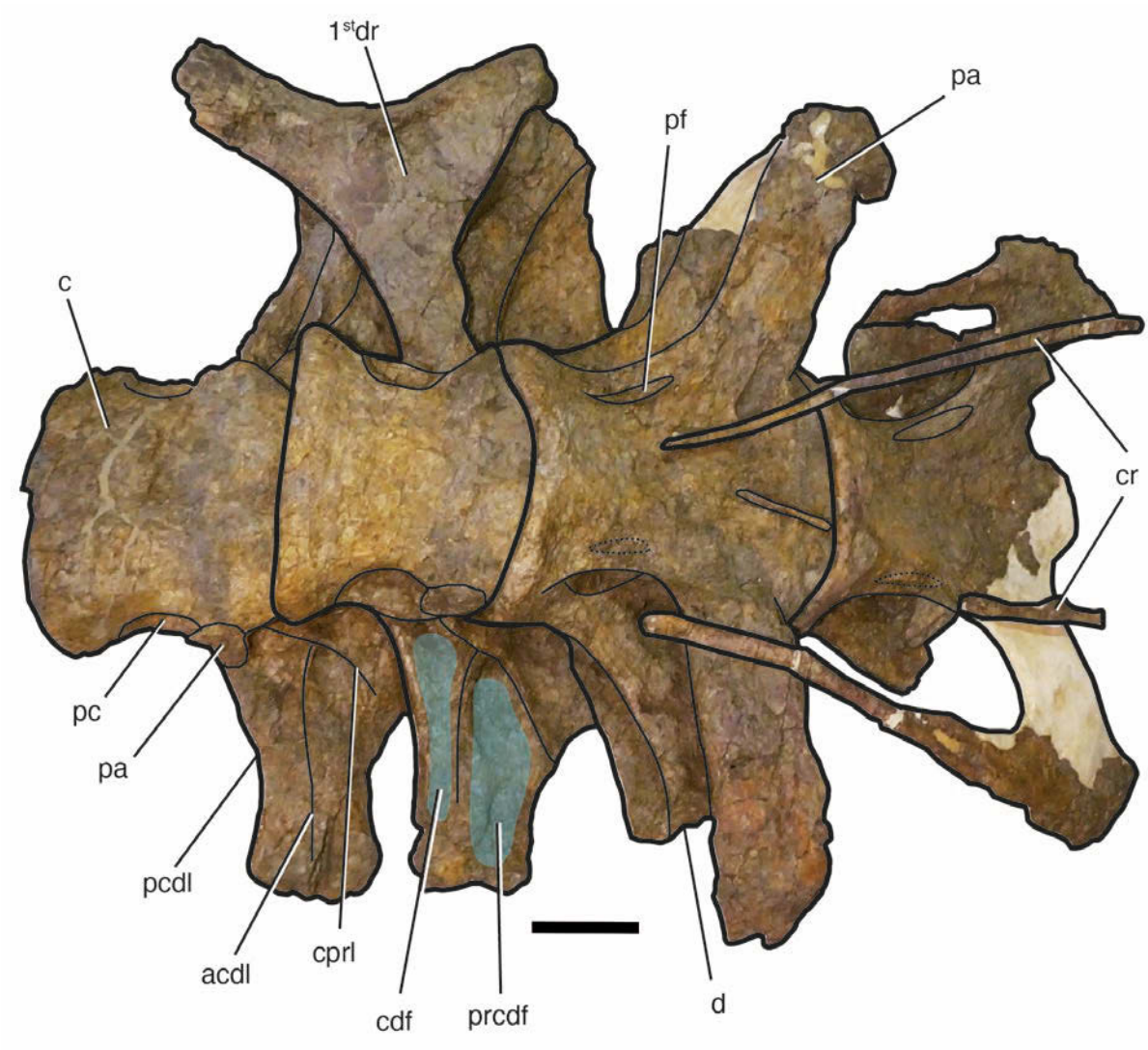

Supplementary Figure 6. Dorsal and cervical vertebrae of *Abditosaurus kuehnei* gen. et sp. nov. First and second anterior dorsal and 14th and 13th posterior cervical vertebrae (MCD-9882), in ventral view. Scale bar equals 10 cm. 1st dr, first dorsal rib; acdl, anterior centrodiapophyseal lamina; c, centrum; cdf, centrodiapophyseal fossa; cprl, centroprezygapophyseal lamina; cr, cervical rib; d, diapophysis; pa, parapophysis; pc, pleurocoel; pcdl, posterior centrodiapophyseal lamina; pf, pneumatic foramen; prcdf, prezygapophyseal centrodiapophyseal fossa.

In the anterior and first middle dorsal vertebrae, the transverse processes are low, laterally directed, and parallel to the horizontal plane, as in most titanosaurs (e.g.

Lohuecotitan[8] , *Rapetosaurus*[24], *Isisaurus*[28], *Opisthocoelicaudia*[41]; although in *Barrosasaurus*[124] and *Pitekunsaurus*[126] they project slightly dorsally). As in all European and other titanosaurs, the neural arch lacks the hyposphene-hypantrum articulation. In the anterior dorsal vertebrae, the anterior centrodiapophyseal lamina (acdl) does not reach the centrum because it intersects the centroprezygapophyseal lamina (cprl), an autapomorphy of *Abditosaurus* (Suppl. Fig. 6).

The middle dorsal vertebrae bear a large and triangular neural spine (Suppl. Fig. 7–10), moderately tall (~40% vertebral height) and angled posterodorsally (49º). The strongly posterodorsally inclined neural spine is like those of the middle dorsal vertebrae of most European titanosaurs, *Rinconsaurus*[95], *Overosaurus*[26], *Trigonosaurus*[102], *Opisthocoelicaudia*[41], *N. australis*[98], and *Dreadnoughtus*[127]. A single dorsoventrally extended prsl along almost the entire length of the neural spine is a character that *Abditosaurus* shares with *Rapetosaurus*[24], *Saltasaurus*[25], *Isisaurus*[28], *Lirainosaurus*[38], *Rinconsaurus*[95], *Paludititan*[101], differing from the reduced and dorsoventrally restricted prsl of *Opisthocoelicaudia*[41] and *Magyarosaurus* (sensu Curry Rogers[24]). The surface of the spinopostzygapophyseal fossa (spof) is pneumatized with scattered foramina, an autapomorphy of *Abditosaurus*. The intrapostzygapophyseal (tpol) and postspinal (posl) laminae are absent, the latter absence being a character shared with *Overosaurus*[26]. The long axes of the pre- and postzygapophyses are at a low angle relative to the horizontal plane, as in *Argentinosaurus*[23]. The postzygapophyseal spinodiapophyseal fossa (posdf) is mediolaterally elongated and small. The cpol, the cpof and the pocdf are strongly perforated by several foramina, the presence of which in the cpof and pocdf is autapomorphic of the new species. In the middle dorsal vertebrae, a secondary prdl is an autapomorphic character that divides the prpadf into a small prpadf-1 and

a ventral and larger prpadf-2 (Suppl. Fig. 9). Unlike some other Ibero-Armorican titanosaurs and many other titanosaurs, the centroprezygapophyseal (cprl) lamina is absent. The diapophyses are laterally directed and are located dorsal to the prezygapophyses, as in *Rapetosaurus*[24], *Saltasaurus*[25], *Overosaurus*[26], *Isisaurus*[28], *Opisthocoelicaudia*[41], *N. australis*[98], *Trigonosaurus*[102], and *Lirainosaurus*[125]. *Abditosaurus* is unique in having the diapophyses ventral to the postzygapophyses in the anterior and first middle dorsals (Suppl. Fig. 7 and 8).

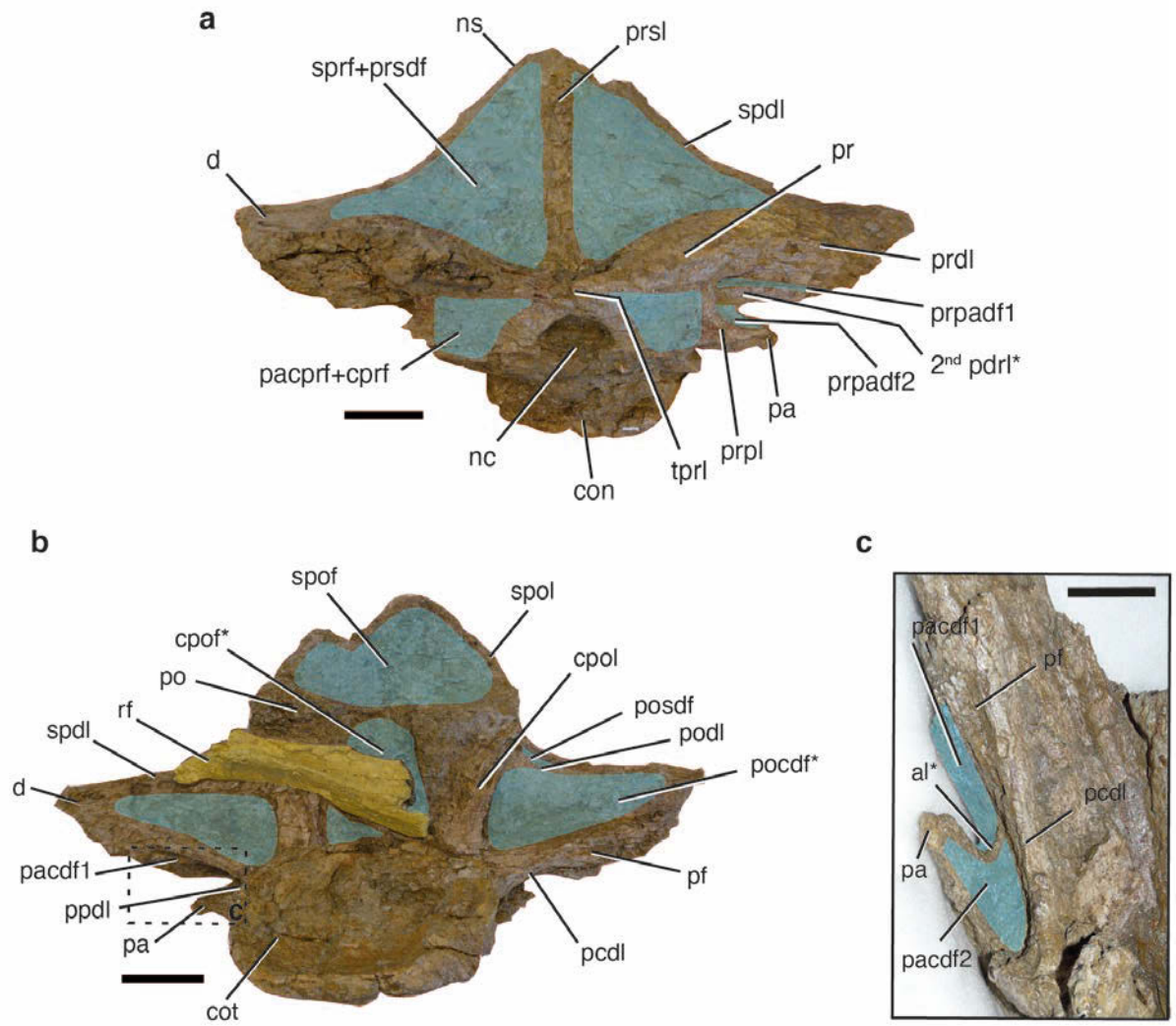

Supplementary Figure 7. Middle dorsal vertebrae of *Abditosaurus kuehnei* gen. et sp. nov. **a**, third dorsal vertebra (MCD-6718) in anterior view; **b**, the same specimen in posterior view; **c**, ventral view of the left transverse process. 2nd prdl, secondary prezygodiapophyseal lamina; con, condyle; cot, cotyle; cpof, centropostzygapophyseal fossa; cpol, centropostzygapophyseal lamina; cprf, centroprezygapophyseal fossa; d, diapophysis; nc, neural canal; ns, neural spine; pa, parapophysis; pacdf, parapophyseal centrodiapophyseal fossa; pacprf, parapophyseal centroprezygapophyseal fossa; pcdl, posterior centrodiapophyseal lamina; pf, pneumatic foramen; po, postzygapophysis; pocdf, postzygapophyseal

centrodiapophyseal fossa; podl, postzygodiapophyseal lamina; posdf, postzygapophyseal spinodiapophyseal fossa; ppdl, paradiapophyseal lamina; pr, prezygapophysis; prdl, prezygodiapophyseal lamina; prpadf, prezygapophyseal paradiapophyseal fossa; prpl, prezygoparapophyseal lamina, prsdf, prezygapophyseal spinodiapophyseal fossa; prsl, prespinal lamina; rf, rib fragment; spdl, spinodiapophyseal lamina; spof, spinopostzygapophyseal fossa; spol, spinopostzygapophyseal lamina; sprf, spinoprezygapophyseal fossa; tprl, intraprezygapophyseal lamina. The adhered rib fragment (shaded yellow) is part of dorsal rib MCD-6722. Scale bar equals 10 cm in a and b and approximately 5 cm in c. * indicates autapomorphic character.

Supplementary Figure 8. Third dorsal vertebra of *Abditosaurus kuehnei* gen. et sp. nov. Downloadable and interactive 3D digital model (PLY file) of the 3rd dorsal vertebra (MCD-6718) available here: https://doi.org/10.6084/m9.figshare.14865717

The pcdl bears a dorsal elliptical pneumatic foramen, a character shared with *Lohuecotitan*[8], *Rapetosaurus*[24], and *Saltasaurus*[25]. In the mid-dorsals the parapophyseal centrodiapophyseal fossae (pacdf) are internally divided by an oblique, posterodorsally-oriented accessory lamina that divides the pacdf into a dorsal and large pacdf-1 and a ventral and small pacdf-2.

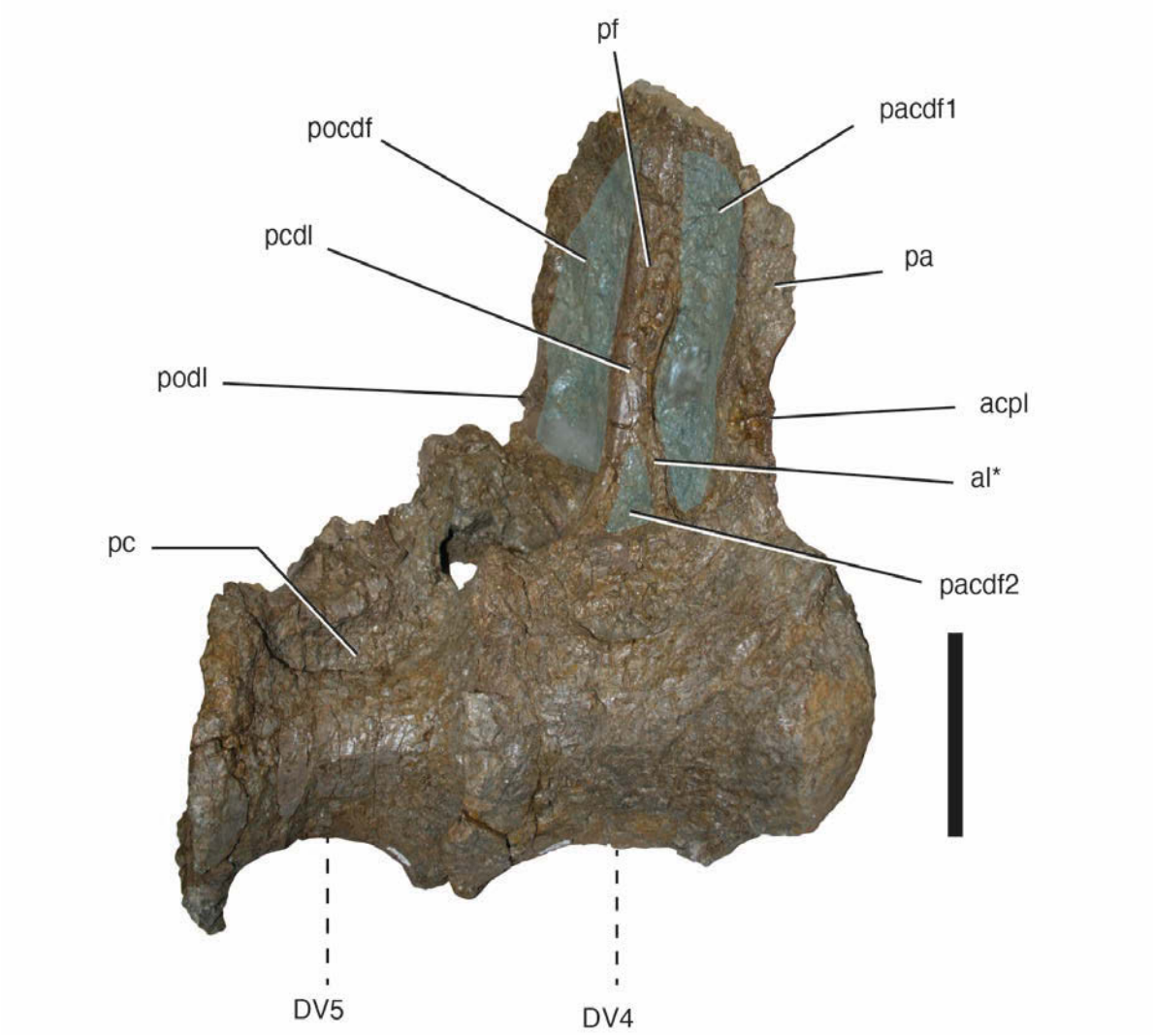

Supplementary Figure 9. **Middle dorsal vertebrae of *Abditosaurus kuehnei* gen. et sp. nov.** (MCD-6729, MCD-6730) in ventrolateral view. Scale bar equals 10 cm. acpl, anterior centroparapophyseal lamina; al, accessory lamina; pa, parapophysis; pacdf, parapophyseal centrodiapophyseal fossa; pc, pleurocoel; pcdl, posterior

centrodiapophyseal lamina; pf, pneumatic foramen; pocdf, postzygapophyseal centrodiapophyseal fossa; podl, postzygodiapophyseal lamina. * indicates autapomorphic character.

Supplementary Figure 10. Middle dorsal vertebrae of *Abditosaurus kuehnei* gen. et sp. nov. Downloadable and interactive 3D digital model (PLY file) of the 4th (MCD-6730) and 5th (MCD-6729) dorsal vertebrae available here: https://doi.org/10.6084/m9.figshare.14865726

Dorsal ribs (Suppl. Fig. 11, 12; Suppl. Table 4) – Six to seven pairs of dorsal ribs are partially preserved, the second and third left ribs being complete. The proximodistal length increases from the anteriormost to the posterior ribs up to the fourth dorsal rib which probably reaches the maximum length. All the recovered ribs are double-headed or dichocephalous, with the capitulum and tuberculum at a right angle and united by a capitulotubercular web but lacking proximal pneumatocoels. A distinct,

proximodistally elongated ridge extends distally from the tuberculum onto the rib shaft. The cross-section at the rib midshaft is plank-like, with an asymmetric 'D'-shape, with convex anterior convex and flat posterior profiles. In both the second and third dorsal ribs, the medial and lateral margins of the shaft merge distally to produce a rounded distal end, a spoon-like, expansion (as in *Opisthocoelicaudia*[41]). This bears longitudinal striae on both the anterior and posterior surfaces.

More particularly, some characters distinguish the dorsal ribs. In the first pair of dorsal ribs, the capitulum and the tuberculum projects equally in a proximal direction, and the latter is longer than the former. In anterior view the conjunction of their long axes and the rib shaft results in a triradiate 'Y' shape. The posterior surface of the distalmost part of the shaft bears striae for muscle insertion. There are no signs of distal expansion in the rib shaft. In the second pair of dorsal ribs the tuberculum projects proximally and points subparallel to the long axis of the rib shaft. The capitulum, which is longer than the tuberculum, projects medially at a right angle to the tuberculum and the rib shaft, and joints the latter with a curved, concave outline. The capitulotubercular web is very thin and more extensive than in the first dorsal ribs. The posterior surface of the distal end bears an anteroposterior thickening or bulge with striae for muscle or tendon insertion on its medial margin. In the third pair of dorsal ribs the tuberculum is poorly developed relative to the capitulum, and projects less proximally than in the second dorsal ribs. The capitulum is longer than the tuberculum, more developed mediolaterally, and projects proximomedially. The anteroposteriorly developed ridge differs from ridges in the preceding first and second ribs in its stronger development, and lateral projection. Characteristically, the dorsal third of the rib shaft twists relative to the mediolateral plane where the tuberculum and capitulum are placed. The shaft expands distally and produces a

distal peduncle where the rib articulates with the sternal plates. The entire distal end bears muscle striae.

Supplementary Figure 11. Dorsal ribs of *Abditosaurus kuehnei* gen. et sp. nov. From left to right, first (MCD-6719), second (MCD-6720), and third (MCD-6986) left dorsal ribs, respectively, in anterolateral view. Scale bar equals 10 cm. b, bulge; cap, capitulum; ctw, capitulotubercular web; r, ridge; tu, tuberculum. * indicates autapomorphic character.

Supplementary Figure 12. Second left dorsal rib of *Abditosaurus kuehnei* gen. et sp. nov. Downloadable and interactive 3D digital model (PLY file) of the left second dorsal rib (MCD-6720) available here: https://doi.org/10.6084/m9.figshare.14865741

Chevrons (Suppl. Fig. 13–15) – The anterior chevrons (MNCN 59539, MNCN 62760) are proximally opened and have a sturdy appearance, representing the 'straight closed Y-shaped' morphotype of Otero et al.[128]. The proximal rami have circular cross-sections, and the preserved part of the distal blade has a lenticular cross-section. The junction between the proximal rami at the distal margin of the haemal canal is strongly fused with a notable thickening. The articular facets are rounded and ball-shaped with no apparent subsurfaces differentiated.

The middle chevron (MNCN 59295) is proximally opened, fits the 'curved Y-shaped' morphotype of Otero et al.[128] and has the proximal and distal rami transversely

compressed with elliptical (proximal rami) to lenticular (distal blade) cross-sections. Martín Jiménez et al.[79] recognized the proximal articulations as being “slightly differentiated in two subfacets”, with no groove between them. With the articular facets articulated to the vertebra the three chevrons point posterodistally at an angle to the caudal axis. The anterior chevrons are straight whereas the distal blade of the middle chevron slightly expands anteroposteriorly.

The open Y-shape of the anterior and middle chevrons is characteristic of several neosauropods, including most macronarians[128]. As indicated by Martín Jiménez et al.[79], the presence of a deep haemal canal in the anterior chevrons (as in MNCN 59539 and MNCN 62760) was considered a synapomorphy of Titanosauria[46,129]. Specifically, the middle chevron of *Abditosaurus* differs from those of *Lohuecotitan*[8] and *Aeolosaurus*[130] in lacking two well-individualized subfacets at the proximal end.

Supplementary Figure 13. Anterior chevron of *Abditosaurus kuehnei* gen. et sp. nov. Downloadable and interactive 3D digital model (PLY file) of the anterior chevron (MNCN-59539) available here:

https://doi.org/10.6084/m9.figshare.14865807

Supplementary Figure 14. Anterior chevron of *Abditosaurus kuehnei* gen. et sp. nov. Downloadable and interactive 3D digital model (PLY file) of the anterior chevron (MNCN-62760) available here: https://doi.org/10.6084/m9.figshare.14865810

Supplementary Figure 15. Middle chevron of *Abditosaurus kuehnei* gen. et sp. nov. Downloadable and interactive 3D digital model (PLY file) of the middle chevron (MNCN-59295) available here: https://doi.org/10.6084/m9.figshare.14865816

Scapula (Suppl. Fig. 16, 17; Suppl. Table 5) – The scapula and coracoid are complete and not co-ossified. The acromial plate is perpendicular to the long axis of the scapular blade and dorsally expanded to twice the dorsoventral breadth of the posterior end. In extent, the dorsal expansion is intermediate between the weak to moderate expansion of *Isisaurus*[28], *Saltasaurus*[35], *N. australis*[48], and *Pitekunsaurus*[126], and the strongly expanded acromial plates of *Mansourasaurus*[16] and *Dreadnoughtus*[51]. The acromial ridge runs dorsoventrally nearly perpendicular to the long axis of the scapular blade, at an acute angle very similar to that of *Rapetosaurus*[24], *Argyrosaurus* ?*superbus*[37], *Opisthocoelicaudia*[41] and *Dreadnoughtus*[50], differing from the obtuse angle of *Alamosaurus*[131], and near the vertical disposition of *Antarctosaurus*[36] and *Pitekunsaurus*[126]. The scapular blade has a nearly 'D'-shaped cross section at the anterior end, and there is no a ventral ridge on the medial surface, unlike in *Atsinganosaurus*[11], *Mansourasaurus*[16], *Lirainosaurus*[39], *Ampelosaurus*[41], and *Opisthocoelicaudia*[41]. Both the dorsal and medial margins of the scapular blade expand distally, the posterodorsal expansion being more pronounced than the posteroventral one, as in *Isisaurus*[28], *Laplatasaurus*[36], *Opisthocoelicaudia*[41], *Saltasaurus*[48] and *Alamosaurus*[131], but differing from *Rapetosaurus*[24], *Lirainosaurus*[39], *Ampelosaurus*[40], and *Dreadnoughtus*[50], where the posterior expansion is absent or minimal. The posterior end of the scapular blade preserves part of the suprascapular cartilage and autapomorphically two lateral fossae or depressions on its lateral surface. The co-occurrence of a subtle posteroventral process on the medial margin of the acromial plate, a prominent process in the anteroventral corner, and a very prominent bulge on the dorsomedial margin of the scapular blade is unique to *Abditosaurus*. The scapula contributes more to the glenoid than does the coracoid, differing from

Lirainosaurus (coracoid contributes more than scapula[39]), and *Opisthocoelicaudia* (scapular contribution subequal to that of coracoid[41]), but similarly to *Mansourasaurus*[16].

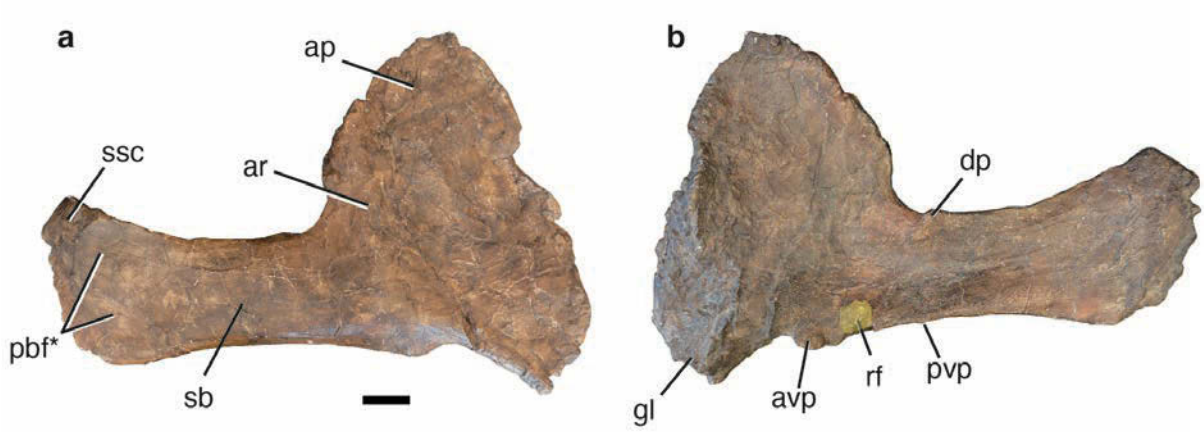

Supplementary Figure 16. Scapula of *Abditosaurus kuehnei* gen. et sp. nov. a, right scapula (from a cast of MCD-6724) in lateral view. **b**, the same specimen in medial view. Scale bar equals 10 cm. ap, acromial plate; ar, acromial ridge; avp, anteroventral process; pbf, posterior blade fossae; dp, dorsal process; gl, glenoid; pvp, posteroventral process; rf, rib fragment; sb, scapular blade; ssc, suprascapular cartilage. The adhered rib fragment (yellow-shaded) is part of dorsal rib MCD-6728. * indicates autapomorphic character.

Supplementary Figure 17. Scapula of *Abditosaurus kuehnei* gen. et sp. nov. Downloadable and interactive 3D digital model (PLY file;_ from a cast of MCD-6724) available here: https://doi.org/10.6084/m9.figshare.14865744

Coracoid (Suppl. Fig. 18, 19; Suppl. Table 5) – The coracoid is described with the glenoid surface oriented posteroventrally. It is longer than tall and has a quadrangular outline, a character shared with *Saltasaurus*[36], *Lirainosaurus*[39], *Ampelosaurus*[40], *Opisthocoelicaudia*[41], *N. australis*[48], *Dreadnoughtus*[50], and *Alamosaurus*[49].As in many titanosaurs, it lacks the ridge originating near the midpoint of the anterodorsal border of the lateral surface, which is present in *Rapetosaurus*[24], *Opisthocoelicaudia*[41], *Dreadnoughtus*[50] and *Saltasaurus*[132]. The absence of an infraglenoid groove is a character that *Abditosaurus* shares with *Rapetosaurus*[24], *Isisaurus*[28], *Lirainosaurus*[39], *Ampelosaurus*[40], *Narambuenatitan*[42], and *Alamosaurus*[49]. The coracoid foramen is far from the scapular articulation, as in *Isisaurus*[28], *Saltasaurus*[36], *Opisthocoelicaudia*[41], *N. australis*[48], *Alamosaurus*[49],

Dreadnoughtus[50], and *Uberabatitan*[122], and differing from *Atsinganosaurus*[11], *Lirainosaurus*[39], *Ampelosaurus*[40], and other derived titanosaurs[16,24,42]. The foramen is elliptical and autapomorphically twists its orientation from the lateral through the medial surface. In articulation with the scapula, the dorsal margin of the coracoid is situated below the level of the scapular acromial plate.

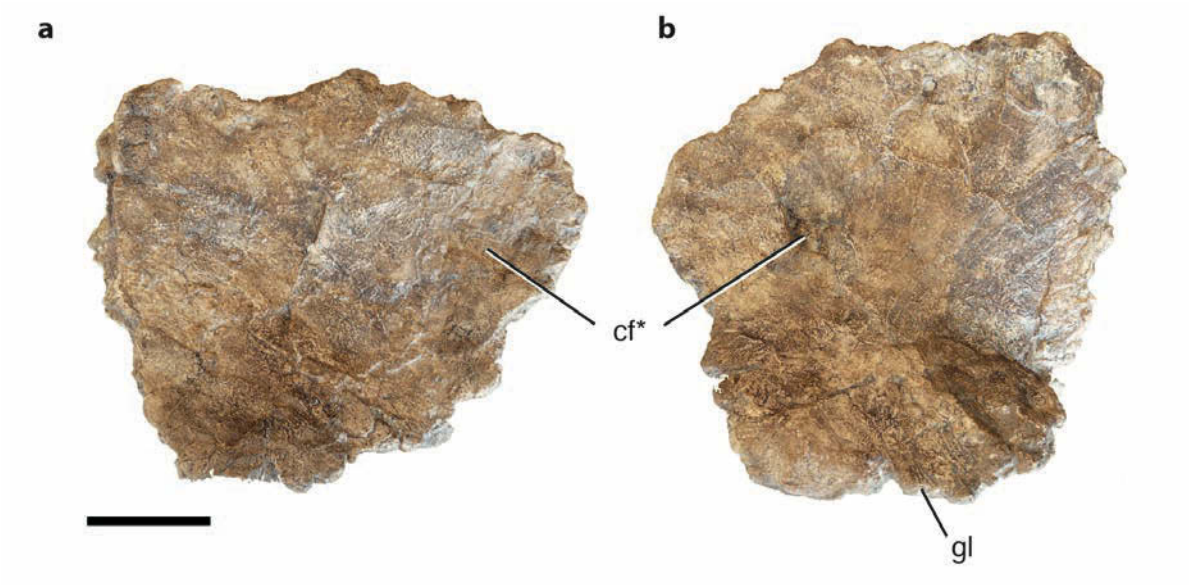

Supplementary Figure 18. Coracoid of *Abditosaurus kuehnei* gen. et sp. nov. a, right coracoid (from a cast of MCD-6742) in medial view. **b**, the same specimen in lateral view. Scale bar equals 10 cm. cf, coracoid foramen; gl, glenoid. * indicates autapomorphic character.

Supplementary Figure 19. Coracoid of *Abditosaurus kuehnei* gen. et sp. nov. Downloadable and interactive 3D digital model (PLY file; from a cast of MCD-6742) available here: https://doi.org/10.6084/m9.figshare.14865750

Sternal plate (Suppl. Fig. 20, 21) – The sternal plate has a semilunate morphology with a strongly concave lateral surface, a character typical of titanosaurs. Unlike almost all titanosaurs[6], it lacks an anteroventral ridge on the ventral surface (as in *Mnyamawamtuka*[29]. The sternal plate length: humeral length ratio iofn *Abditosaurus* (0.68) is very close to the value of saltasaurids (>0.7)[44].

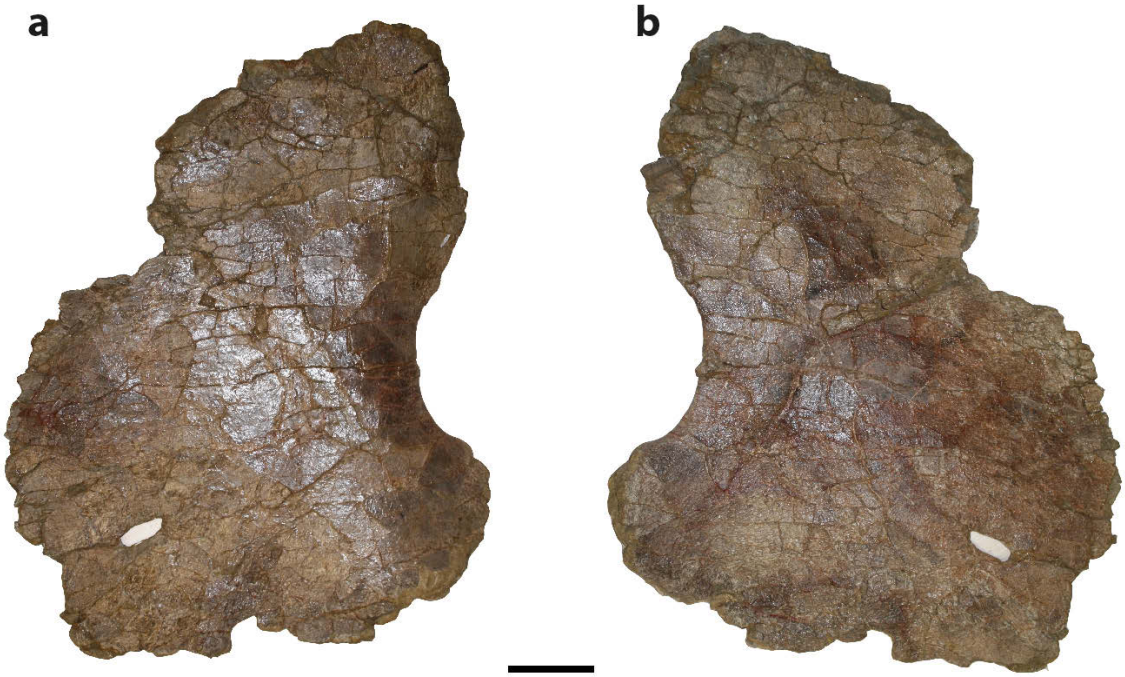

Supplementary Figure 20. Sternal plate of *Abditosaurus kuehnei* gen. et sp. nov.

a, left sternal plate (MCD-6716) in ventral view. **b**, the same specimen in dorsal view. Scale bar equals 10 cm.

Supplementary Figure 21. Sternal plate of *Abditosaurus kuehnei* gen. et sp. nov. Downloadable and interactive 3D digital model (PLY file) of the left sternal plate (MCD-6716) available here: https://doi.org/10.6084/m9.figshare.14865756

Sternal rib (Suppl. Fig. 22) – This element was found isolated and is elongated, rod-like, with longitudinal striations and tapered, and irregular ends. The discovery of an ossified sternal ribs is *Abditosaurus* is unique among Titanosauria and represents the first unequivocal evidence of these elements in Titanosauriformes. Further, it challenges the assumption that the loss of ossified sternal ribs might be a synapomorphy of this clade[46]. The preservation of a sternal ribs in *Abditosaurus* suggests that the ossification of these elements might be related to the very advanced ontogenetic age of the holotypic individual.

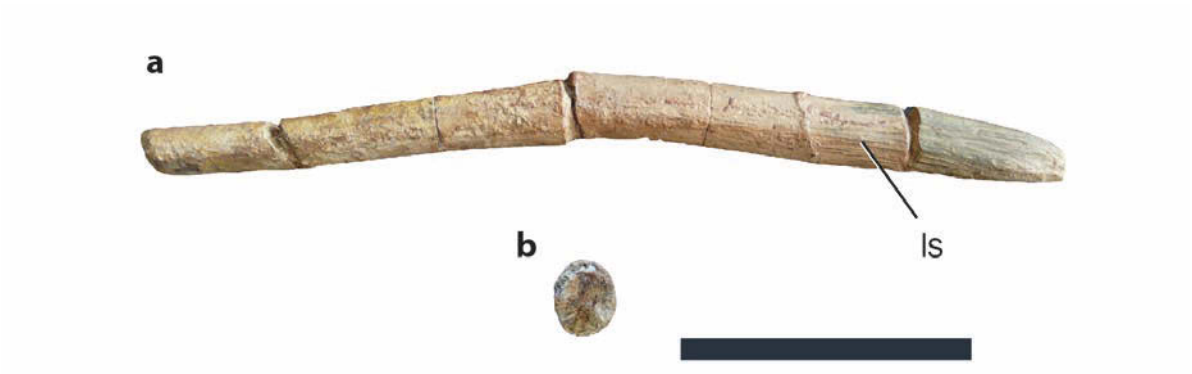

Supplementary Figure 22. Sternal rib of *Abditosaurus kuehnei* gen. et sp. nov. **a**, sternal rib (MCD-6747) in longitudinal view. **b**, cross-section at midshaft. Scale bar equals 10 cm. ls, longitudinal striae.

Humerus (Suppl. Fig. 23–25; Suppl. Table 6) – The humerus is a robust element, with a robustness index (RI[57]) value similar to those of *Opisthocoelicaudia*, *N. australis*, *Saltasaurus*, and *Dreadnoughtus*[50] and remarkably different from the more gracile humeri of other Ibero-Armorican taxa as well as some other titanosaurs (e.g., *Rapetosaurus*[24]). The mediolateral development of the proximal end (43% of the total length of the bone) is similar to those described in *Saltasaurus*, *N. australis*[33], and *Opisthocoelicaudia*[41]. The deltopectoral crest is robust and strongly expanded mediolaterally to reach the midline of the shaft, as in *Nullotitan*[31], *Saltasaurus*[33], *Aeolosaurus rionegrinus*[33], *Opisthocoelicaudia*[41], *N. australis*[48], *Alamosaurus*[49], *Dreadnoughtus*[50], and an unidentified lithostrotian[133], but differing from the unexpanded or moderately expanded crests of all other Ibero-Armorican species and many other titanosaurs[16,28,32,37,99,134,135]. It projects unambiguously medially, similarly to the conditions in *Gondwanatitan*[30], *Nullotitan*[31], and *Jainosaurus*[32]. Unlike those of other Ibero-Armorican titanosaurs, the *Abditosaurus* humerus exhibits a distally expanded deltopectoral crest, a synapomorphy of Saltasauridae[44,46] shared with *Opisthocoelicaudia*[41], *Saltasaurus*[47], *N. australis*[48], and *Alamosaurus*[49]. The distal

condyles are clearly divided, as in saltasaurids[44,46], and the articular surface of the radial condyle faces anterodistally, as in *Paralititan*[34] and *Saltasaurus*[47].

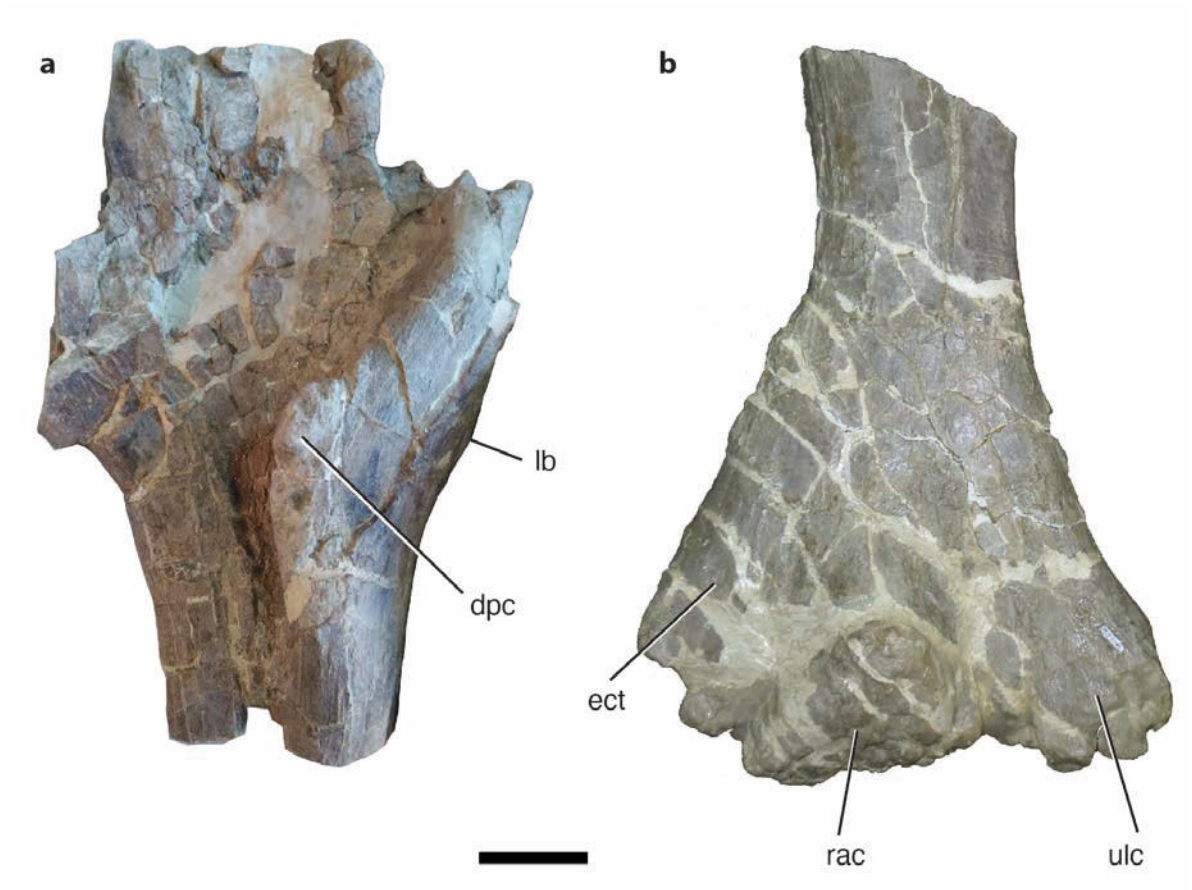

Supplementary Figure 23. Humeri of *Abditosaurus kuehnei* gen. et sp. nov. **a**, proximal half of the left humerus (MNCN-79834) in anterior view. **b**, distal half of the right humerus (MCD-6988) in anterior view. Scale bar equals 10 cm. dpc, deltopectoral crest; ect, ectepicondylar area; lb, lateral bulge; rac, radial condyle; ulc, ulnar condyle.

Supplementary Figure 24. Humerus of *Abditosaurus kuehnei* gen. et sp. nov. Downloadable and interactive 3D digital model (PLY file) of the proximal half of the left humerus (cast of MNCN-79834) available here: https://doi.org/10.6084/m9.figshare.14865765

Supplementary Figure 25. Humerus of *Abditosaurus kuehnei* gen. et sp. nov. Downloadable and interactive 3-D digital model (ply file) of the proximal half of the distal half of the right humerus (MCD-6988) available here: https://doi.org/10.6084/m9.figshare.14865777

Radius (Suppl. Fig. 26, 27; Suppl. Table 6) – The radius has a mediolaterally expanded distal end, bevelled posterolaterally at more than 20º relative to the long

axis of the shaft, and a well-defined interosseus ridge, as in other lithostrotian sauropods[44]. The interosseous ridge extends proximodistally and is laterally positioned, as in *Opisthocoelicaudia*[41] but unlike the posteriorly centred or the obliquely oriented ridge of *Rapetosaurus*[24], *Saltasaurus*[47], *N. australis*[48], *Dreadnoughtus*[50], and *Uberabatitan*[122]. Its development and location slightly resemble that of *Diamantinasaurus*[136]. Unlike the rounded shape of *Rapetosaurus*[24] or *Dreadnoughtus*[50], the distal surface is elliptical and anteroposteriorly asymmetrical, as in *N. australis*[48]. Autapomorphically, *Abditosaurus* presents a small, oblique ridge on the posterodistal surface.

Supplementary Figure 26. Radius of *Abditosaurus kuehnei* gen. et sp. nov. **a**, distal half of the right radius (MCD-6748) in anterior view. **b**, the same specimen in posterior view. **c**, the same specimen in distal view, anterior side up. Scale bar equals 10 cm. ior, interosseous ridge; pdr, posterodistal ridge. * indicates autapomorphic character.

Supplementary Figure 27. Radius of *Abditosaurus kuehnei* gen. et sp. nov. Downloadable and interactive 3D digital model (PLY file) of the distal half of the right radius (MCD-6748) available here: https://doi.org/10.6084/m9.figshare.14865780

Ilium (Suppl. Fig. 28) – The left ilium only preserves the preacetabular process and part of the long preacetabular blade. In lateral view, the anteroventral tip of the preacetabular process has a roughly straight edge at an angle to the concave profile of the preacetabular blade. In dorsal view, it projects anterolaterally, as in *Garrigatitan*[6] and *Lohuecotitan*[8] but differing from *Lirainosaurus*[39]. Mediolaterally, the

preacetabular blade is thick and robust and thickens at the preacetabular process. Internally, the ilium is pneumatized (camellate texture), as in *Garrigatitan*[6], *Lohuecotitan*[8], *Atsinganosaurus*[11], *Lirainosaurus*[39], *Alamosaurus*[51], *Saltasaurus*, *Neuquensaurus*, *Rocasaurus*[52], and *Diamantinasaurus*[136], among others.

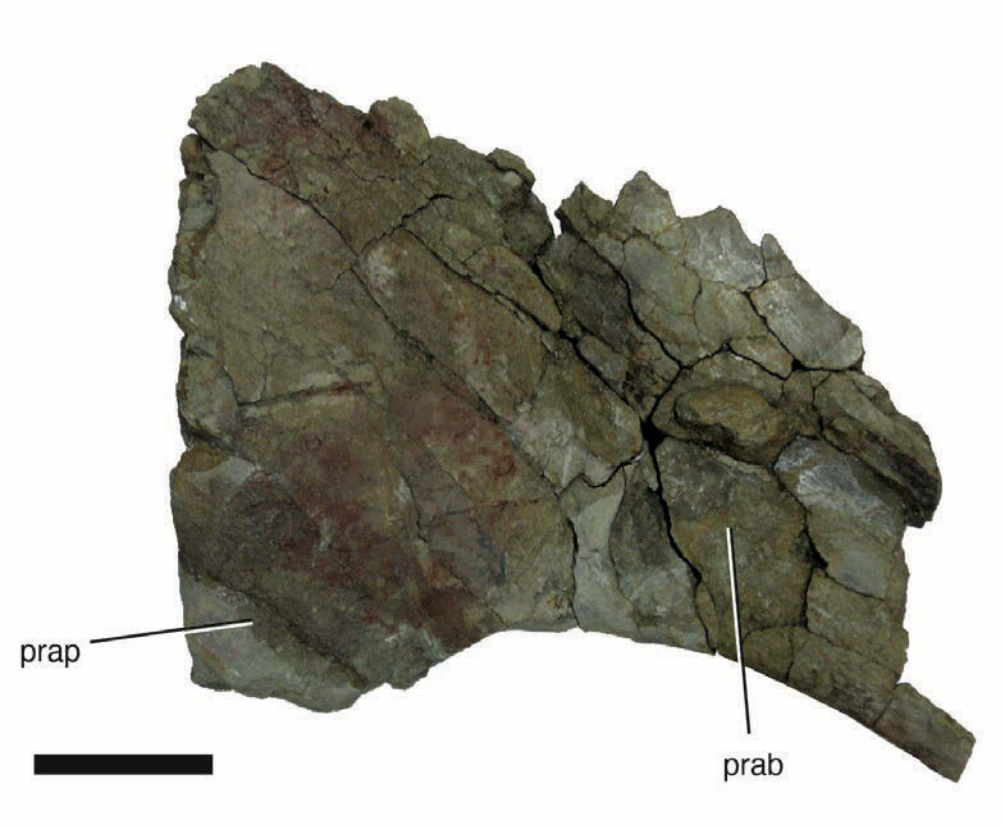

Supplementary Figure 28. Ilium of *Abditosaurus kuehnei* gen. et sp. nov. Anterior portion of the left ilium (MCD-6731) in lateral view. Scale bar equals 10 cm. prab, preacetabular blade; prap, preacetabular process.

Femur (Suppl. Fig. 29; Suppl. Table 7) – The preserved femur exhibits a prominent, proximally located lateral bulge, which differs from most other European titanosaurs as well as a posterior accessory ridge. The shaft is more mediolaterally than anteroposteriorly developed with an eccentricity index >185%, as in most titanosaurs[53].

Supplementary Figure 29. Femur of *Abditosaurus kuehnei* gen. et sp. nov. Downloadable and interactive 3D digital model (PLY file) of the partial left femur (MCD 6987) available here: https://doi.org/10.6084/m9.figshare.14865786

Tibia (Suppl. Fig. 30, 31; Suppl. Table 7) – The tibia is gracile, like most other European titanosaurs and, as in most titanosaurs, the proximal end is mediolaterally compressed, but this compression is not as well developed as in *Atsinganosaurus*[11] and *Lirainosaurus*[39] and contrasts with the rounded shape of *Lohuecotitan*[8] and *Ampelosaurus*[40]. A small but prominent bulge at the posterior margin of the proximal end is also observed in *Neuquensaurus*[35]. The cnemial crest projects anteriorly, as in *Gondwanatitan*[30]. The distal end is longer mediolaterally than anteroposteriorly, as is typical for titanosaurs[44,54]. The anteromedial ridge is more pronounced than in *Lohuecotitan*[8], *Atsinganosaurus*[11], and *Lirainosaurus*[39], and a mediolaterally expanded posteroventral (or lateroposterior) process is shared with *Gondwanatitan*[30], *Dreadnoughtus*[50] and *Laplatasaurus*[56]. The distal end is heart-shaped with the distal processes strongly protruding and directed laterally.

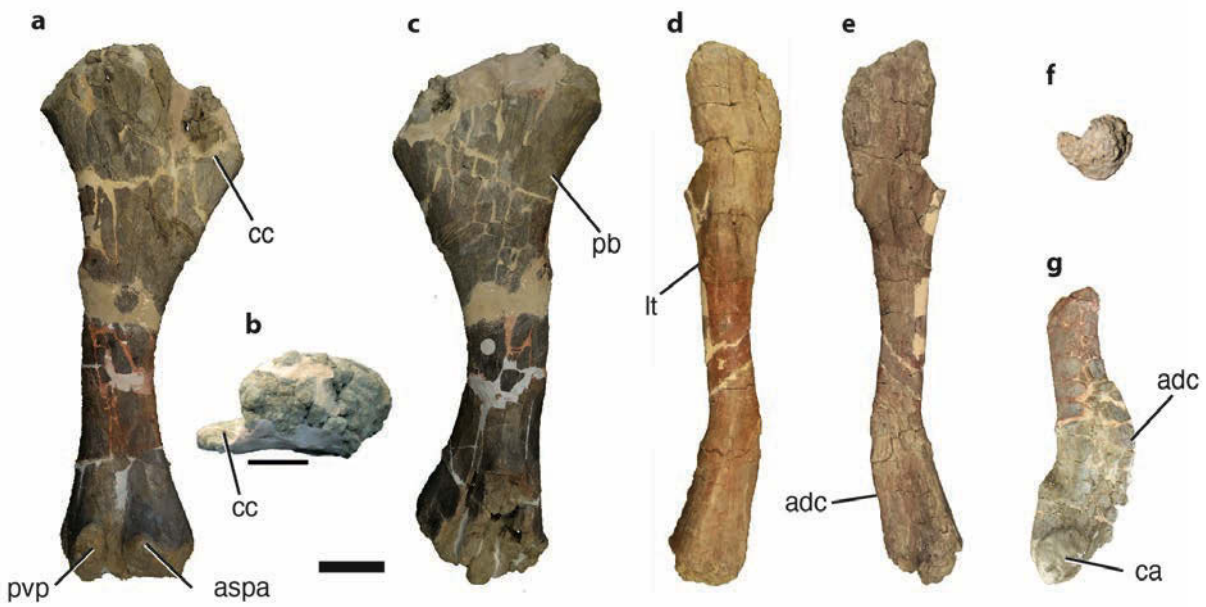

Supplementary Figure 30. Tibia, fibula and calcaneum of *Abditosaurus kuehnei* gen. et sp. nov. **a**, right tibia (MNCN-79837-79838-79848) in lateral view. **b**, the same specimen in proximal view. **c**, the same specimen in medial view. **d**, right fibula (MCD-

6723) in lateral view. **e**, the same specimen in medial view. **f**, the same specimen in distal view (medial side up). **g,** distal half of the left fibula (MNCN-79847) with adhered calcaneum in medial view. Scale bar equals 10 cm. adc, anterodistal crest; aspa, articular surface for ascending process of astragalus; ca, calcaneum; cc, cnemial crest; lt, lateral trochanter; pb, posterior bulge; pvp, posteroventral process.

Supplementary Figure 31. Tibia of *Abditosaurus kuehnei* gen. et sp. nov. Downloadable and interactive 3D digital model (PLY file) of the right tibia (MNCN-79837-79838-79848) available here: https://doi.org/10.6084/m9.figshare.14865792

Fibula (Suppl. Fig. 30, 32; Suppl. Table 7) – The sigmoid shape of the fibulae is a character shared with most other Campanian–Maastrichtian titanosaurs except for *Ampelosaurus*[40], *Laplatasaurus*[56], *Uberabatitan*[122], and *Bonatitan*[137]. The presence of a prominent lateral trochanter, a synapomorphy of Saltasaurinae[49], is shared with *Jainosaurus*[33], *Saltasaurus*[48], *Neuquensaurus*[48], *Dreadnoughtus*[50], *Alamosaurus*[55], *Laplatasaurus*[56], *Bonatitan*[137], and *Aeolosaurus sp.*[135]. Unlike *Lirainosaurus*[39] and *Jainosaurus* cf. *septentrionalis*[134], the shaft is distinctively elliptical in cross-section. *Abditosaurus* is unique in having a distal end bevelled posteriorly at 20º with respect to the long axis. The distal articular surface is triangular, as in *Rapetosaurus*[24], *Lirainosaurus*[39], *Alamosaurus*[55], and *Laplatasaurus*[56].

Supplementary Figure 32. Fibula of *Abditosaurus kuehnei* gen. et sp. nov. Downloadable and interactive 3D digital model (PLY file) of the right fibula (MCD-6723) available here: https://doi.org/10.6084/m9.figshare.14865801

Calcaneum (Suppl. Fig. 30) – The calcaneum is a small, convex, oval element, as in *Euhelopus*[57], and similar to the purported calcaneum reported of *Elaltitan*[37] (although the authors later rejected this interpretation, Mannion, pers. comm., 2018).

2.3 Appendicular osteohistology (Suppl. Fig. 33)

Humerus (MCD-7244) – The histological samples from the posterior side of the left humerus (MCD-7244.1, Suppl. Fig. 33) show extensive bone remodelling. The inner cortex is defined by large medullary cavities, sometimes infilled with secondary carbonate. The expansion of the medullary cavities decreases gradually outwards, merging into the middle cortex. The outer cortex is of Haversian tissue, with at least three overlapping generations of secondary osteons. For this reason, no remains of primary bone or lines of arrested growth (LAGs) are observed throughout the thickness of the sample. A very thin layer of avascular lamellar bone is observed in the periosteal region of the bone, here interpreted as the external fundamental system (EFS). The combination of the aforementioned histological features is consistent with type G bone tissue[138].

Femur (MCD-7245) – The samples from the anterior side of the left femur (MCD-7245.A1) exhibit nearly identical histological characteristics to the sample from the posterior side of the humerus (MCD-7244.1); in other words, extensive bone remodelling and large medullary cavities merging into well-developed Haversian bone with three generations of secondary osteons that obliterate any trace of the primary bone tissue, thus being classified as type G bone tissue[138]. By contrast, the sample from the posterior side of the femur (MCD-7245.B1, Suppl. Fig. 33) exhibits a less mature bone tissue. The medullary cavity is well-developed with large vacuities that gradually merge into the Haversian tissue that characterizes the middle cortex. However, the secondary osteons decrease in size and number toward the outer cortex, revealing primary laminar fibro-lamellar bone tissue. Along the outer cortex, a minimum of six LAGs can be counted, with no significant reduction in their thickness outward. No EFS is observed in the most external region of the periosteum. Due to

the differential combination of histological features observed in the sample from the posterior side of the femur, it can be divided into two distinctive zones. Whereas the inner and the middle cortex aligns with the definition of type F bone tissue[138], the upper cortex corresponds well with type E tissue[138].

Tibia (MCD-7243) – As in the humerus and femur, the medial sample from the tibia (MCD-7243.1, Suppl. Fig. 33) exhibits extensive bone remodelling, with abundant medullary cavities in the inner cortex. These vacuities decrease in size outward until they merge into the middle cortex, which is characterized by well-developed Haversian bone tissue that extends toward the outer cortex. Three generations of secondary osteons erase any trace of the primary bone tissue or LAGs. As in other samples, a thin (0.01 mm-thick) layer of avascular lamellar bone is present at the periosteum, which is interpreted as the EFS. The aforementioned combination of bone characteristics is consistent with type G[138] (Suppl. Fig. 33).

The combination of histological features of the tibia, humerus, and the anterior side of the femur can be correlated with type G bone tissue[138], whereas the sample from the posterior side of the femur is similar to that of type F. The dissimilarity between the types of bone tissue from elements from the same individual can be explained by an intraskeletal histovariability related to the different medullary cavity expansion rates of the appendicular bones[139]. Nevertheless, given the generalized high degree of bone remodelling with several generations of secondary osteons in the outer cortex of all samples, it can be concluded that *Abditosaurus* falls histologically within HOS-14[138, 140], a histologic ontogenetic stage characteristic of a very old-aged individual (senile stage[141]). In addition, various other lines of evidence points to the

fact that the Orcau-1 specimen was a senile individual. Thus, the occurrence of an ossified calcaneum and sternal rib (both of which are very rare in titanosaurs) in *Abditosaurus* might indicate that the ossification of these bones is related to advanced ontogenetic age.

The presence of primary laminar fibro-lamellar tissue in the outer cortex of the femur of *Abditosaurus* contrasts with the occurrence of the modified laminar bone (MLB) showed by several insular European titanosaurs (i.e., *Lirainosaurus*[9], *Ampelosaurus*[10], *Magyarosaurus*[141]). Although MLB is not observed in *Garrigatitan*[6], the occurrence of a well-vascularized EFS and vascular canals open to the periosteal surface of the bone lead the authors to speculate that some kind of size reduction comparable to other titanosaurs from the Late Cretaceous European archipelago took place in this recently-named French taxon[8].

By contrast, primary laminar fibro-lamellar bone tissue seems to be the plesiomorphic histological condition in titanosaurs and has been reported in several taxa such as the North American *Alamosaurus*[10, 142], the South American *Patagotitan*[107], *Dreadnoughtus*[143], and *Bonitasaura*[144], and the Madagascan *Rapetosaurus*[145]. These observations suggest that *Abditosaurus* did not have metabolic adaptations derived from insular conditions like other European titanosaurs[10] but rather showed similar growth rates to non-insular titanosaurs.

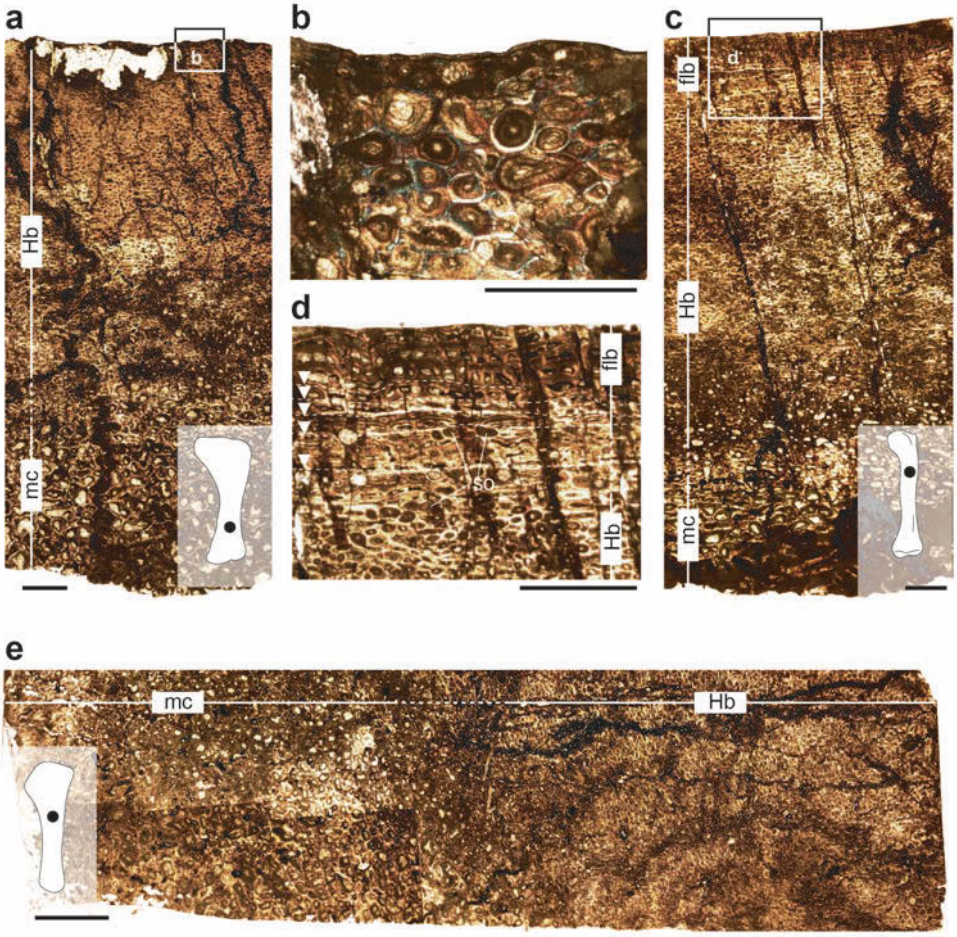

Supplementary Figure 33. Osteohistological characterization of *Abditosaurus kuehnei* gen. et sp. nov. **a**, thin section of the posterior side of the humerus (MCD-7244.1). **b**, detail of the high bone remodeling displayed by Haversian bone tissue reaching the external bone. **c**, composed thin section of the posterior side of the femur (MCD-7245.B1). **d**, close-up detail of the fibro-lamellar bone that occurs at the periosteal region. White triangles and dashed lines illustrate the location of the preserved LAGs. **e**, composed histological log of the posterior side of the tibia (MCD-7243.1) showing the extensive bone remodeling. Dashed line indicates the transitional zone between the bone tissues of the medullary region and the cortex region. flb, fibro-lamellar bone tissue; Hb, Haversian bone tissue; mc, medullar cancellous bone; so, secondary osteons. Scale bar equals 2 mm (a, c, d, e) and 1 mm (b), respectively.

2.4 Titanosaur evolution in the Ibero-Armorican island

At the very end of the Cretaceous, Europe consisted of an extensive archipelago in which the main landmasses were the Ibero-Armorican Island and the Haţeg Island[146]. These were the palaeogeographical settings where the dinosaur faunas evolved from the early Campanian to the latest Maastrichtian and, despite some remarkable differences, the two regions show faunal similarities[3,20,147] , such as the presence of several clades of titanosaurian sauropods. Moreover, on the Ibero-Armorican Island, the evolution of dinosaur faunas features the 'Maastrichtian Dinosaur Turnover' [2,3,15], a replacement of fauna that started in the early Maastrichtian and ended in the early late Maastrichtian (a span of 2.5–2.8 million of years), generally characterized by a shift from a sauropod-dominated to a hadrosauroid-dominated faunal assemblages. Detailed biochronostratigraphic studies in the region pinpoint other intra-clade replacements that occurred. For instance, the temporal distribution of titanosaurian bone and oological fossils shows a late Campanian–early Maastrichtian assemblage composed of small to medium-sized taxa (*Lirainosaurus*, *Atsinganosaurus*, *Ampelosaurus*, *Lohuecotitan*, *Garrigatitan*) that was replaced by an early–late Maastrichtian assemblage of distinct but indeterminate large-bodied taxa (e.g., the large sized specimens reported by Canudo[14] in chron C29r and by Vila et al.[15] in chron C31r-C31n), associated with distinct oospecies assemblages (see below). The pre-turnover assemblages would have been present in the region until the early late Maastrichtian (chron C30r), whereas the new post-turnover titanosaurs would have reached the island by the early Maastrichtian (basal part of chron C31r), coexisting for a period with the former taxa (Fig. 4).

Oospecies chronostratigraphy

In the Upper Cretaceous deposits of Europe, the occurrence of several distinctive oospecies associated with titanosaurs is well documented[22,148-150] and recent biochronostratigraphic studies of the Ibero-Armorican domain have established that the two main assemblages of oospecies from the Campanian–Maastrichtian interval are associated with the pre- and post-turnover titanosaur assemblages of the 'Maastrichtian Dinosaur Turnover' (MDT)[3]. The lower oological assemblage consists of *Megaloolithus siruguei* + *Megaloolithus aureliensis*, and ranges from the upper Campanian (upper part of chron C33) to the lower Maastrichtian (chron C31). Both oospecies are endemic to Europe[149,150], with *M. siruguei* being the more abundant and occurring at several Maastrichtian localities in Spain, France, and Romania[151]. In the Ibero-Armorican region, the spatiotemporal distribution of *M. siruguei* and *M. aureliensis* suggests that they were produced by the pre-turnover titanosaur taxa[3]. The upper assemblage is defined uniquely on the Ibero-Armorican Island solely by the association of *Fusioolithus baghensis* + *Megaloolithus mamillare* and ranges from the lower Maastrichtian (chron C31r) to the uppermost Maastrichtian (chron C29r). Unlike those in the lower assemblage, the oospecies of the upper association have a geographic distribution outside of Europe, in Gondwanan landmasses[152–154]. Thus, *F. baghensis* is recorded in the Campanian–Maastrichtian of South America, India[155,156], and probably Africa[157,158], whereas *M. mamillare* (most probably a senior synonymous of *M. jabalpurensis*) is recorded in South America and India[152,156]. More importantly, both oospecies represent a clade of titanosaurs exclusive to the Campanian–Maastrichtian interval that attained a Gondwanan distribution. In Europe, as both oospecies appear recurrently and characteristically after the lower

early Maastrichtian assemblage (*M. siruguei* + *M. aureliensis*), they can be regarded as the eggshell types produced by the newly arriving, post-turnover titanosaur faunas[2,3]. Consequently, the occurrence of *F. baghensis* eggshells at the *Abditosaurus* locality[22] (Suppl. Fig. 34) indicates the presence of a post-turnover titanosaur taxon with Gondwanan affinities and, in light of phylogenetic analyses (Fig. 3 and Suppl. Fig. 42-65), we suggest that this oospecies might have been produced by saltasaurine titanosaurs. Nevertheless, new data from latest Cretaceous titanosaurs and nesting grounds in South America, as well as the possible discovery of new derived titanosaurs in India and Africa, are required to confirm this hypothesis.

Supplementary Figure 34. *Fusioolithus baghensis* oospecies at the type locality of *Abditosaurus kuehnei* gen. et sp. nov. Radial section of sample IPS59133 from Orcau-1.

2.5 Phylogenetic results

A first maximum parsimony analysis using equally weighted characters was carried out, resulting in 7,152 trees of 918 steps (Consistency Index 0.26, Retention Index 0.53, Rescaled Consistency Index 0.16). The resulting consensus tree is poorly resolved (Suppl. Fig. 35), with all taxa more derived than *Brachiosaurus* recovered in a large polytomy, with only four resolved clades, most notably a very exclusive Saltasauridae formed by *Neuquensaurus*, *Saltasaurus*, *Futalognkosaurus*, *Lirainosaurus* and *Opisthocoelicaudia*. Attempts to increase the resolution of the strict consensus using iterative PCR pruning invariably resulted in the pruning of most of the taxa, including *Abditosaurus kuehnei* gen. et sp. nov. and most other European taxa.

A second round of analysis using implied weighting[159] was carried out. Due to the high number of missing entries in the dataset, a recurring problem in fossil datasets, the extended version of the implied algorithm was preferred. Missing entries were assumed to have 50.0% of the homoplasy of observed entries; homoplasy in missing entries was not increased beyond 4,000 times the observed homoplasy. Four different concavity constants (k = 5, 10, 12, and 15) were used to weight down the homoplasy (Supplementary Figures 35–39).

The extended implied weighting searches resulted in a single most parsimonious tree for the k = 5 and k = 10 (Supplementary Figures 35–37) and 16 most parsimonious trees for k = 12 and k = 15 (Supplementary Figures 38 and 39), with decreasing fit scores as the k increased. The general topology of the trees is very similar for all the different k, but important differences can be observed in the placement of *Abditosaurus*. The new taxon is always recovered within Saltasauridae,

as are all European titanosaurs, but when an aggressive k value (k = 5) is used, it is recovered as the sister taxon of *Paralititan*, forming a clade with *Maxakalisaurus*, *Neuquensaurus* and *Saltasaurus*, and resulting in a monophyletic Saltasaurinae sensu Wilson and Upchurch[160]. More conservative k values (10,12, and 15) recover *Abditosaurus* as the sister taxon of *Lohuecotitan*, forming a sister clade to *Maxakalisaurus* + *Paralititan*, and recovered as a sister clade to all other Saltasauridae. These more conservative k analyses are identical in the topology of Saltasauridae, and only differ in the topology of non-saltasaurid titanosaurs, and in the topology, but not the composition, of the clade Aeolosauridae, the most inclusive clade containing *Aeolosaurus* but not *Opisthocoelicaudia* or *Saltasaurus*[161]. Nevertheless, these consensus trees are unusual in recovering the clade *Opisthocoelicaudia* + *Lirainosaurus* as sister to Saltasaurini, leaving most of the taxa traditionally included in Opisthocoelicaudiinae and Saltasaurinae (*sensu* Sereno[60]) outside these clades, in successively less inclusive clades of saltasaurid titanosaurs. Thus, even though the general recommendation is to use less aggressive k values for implied weighting analysis (k = 12[162,163]), we consider the topology recovered with k = 5 to be the preferred hypothesis.

All other European Saltasauridae are recovered within Opisthocoelicaudiinae in the k = 5 topology, with *Atsinganosaurus* more closely related to *Argentinosaurus*, *Puertasaurus*, *Mendozasaurus*, and *Patagotitan*. Note that this clade has a similar composition to a traditional Lognkosauria but does not include the internal specifier *Futalognkosaurus* (*sensu* Calvo et al.[164]). The rest of the European Saltasauridae (*Paluditiitan*, *Lohuecotitan*, *Ampelosaurus* and *Lirainosaurus*) are recovered in a clade together with *Opisthocoelicaudia*.

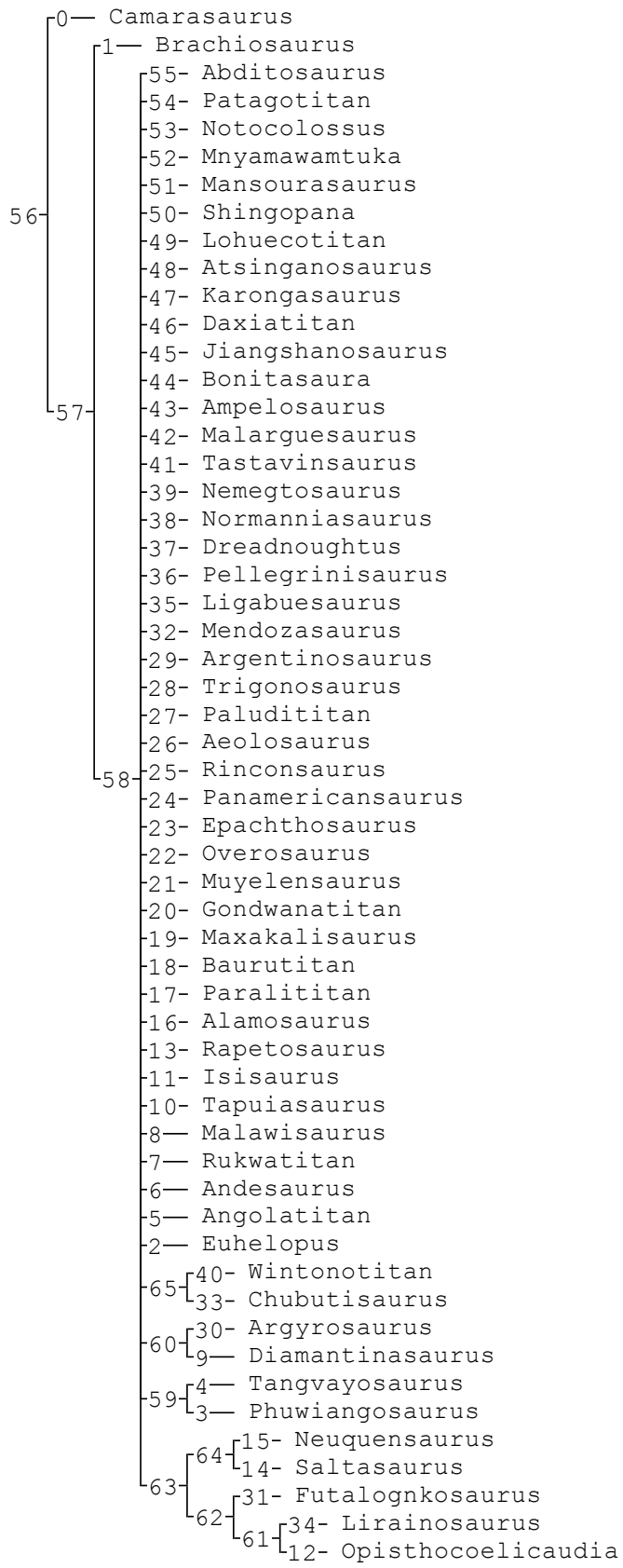

Supplementary Figure 35. Strict consensus of 7420 most parsimonious trees, recovered using equally weighted characters.

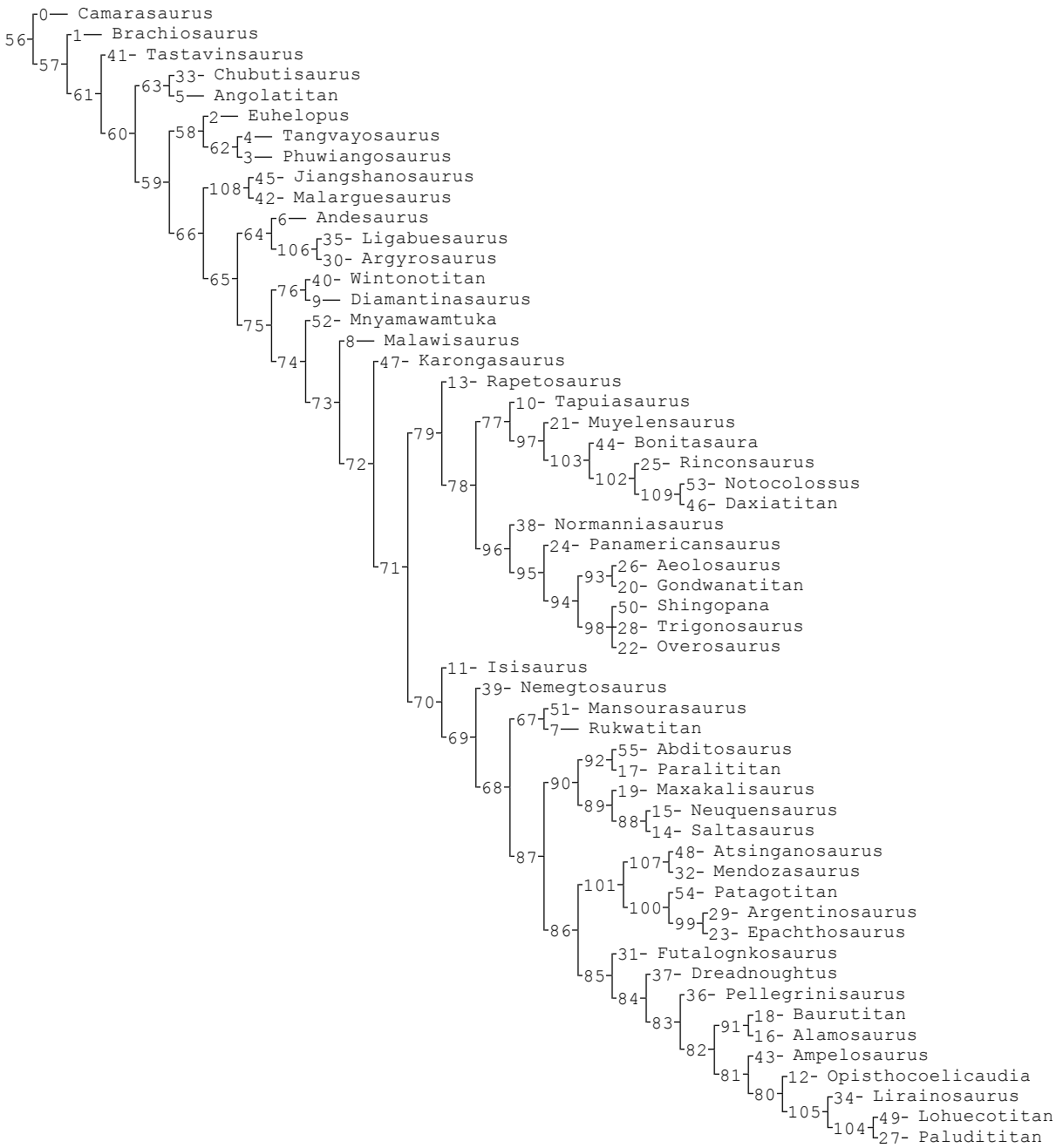

Supplementary Figure 36. Single most parsimonious tree recovered using extended implied weightings with a concavity constant k = 5.

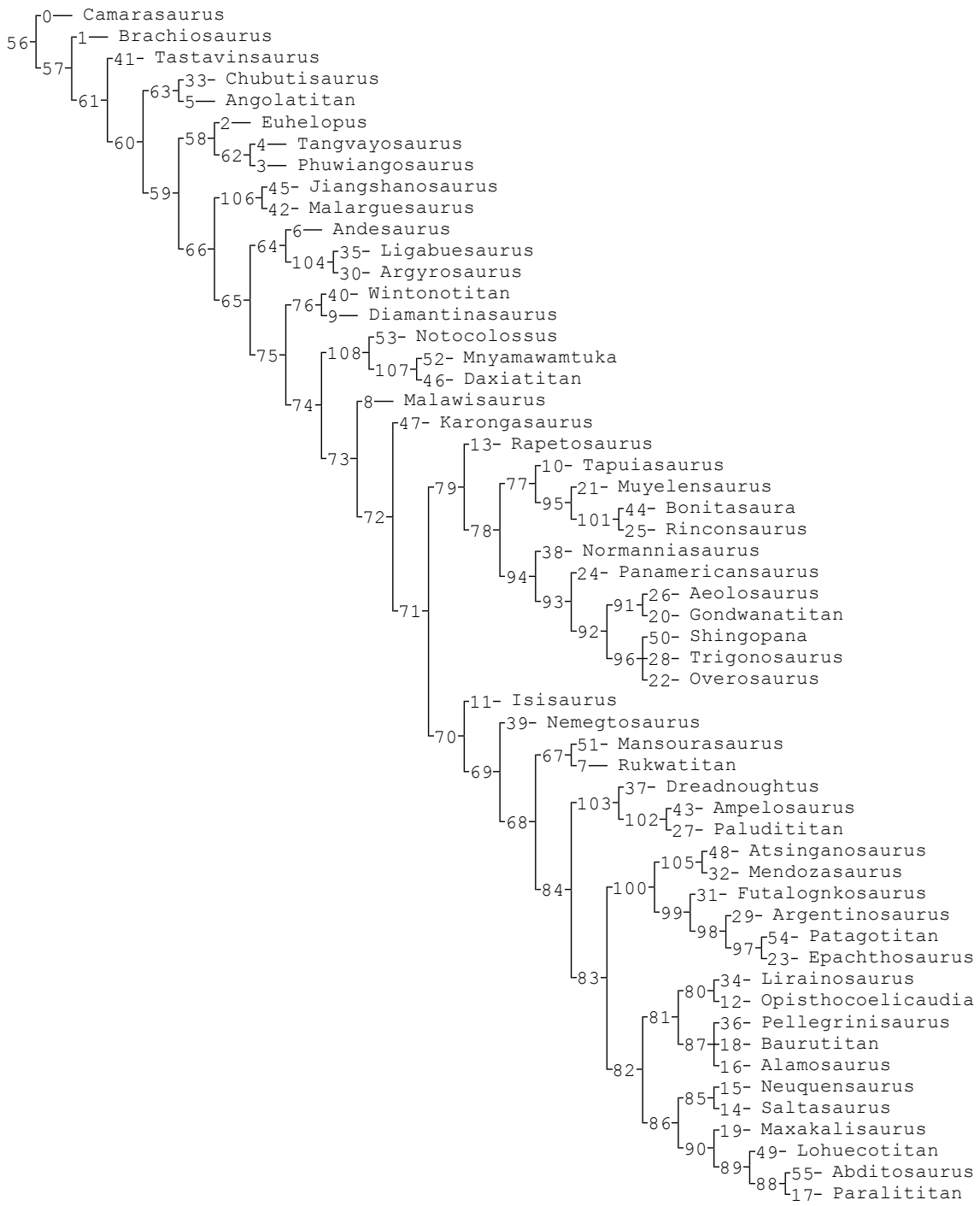

Supplementary Figure 37. Single most parsimonious tree recovered using extended implied weightings with a concavity constant k = 10.

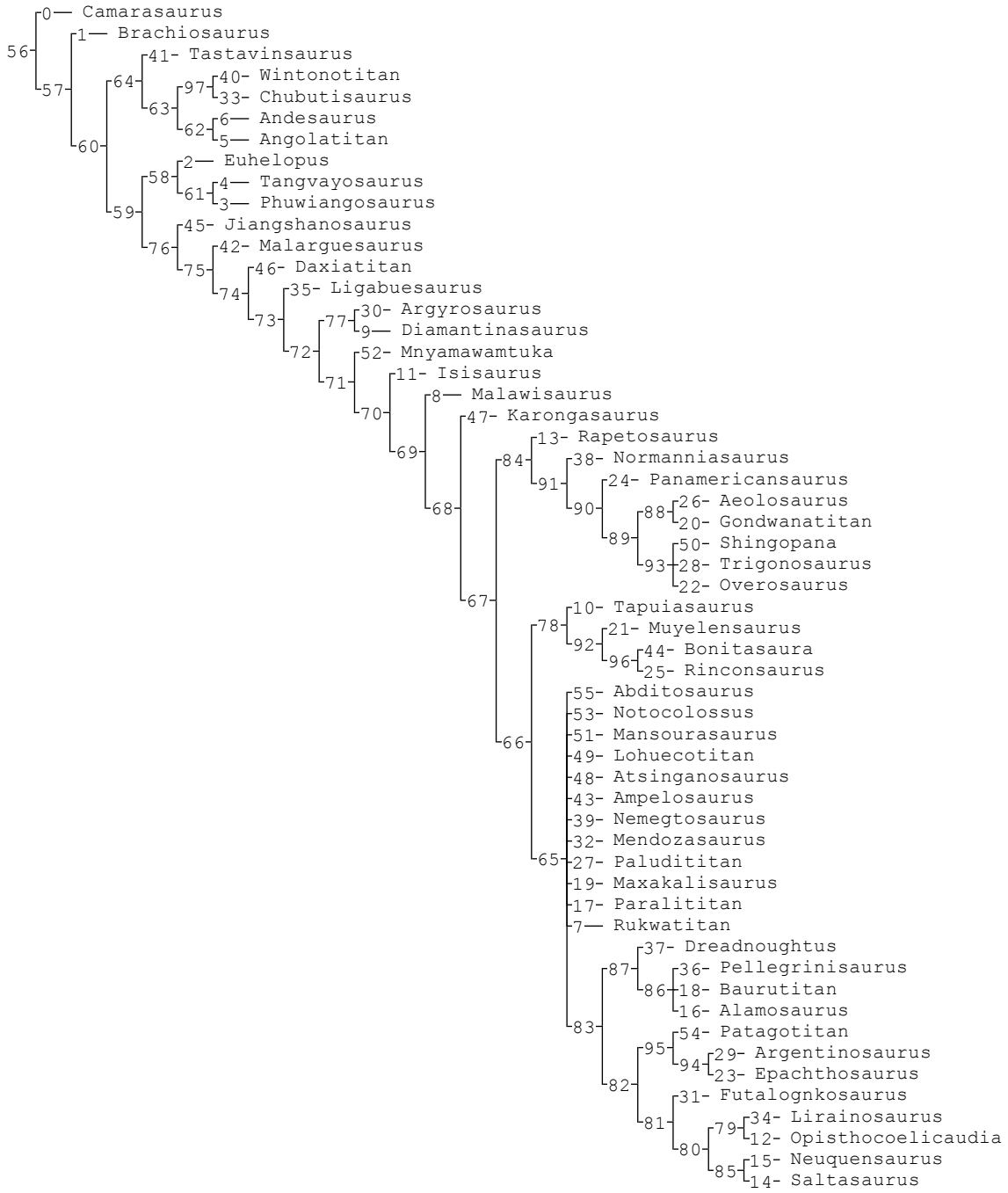

Supplementary Figure 38. Strict consensus of 16 most parsimonious trees recovered using extended implied weightings with a concavity constant k = 12.

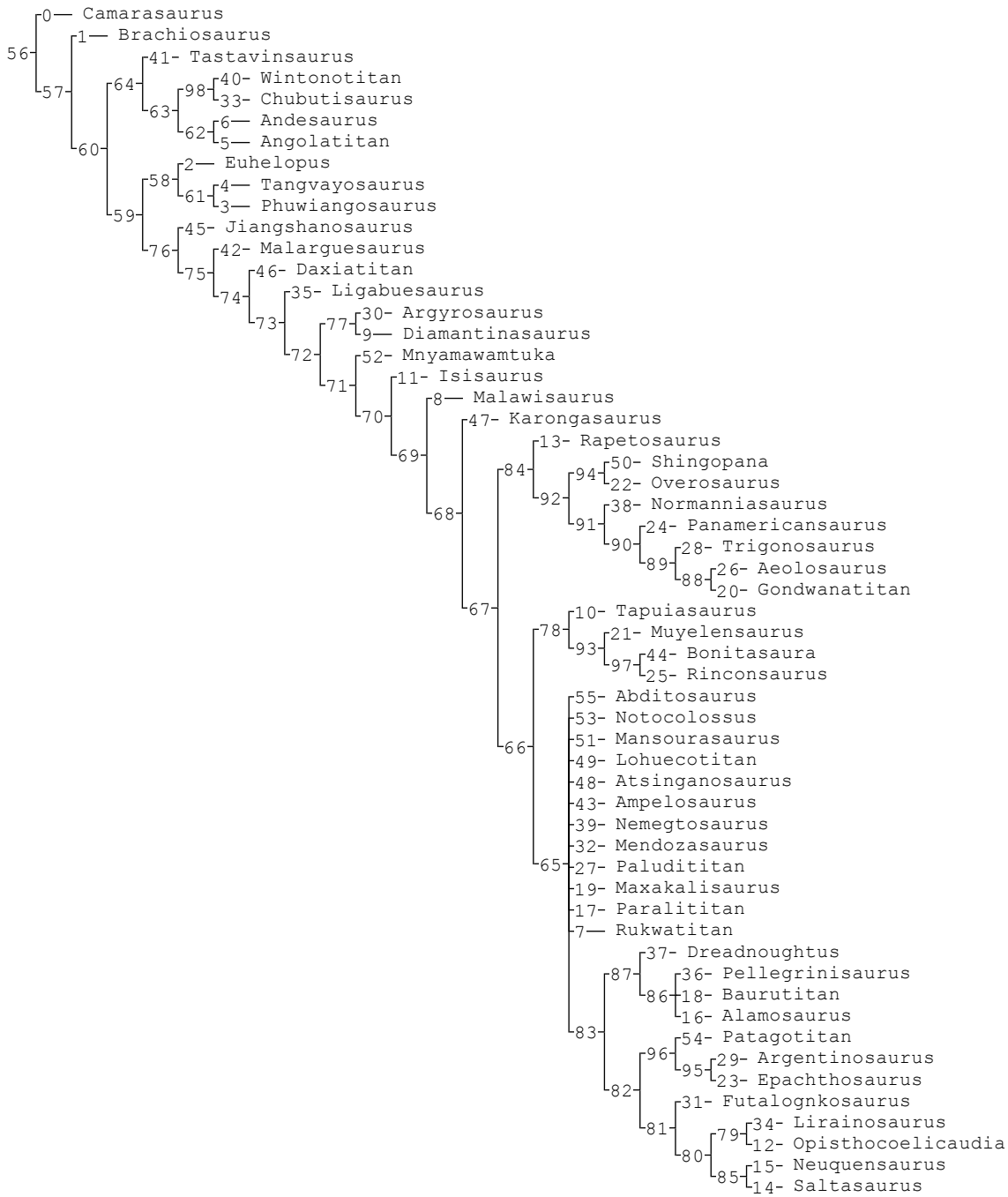

Supplementary Figure 39. Strict consensus of 16 most parsimonious trees recovered using extended implied weightings with a concavity constant k = 15.

The non-clock Bayesian analysis produced a maximum clade credibility tree (MCCT; Supplementary Figure 40), where *Abditosaurus* is again recovered within Saltasaurinae, most closely related to *Paralititan*, whereas all other European titanosaurs are recovered as members of Opisthocoelicaudiinae. *Atsinganosaurus* is recovered as a member of a very restricted Lognkosauria (*Futalognkosaurus* + (*Mendozasaurus* + *Atsinganosaurus*)), and the rest of the European saltasaurids are recovered in a clade with *Opisthocoelicaudia* and *Mansourasaurus*, which has a much more derived position than in the parsimony-based analysis, where it was recovered as a very basal saltasaurid.

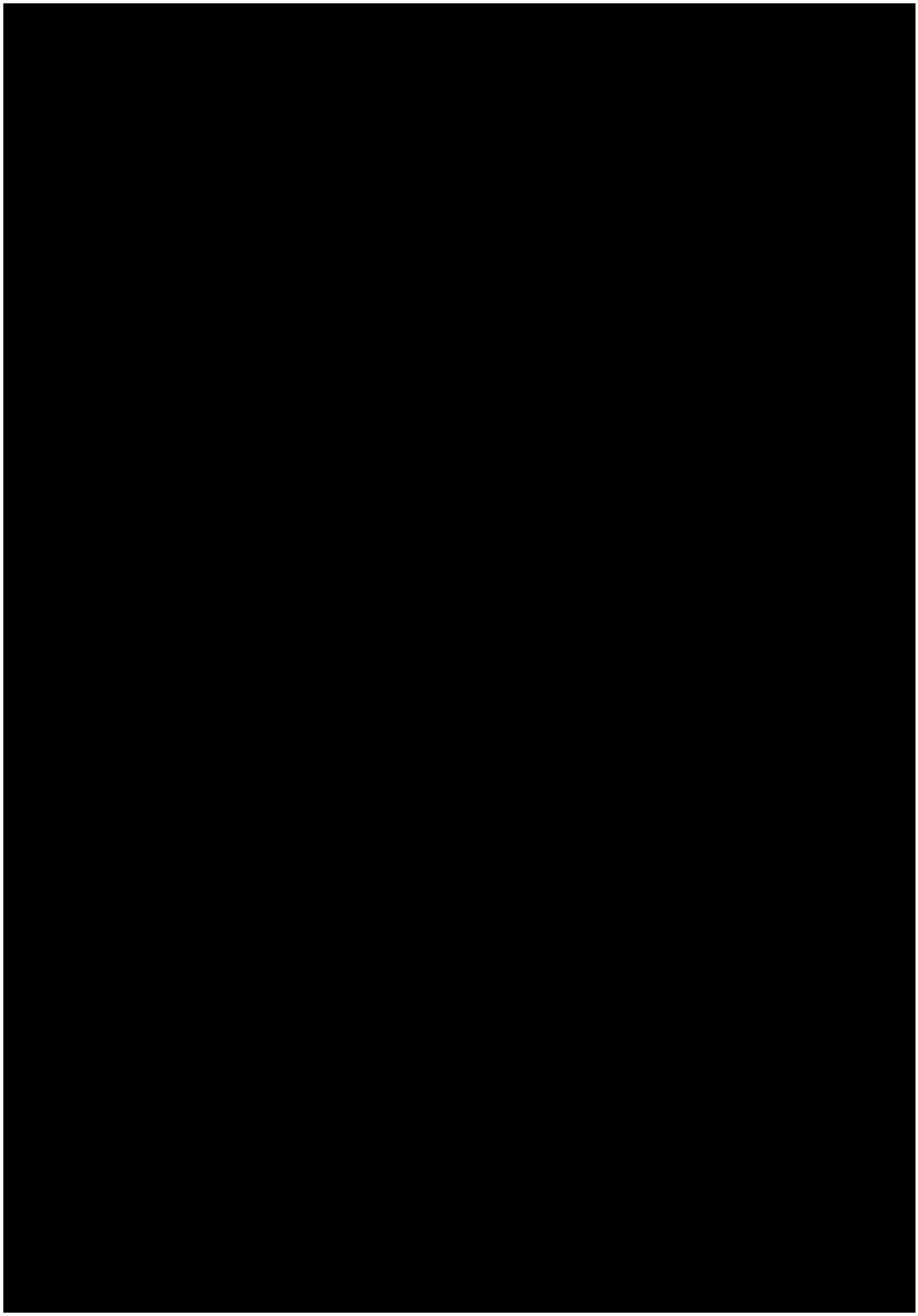

Supplementary Figure 40. Maximum clade credibility tree for the non-clock Bayesian analysis. Numbers in nodes represent posterior probabilities.

As in the non-clock Bayesian analysis and the k = 5 implied weighting analysis, the tip dating analysis resulted in a maximum clade credibility tree (Supplementary Figure 41) where the composition of Saltasauridae remains identical to that recovered by Gorscak and O'Connor[29], although the internal relationships among taxa are slightly different. Two monophyletic clades are recovered, with a more inclusive Lognkosauria (including *Rukwatitan*, *Notocolossus*, and *Epachtosaurus* in addition to the taxa recovered in the non-clock analysis) being sister to all other Saltasauridae. This clade is, in turn, divided into two mutually exclusive clades, Saltasaurinae and Opisthocoelicaudiinae, with *Abditosaurus* recovered as a saltasaurine, and all other European titanosaurs recovered as members of Opisthocoelicaudiinae, forming with *Mansourasaurus* the Afro-Eurasian clade of Sallam et al.[16], but also including the South American *Baurutitan*, *Dreadnoughtus*, and *Pellegrinisaurus* plus the North American *Alamosaurus*. Noteworthy is that *Lohuecotitan* appears more related to this Pan-American clade than to other Eurasian forms.

It is important to note that, due to the low level of completeness of most of the sauropod taxa included in the dataset, the general support for these topologies is very low, as it was in previous iterations of the dataset[16,29], with very low posterior probabilities, which only show support for Saltasaurini (the clade formed by *Saltasaurus*+*Neuquensaurus*). In any case, the same general topology is retrieved by three different methods –low k implied-weighting parsimony, non-clock Bayesian analysis, and tip dating analysis– with *Abditosaurus* recovered as a saltasaurine saltasaurid titanosaur, whereas all other European members of Titanosauria are recovered as opisthocoelicaudiine saltasaurid titanosaurs. We therefore consider

that this general topology is worthy of discussion, although it is likely to change as new data are added and better search algorithms are developed.

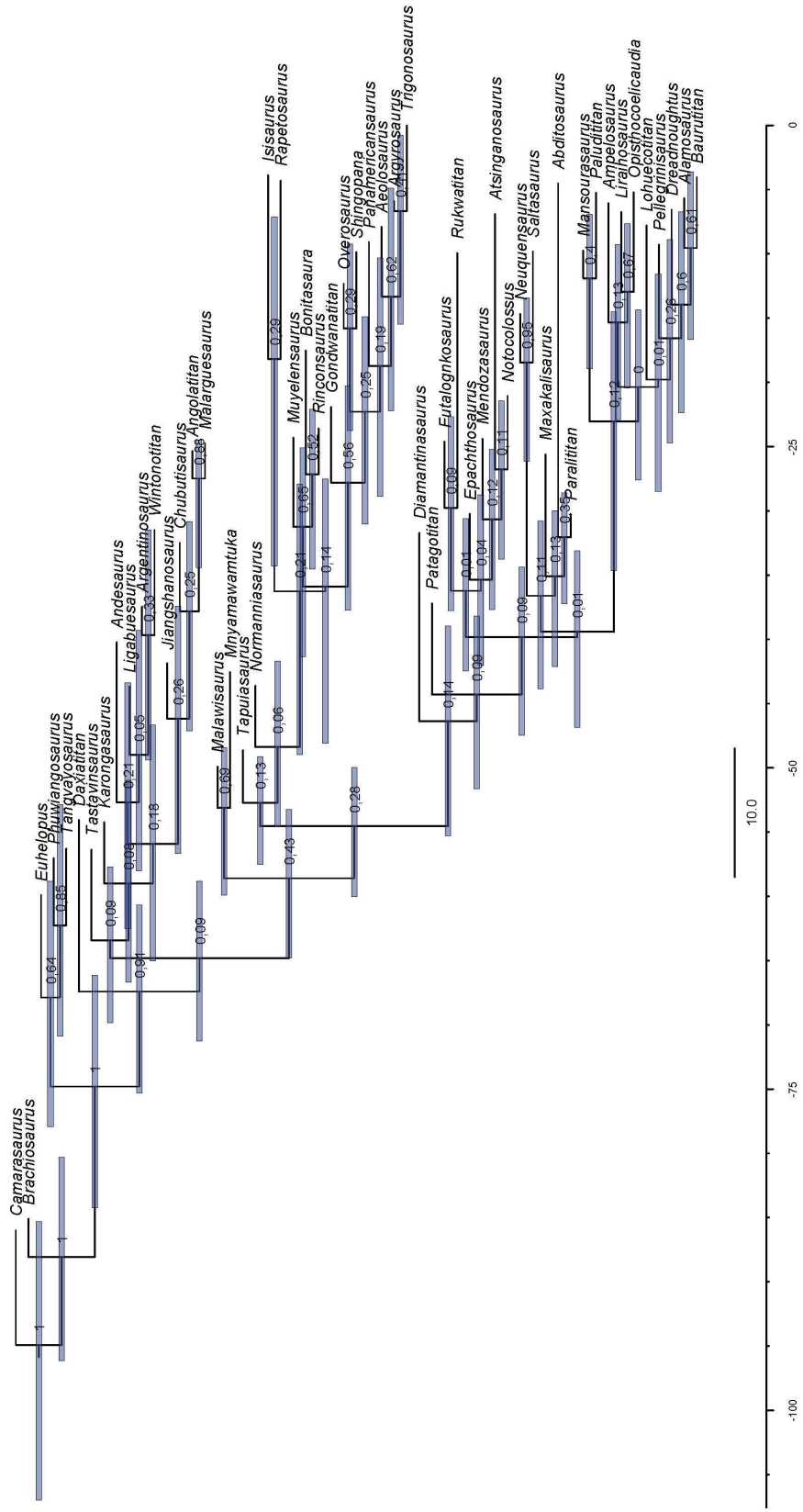

Supplementary Figure 41. Maximum clade credibility tree for the tip-dated Bayesian analysis. Numbers in nodes represent posterior probabilities. Blue bars represent % highest posterior density (HPD) for the timing of the divergence date at each node.

2.6 Palaeobiogeographic results and implications (Suppl. Fig. 42–65; Suppl. Table 3)

Both the starting and harsh multiplier datasets produced similar results under all analysed models (Suppl. Table 3). The most likely model of all 12 combinations is the DEC+J model under harsh multipliers. Nevertheless, this model has been questioned, especially when applied to datasets that include taxa restricted to a single area, as is the case for most fossil-based datasets. Until this ongoing debate is settled, we here prefer to restrict our discussion to the models that do not include founder speciation (the J parameter). The BAYAREALIKE model under starting distribution multipliers (Suppl. Figures 62–65) shows that the ancestors of saltasaurids had a pseudo-Gondwanan distribution (Europe + Africa+ South America) range during the Early Cretaceous (probably due to the lack of data from Antarctica and Oceania). Since then, most of the cladogenesis has resulted in speciation by vicariance, except for *Abditosaurus*, which originated in Africa and later dispersed to Europe. Coinciding with the final break-up of northern South America and Africa (ca. 100 Ma[165–167]), the three main clades (Lognkosauria, Saltasaurinae and Opisthocoelicaudiinae) are present by vicariance in all three continents. Relevant to this work, most European taxa are members of Opisthocoelicaudiinae, and according to the BAYAREALIKE analysis have an ancestral range of Europe, Africa, and South America from the beginning of the Cenomanian (100.5 Ma) to the middle Campanian (80.5 Ma), suggesting that a connection remained available at least for these taxa. In this regard, the vicariance scenario after the final breakup of northern South America and Africa at ca. 100 Ma would constrain the connection not later than the early Cenomanian and imply a Gondwanan distribution of the clade[168], as well as the presence of related titanosaur taxa in Africa and Europe for most of

the Late Cretaceous. *Atsinganosaurus* and *Rukwatitan* are the only representative of Lognkosauria outside of South America, but their Campanian age points towards the presence of related forms yet to be discovered in the early Late Cretaceous of Africa. A late biogeographical reconnection between the three landmasses during the Campanian would be favoured by the hypothesized trans-Atlantic connection of South America and Africa ('Atlantogea' model[169]).

Finally, Saltasaurinae is divided in two clades: Saltasaurini, restricted to South America, and an African clade formed by *Paralititan* and *Abditosaurus*. Apparently, the lack of record of the latter clade from the Turonian to the Maastrichtian does not allow us to precisely determine when *Abditosaurus* or its ancestors reached Europe. However, the co-occurrence of *Abditosaurus* with Gondwanan (fusioolithid) oospecies in the lower Maastrichtian of Europe (and a coeval record in northern Africa[157,158]) dates the arrival of the clade to this continent (see 'oospecies chronostratigraphy' section).

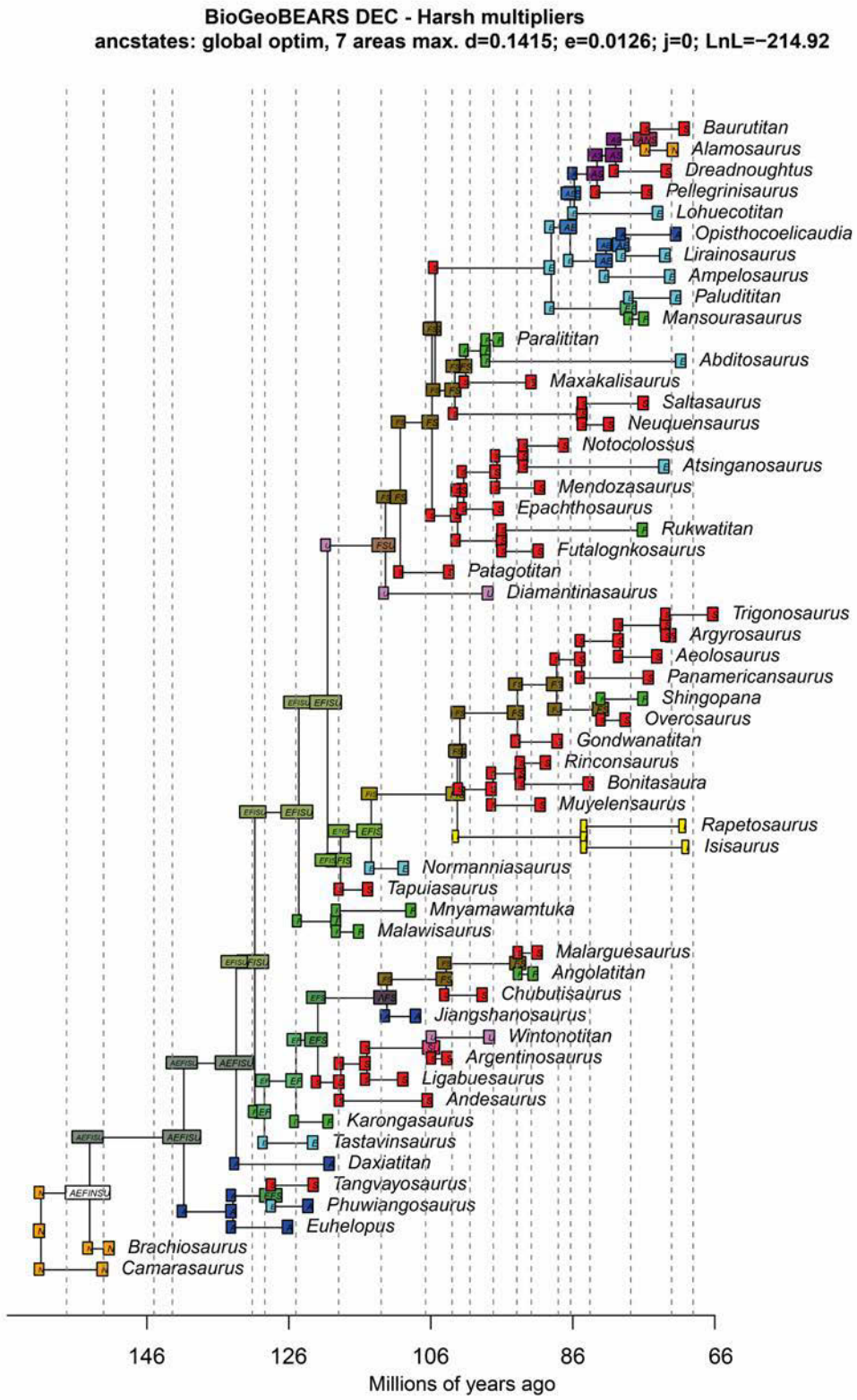

Supplementary Figure 42. **DEC model results on the tip-dated Bayesian phylogenetic analysis using 'harsh' distribution multipliers.** Node boxes indicate most likely ancestral range reconstruction. A: Asia, F: Africa, E: Europe, N: North America, S: South America, I: India.

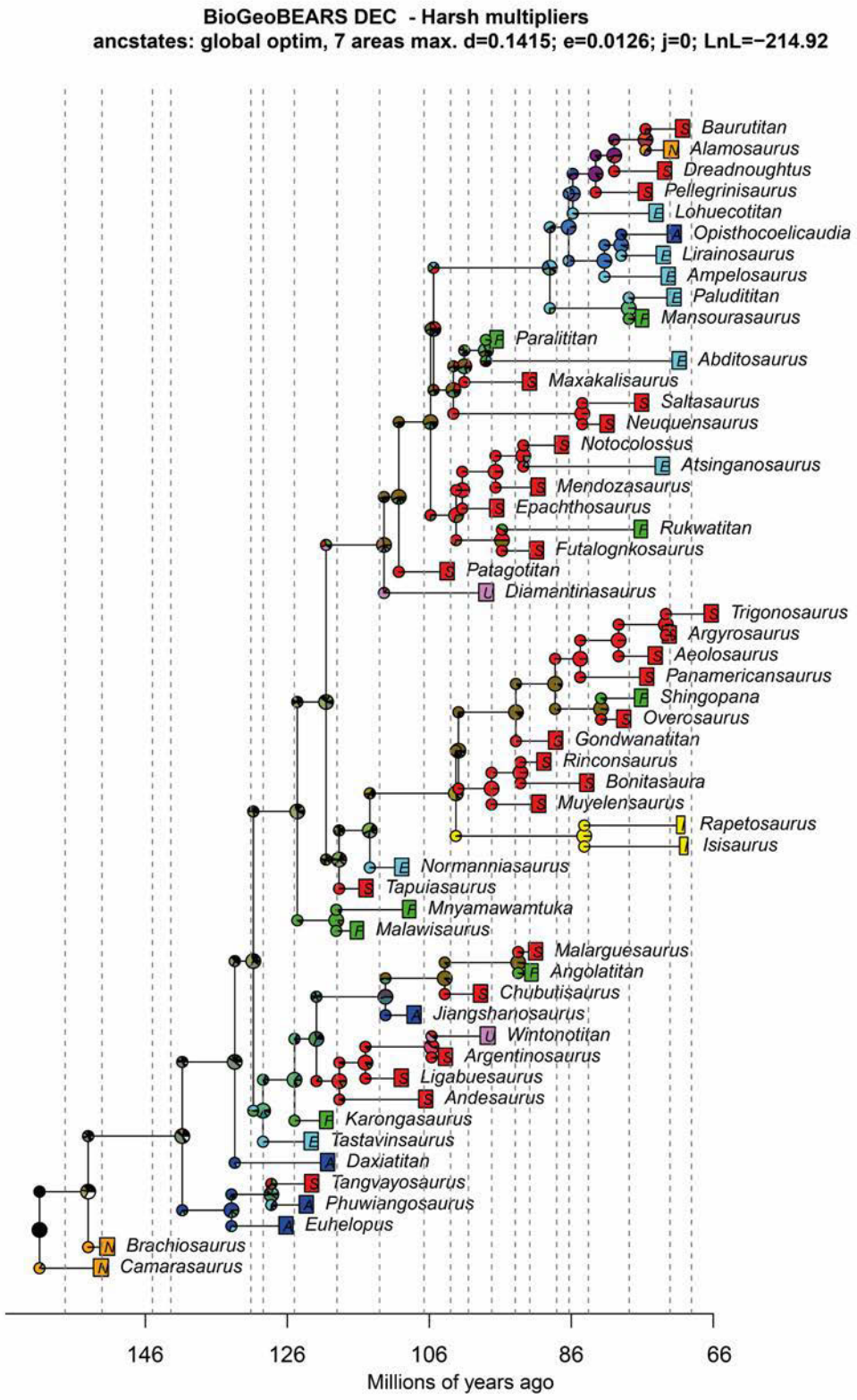

Supplementary Figure 43. **DEC model results on the tip-dated Bayesian phylogenetic analysis using 'harsh' distribution multipliers.** Pie charts indicate relative support for ancestral area reconstruction; branch tips indicate taxon area distribution. A: Asia, F: Africa, E: Europe, N: North America, S: South America, I: India. For multiple area ranges colour coding, see Suppl Figure 42.

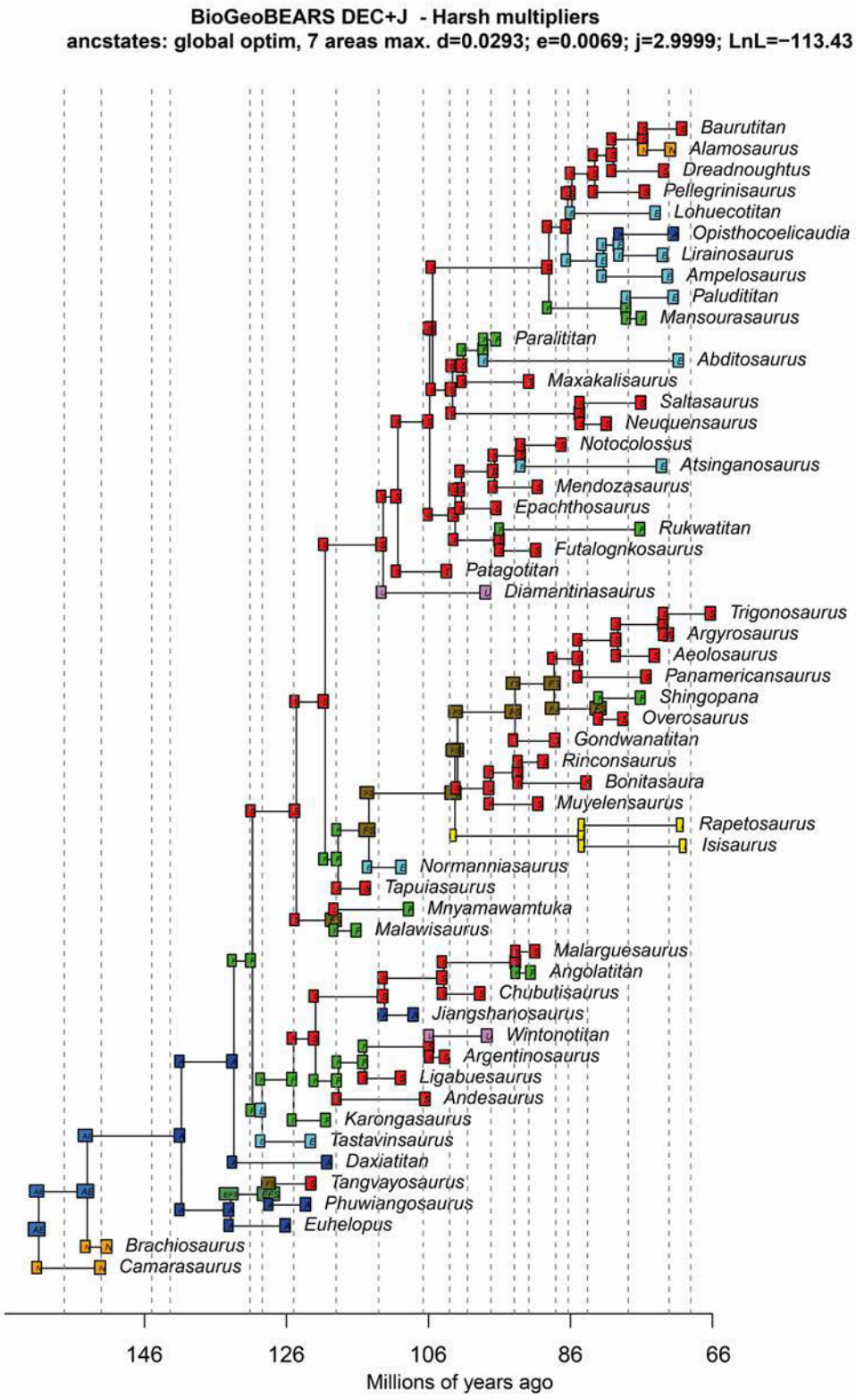

Supplementary Figure 44. **DEC+J model results on the tip-dated Bayesian phylogenetic analysis using 'harsh' distribution multipliers.** Node boxes indicate most likely ancestral range reconstruction. A: Asia, F: Africa, E: Europe, N: North America, S: South America, I: India.

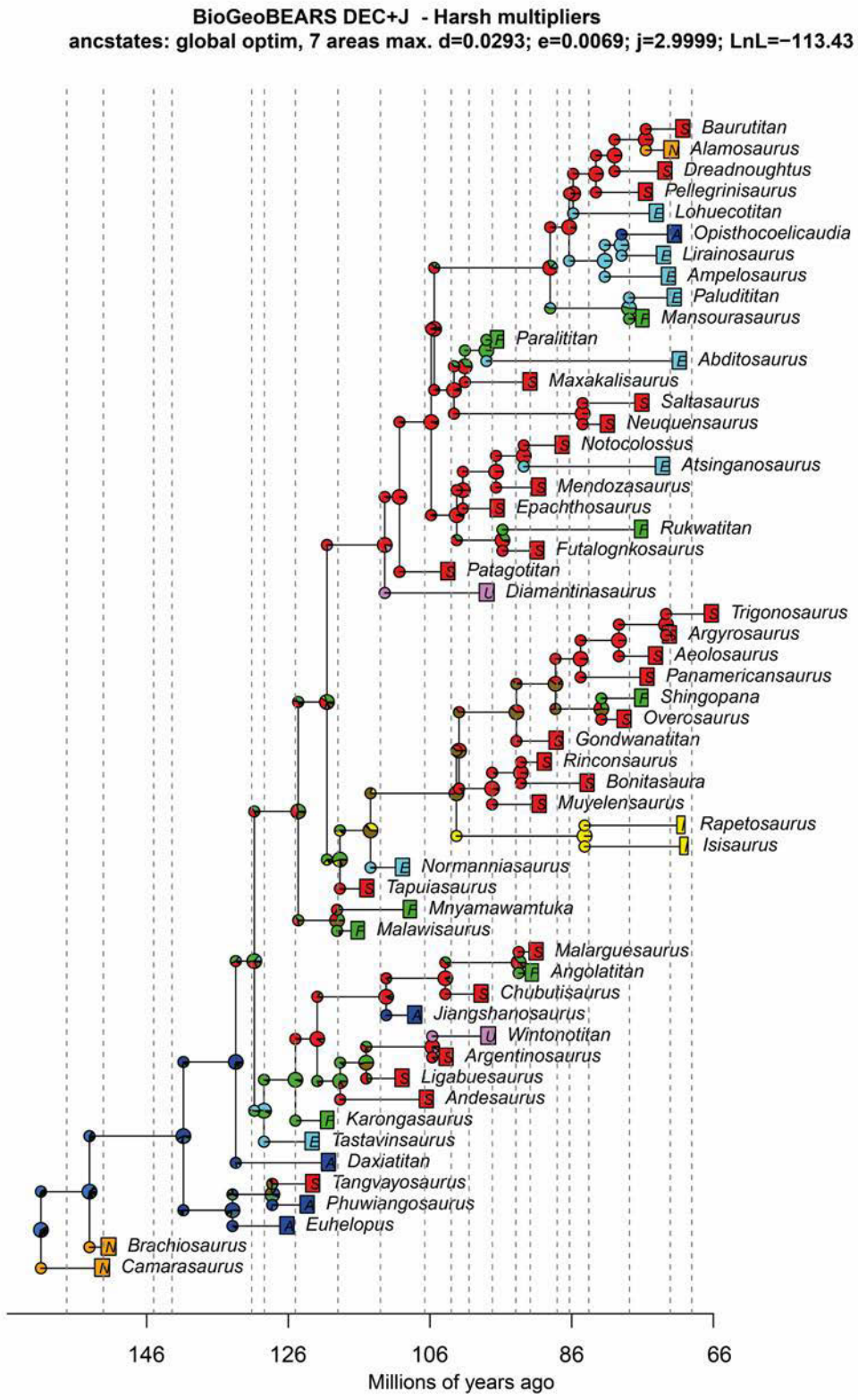

Supplementary Figure 45. **DEC+J model results on the tip-dated Bayesian phylogenetic analysis using 'harsh' distribution multipliers.** Pie charts indicate relative support for ancestral area reconstruction; branch tips indicate taxon area distribution. A: Asia, F: Africa, E: Europe, N: North America, S: South America, I: India. For multiple area ranges color coding, see Suppl. Figure 44.

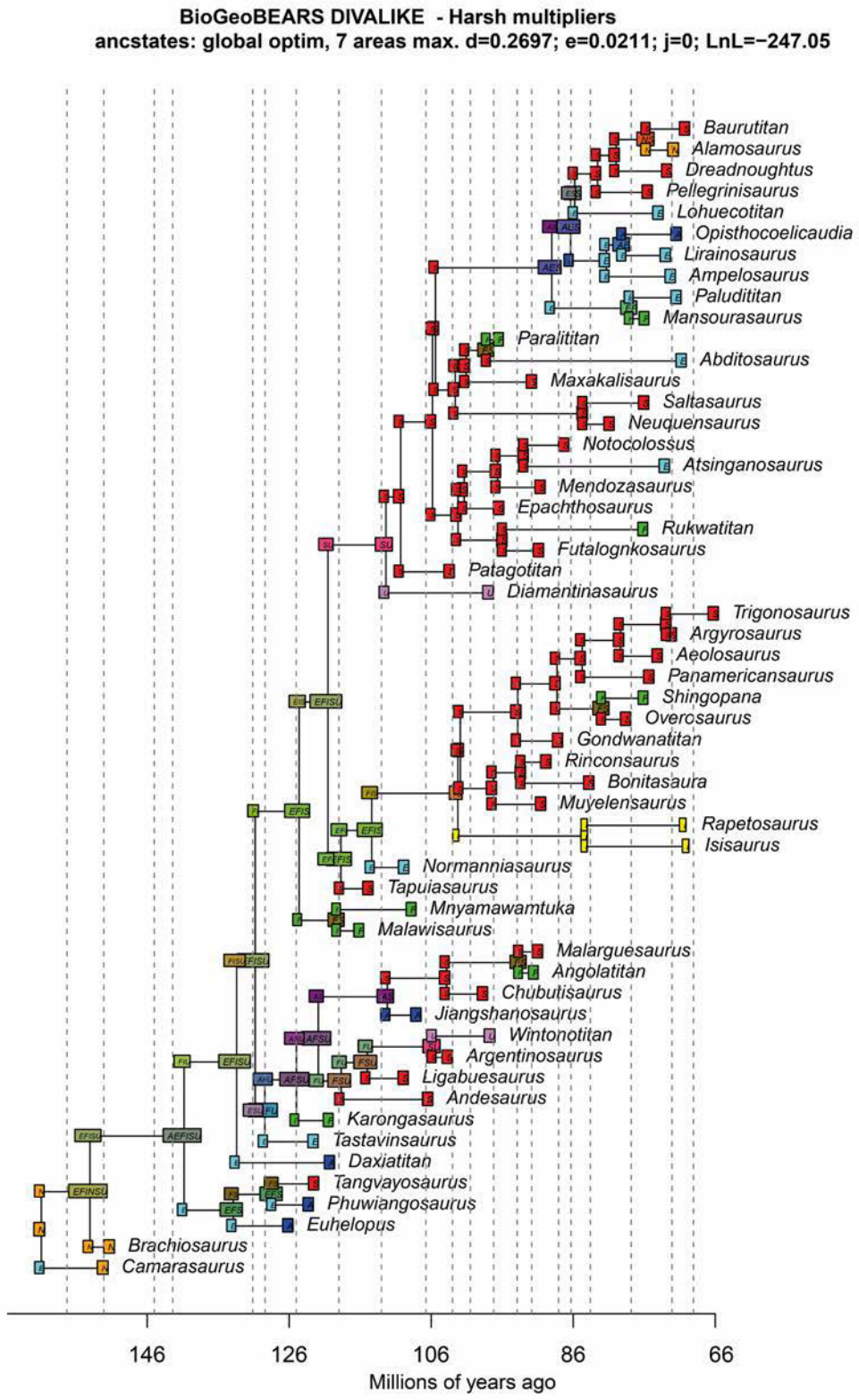

Supplementary Figure 46. **DIVALIKE model results on the tip-dated Bayesian phylogenetic analysis using harsh' distribution multipliers.** Node boxes indicate most likely ancestral range reconstruction. A: Asia, F: Africa, E: Europe, N: North America, S: South America, I: India.

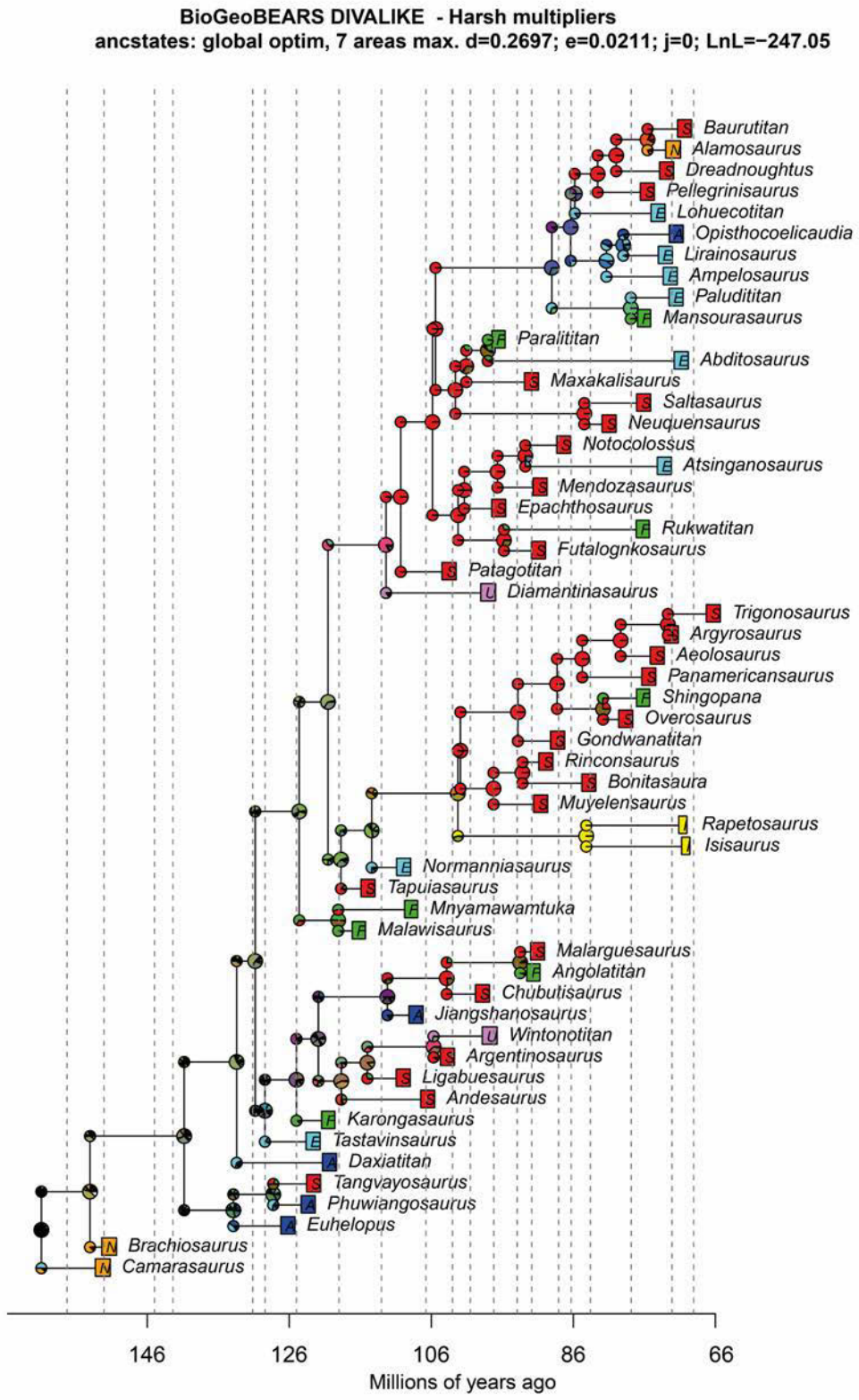

Supplementary Figure 47. **DIVALIKE model results on the tip-dated Bayesian phylogenetic analysis using 'harsh' distribution multipliers.** Pie charts indicate relative support for ancestral area reconstruction; branch tips indicate taxon area distribution. A: Asia, F: Africa, E: Europe, N: North America, S: South America, I: India. For multiple area ranges colour coding, see Suppl. Figure 46.

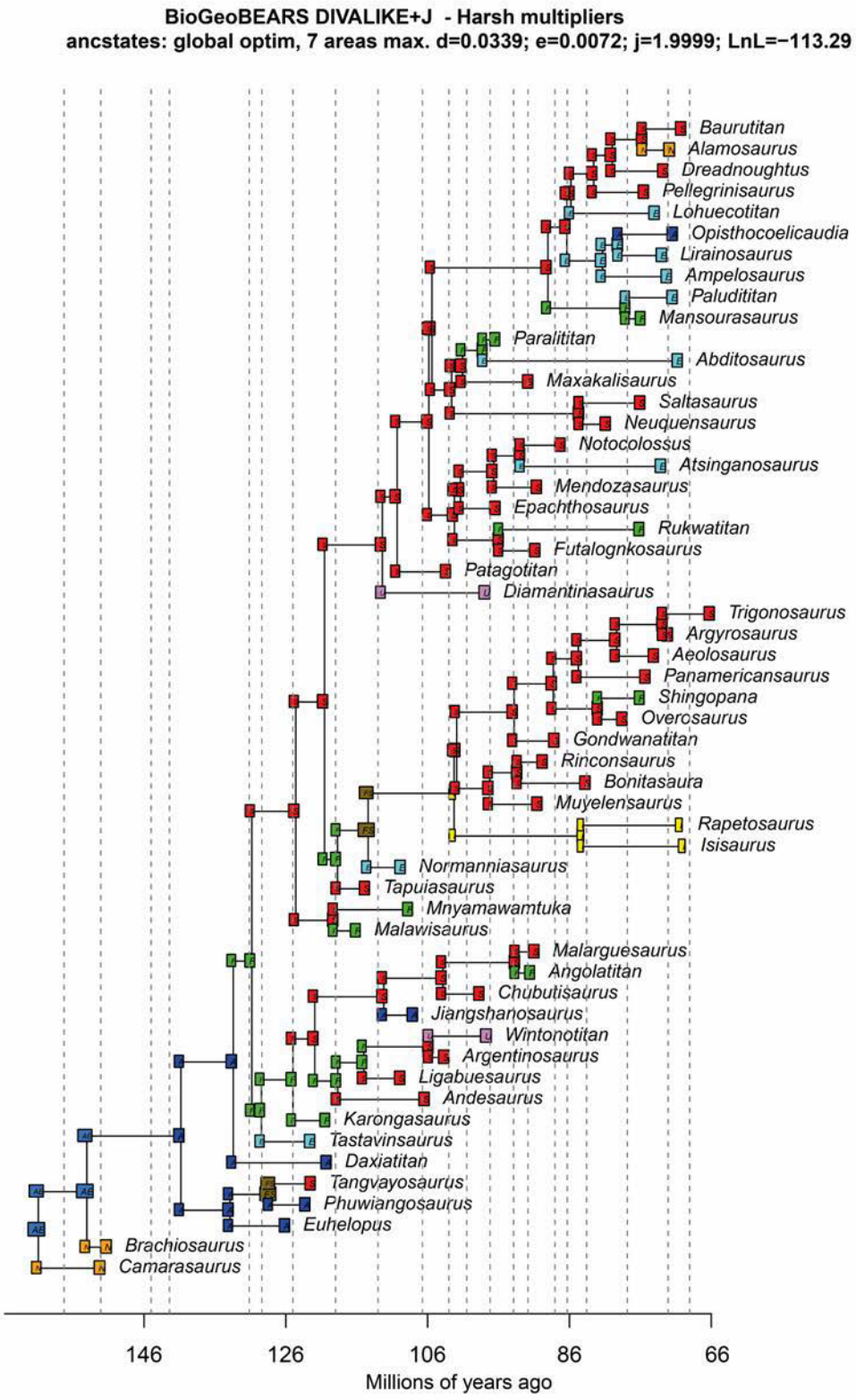

Supplementary Figure 48. **DIVALIKE+J model results on the tip-dated Bayesian phylogenetic analysis using 'harsh' distribution multipliers.** Node boxes indicate most likely ancestral range reconstruction. A: Asia, F: Africa, E: Europe, N: North America, S: South America, I: India.

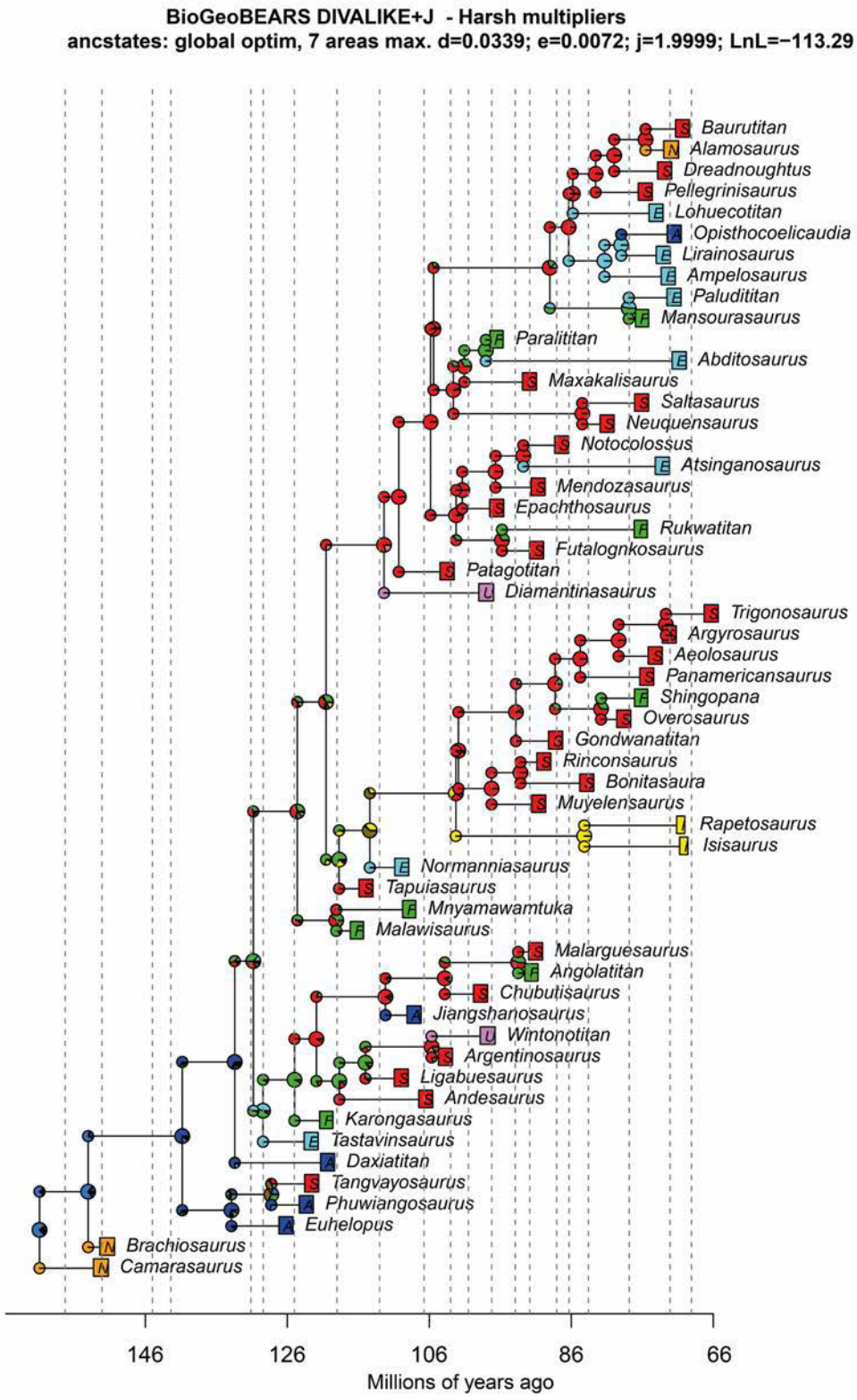

Supplementary Figure 49. **DIVALIKE+J model results on the tip-dated Bayesian phylogenetic analysis using 'harsh' distribution multipliers.** Pie charts indicate relative support for ancestral area reconstruction; branch tips indicate taxon area distribution. A: Asia, F: Africa, E: Europe, N: North America, S: South America, I: India. For multiple area ranges colour coding, see Suppl. Figure 48.

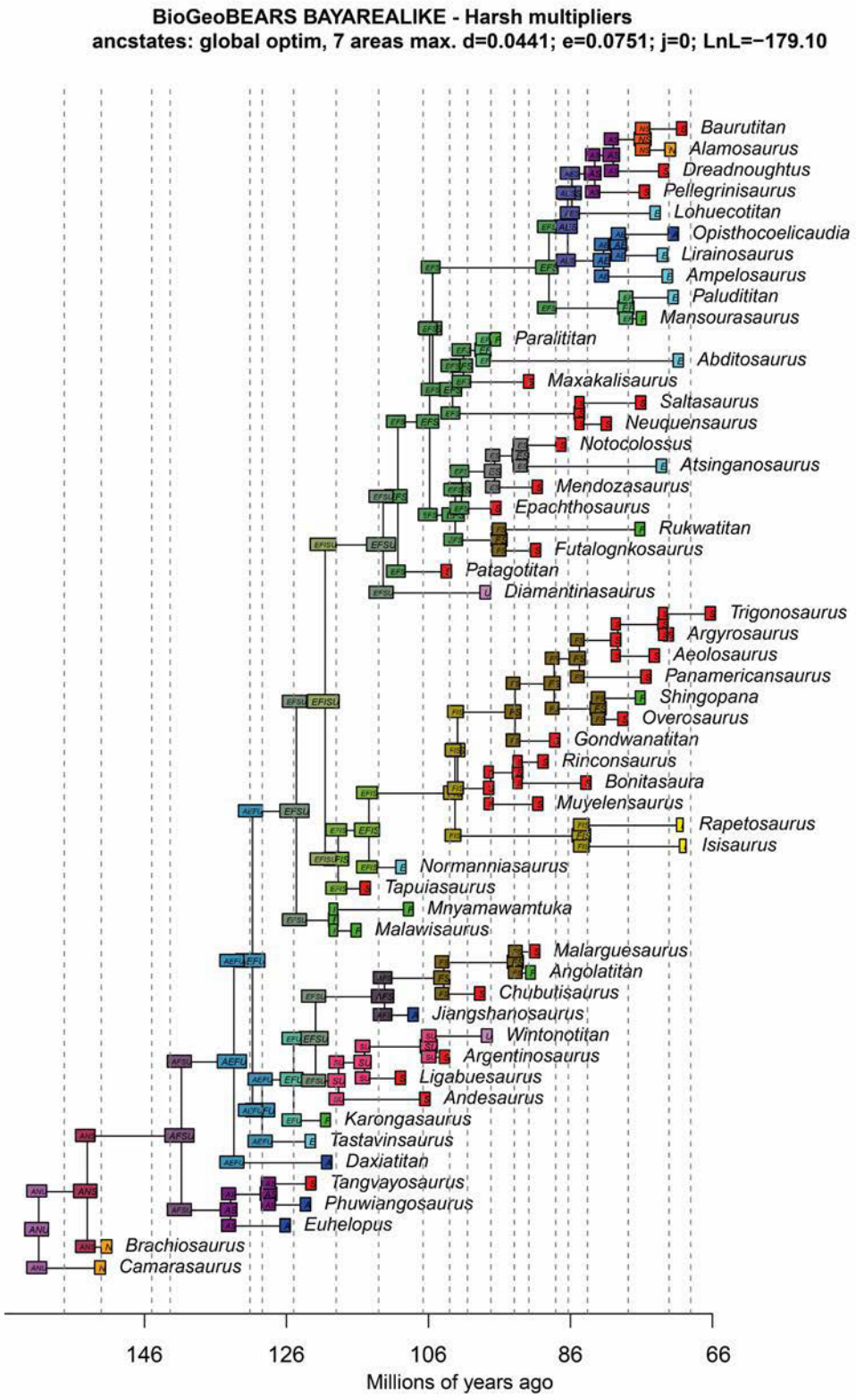

Supplementary Figure 50. **BAYAREALIKE model results on the tip-dated Bayesian phylogenetic analysis using 'harsh' distribution multipliers.** Node boxes indicate most likely ancestral range reconstruction. A: Asia, F: Africa, E: Europe, N: North America, S: South America, I: India.

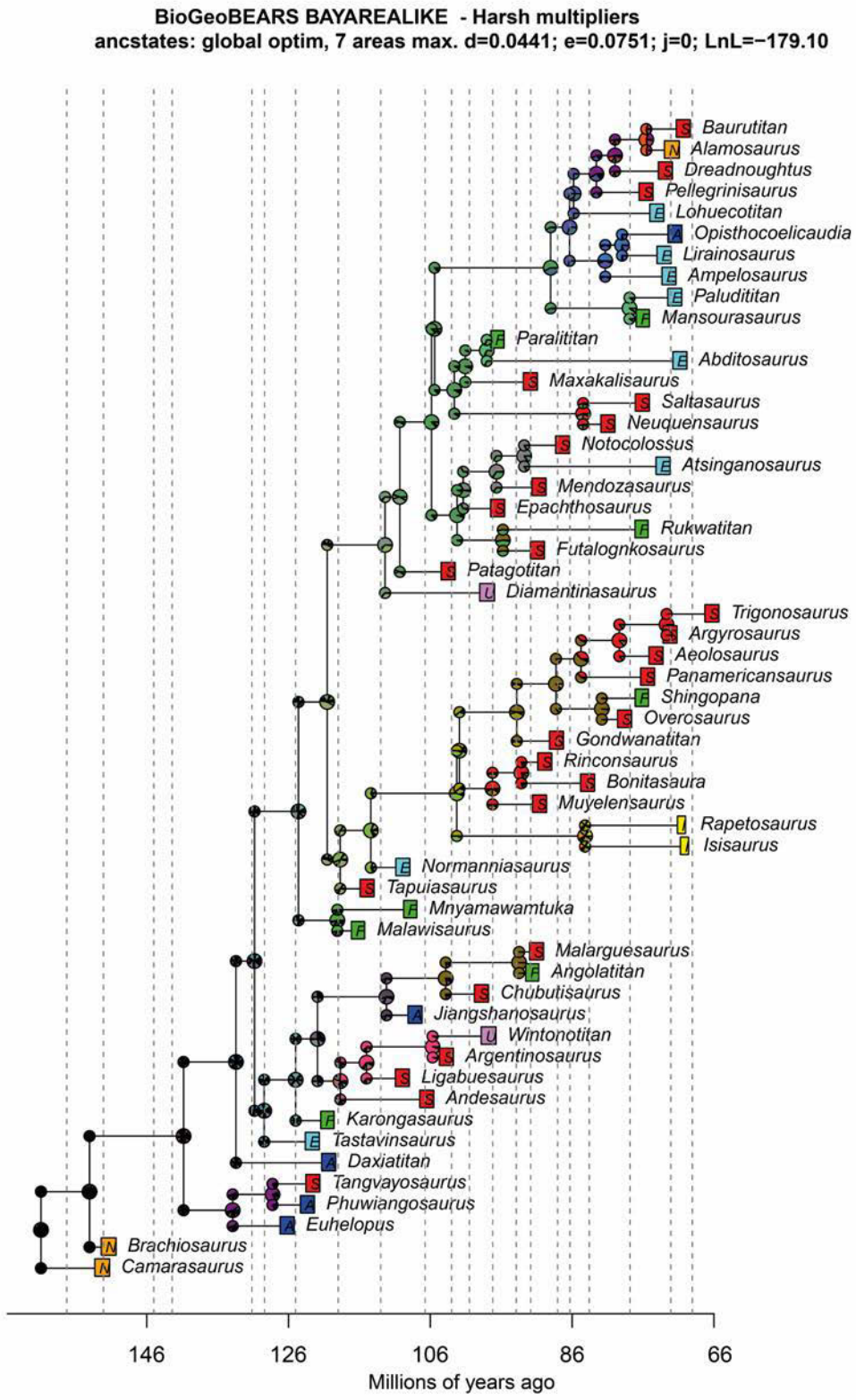

Supplementary Figure 51. **BAYAREALIKE model results on the tip-dated Bayesian phylogenetic analysis using 'harsh' distribution multipliers.** Pie charts indicate relative support for ancestral area reconstruction; branch tips indicate taxon area distribution. A: Asia, F: Africa, E: Europe, N: North America, S: South America, I: India. For multiple area ranges colour coding, see Suppl. Figure 50.

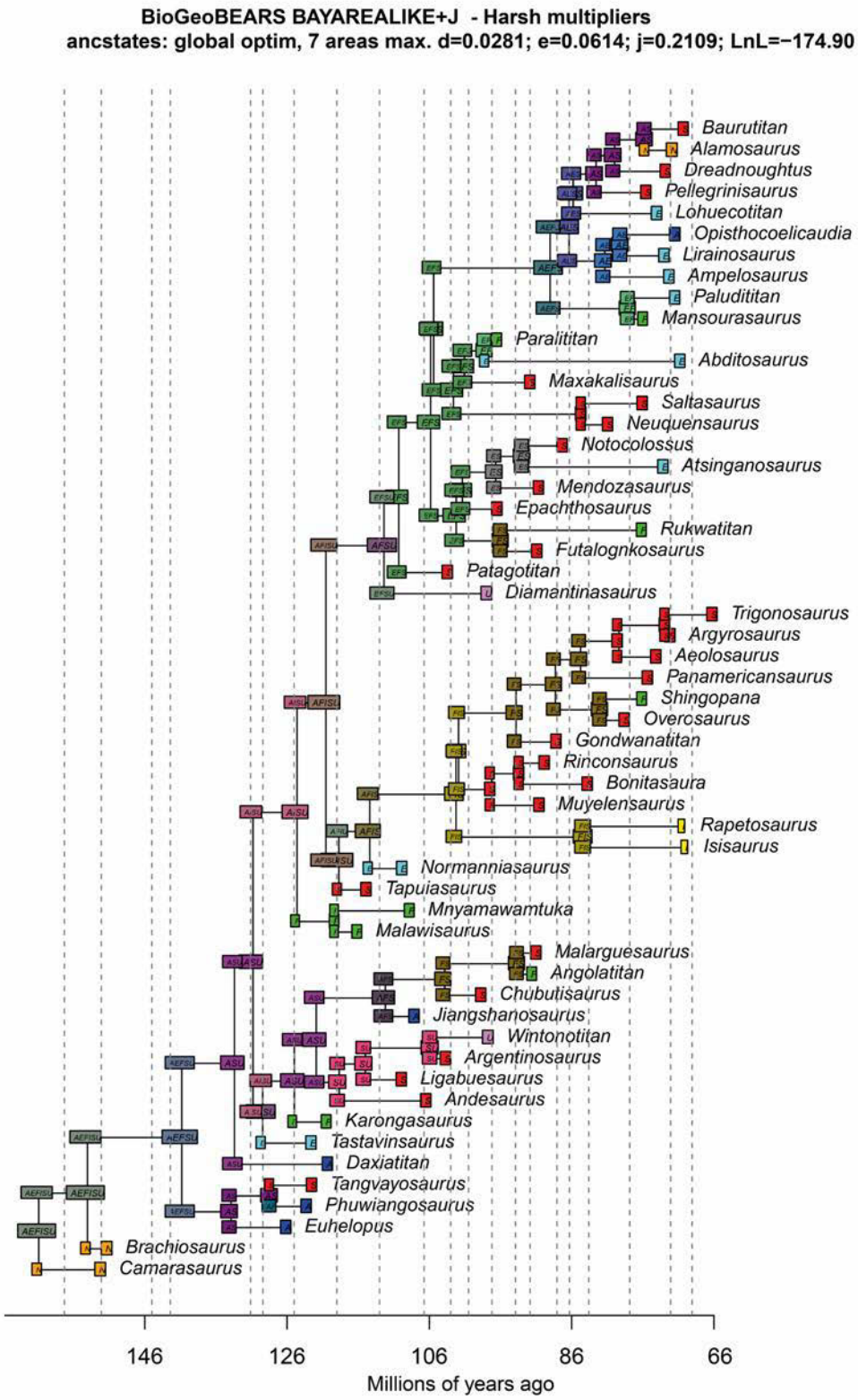

Supplementary Figure 52. **BAYAREALIKE+J model results on the tip-dated Bayesian phylogenetic analysis using 'harsh' distribution multipliers.** Node boxes indicate most likely ancestral range reconstruction. A: Asia, F: Africa, E: Europe, N: North America, S: South America, I: India.

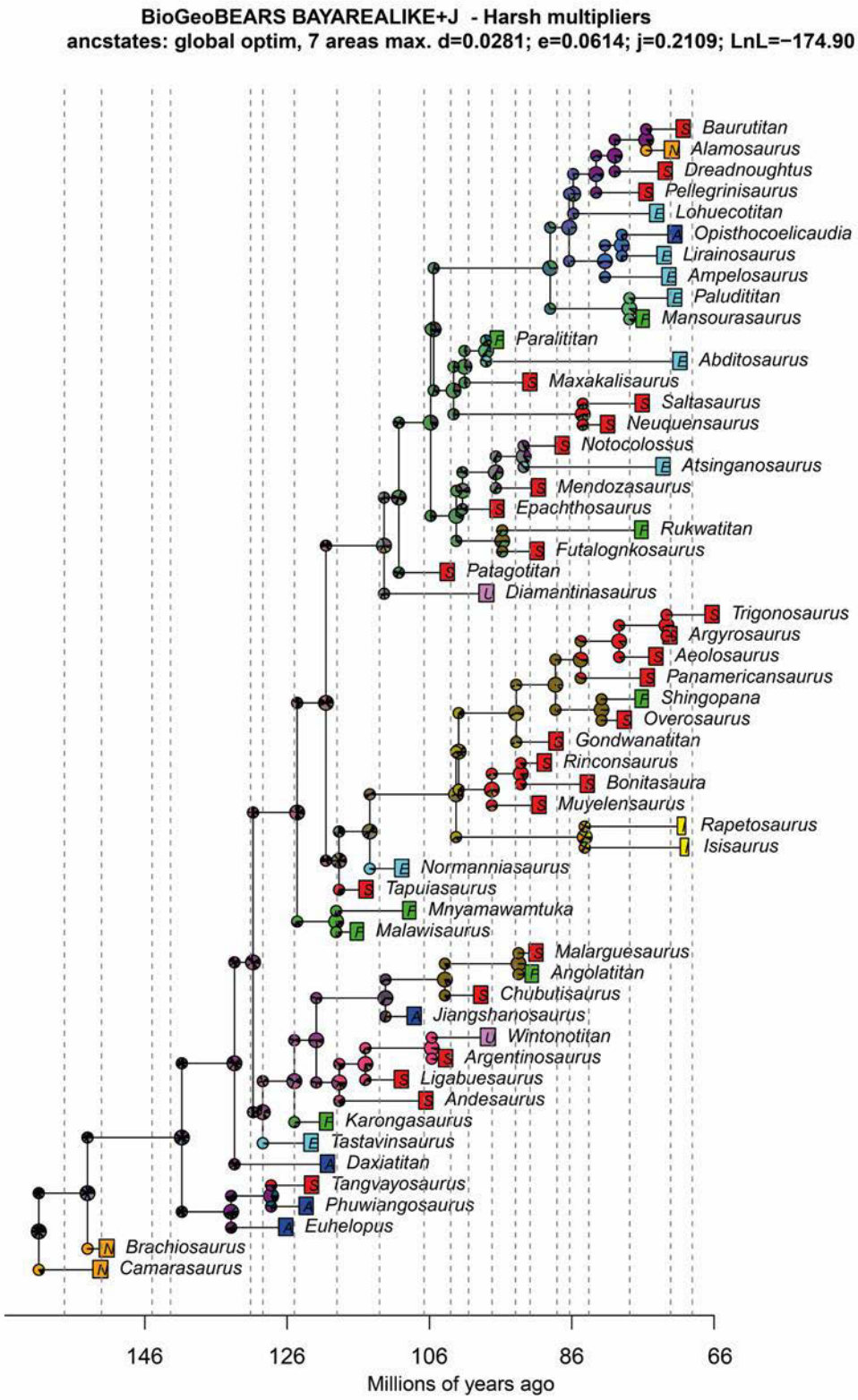

Supplementary Figure 53. **BAYAREALIKE+J model results on the tip-dated Bayesian phylogenetic analysis using 'harsh' distribution multipliers.** Pie charts indicate relative support for ancestral area reconstruction; branch tips indicate taxon area distribution. A: Asia, F: Africa, E: Europe, N: North America, S: South America, I: India. For multiple area ranges colour coding, see Suppl. Figure 52.

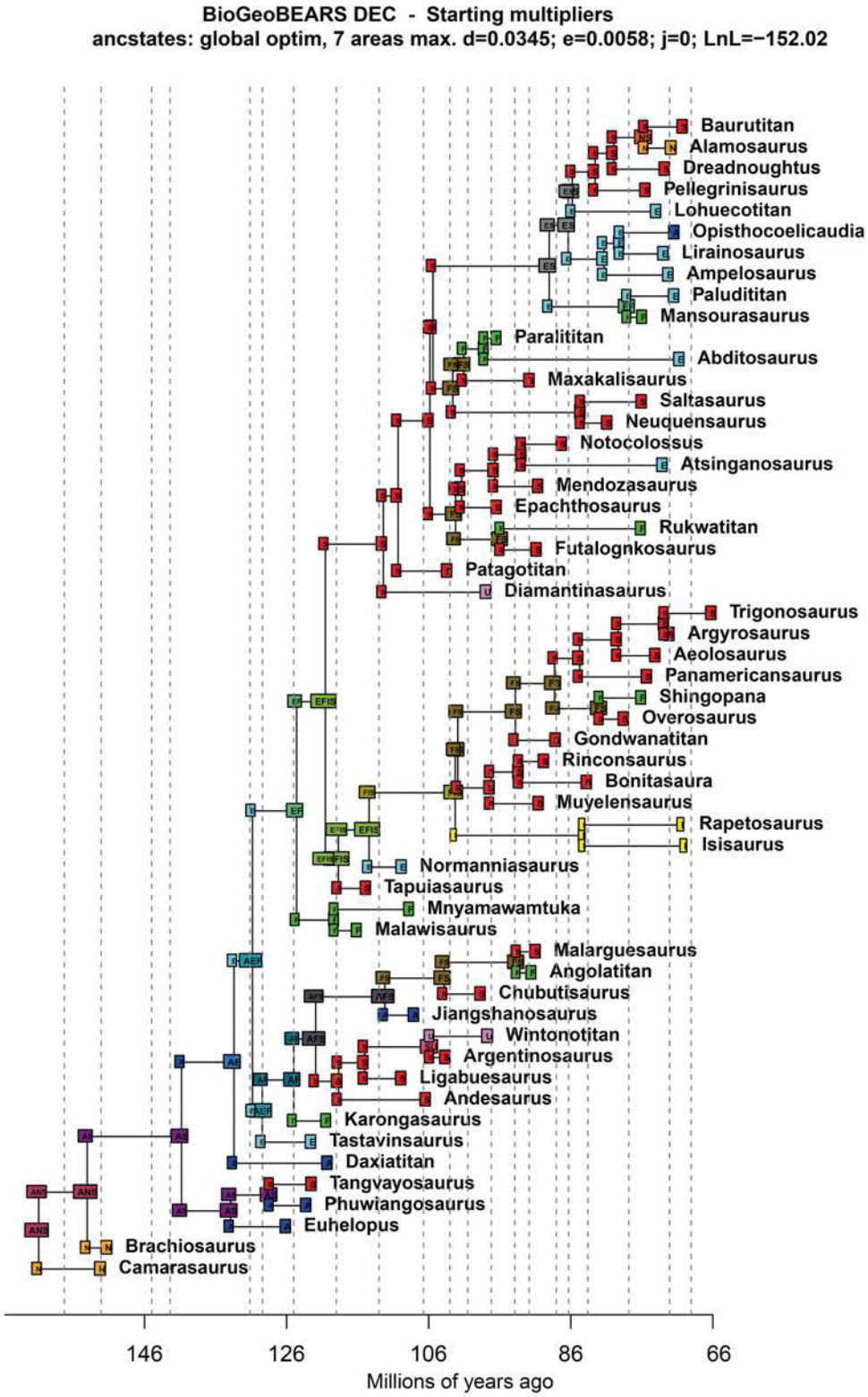

Supplementary Figure 54. **DEC model results on the tip-dated Bayesian phylogenetic analysis using 'starting' distribution multipliers.** Node boxes indicate most likely ancestral range reconstruction. A: Asia, F: Africa, E: Europe, N: North America, S: South America, I: India.

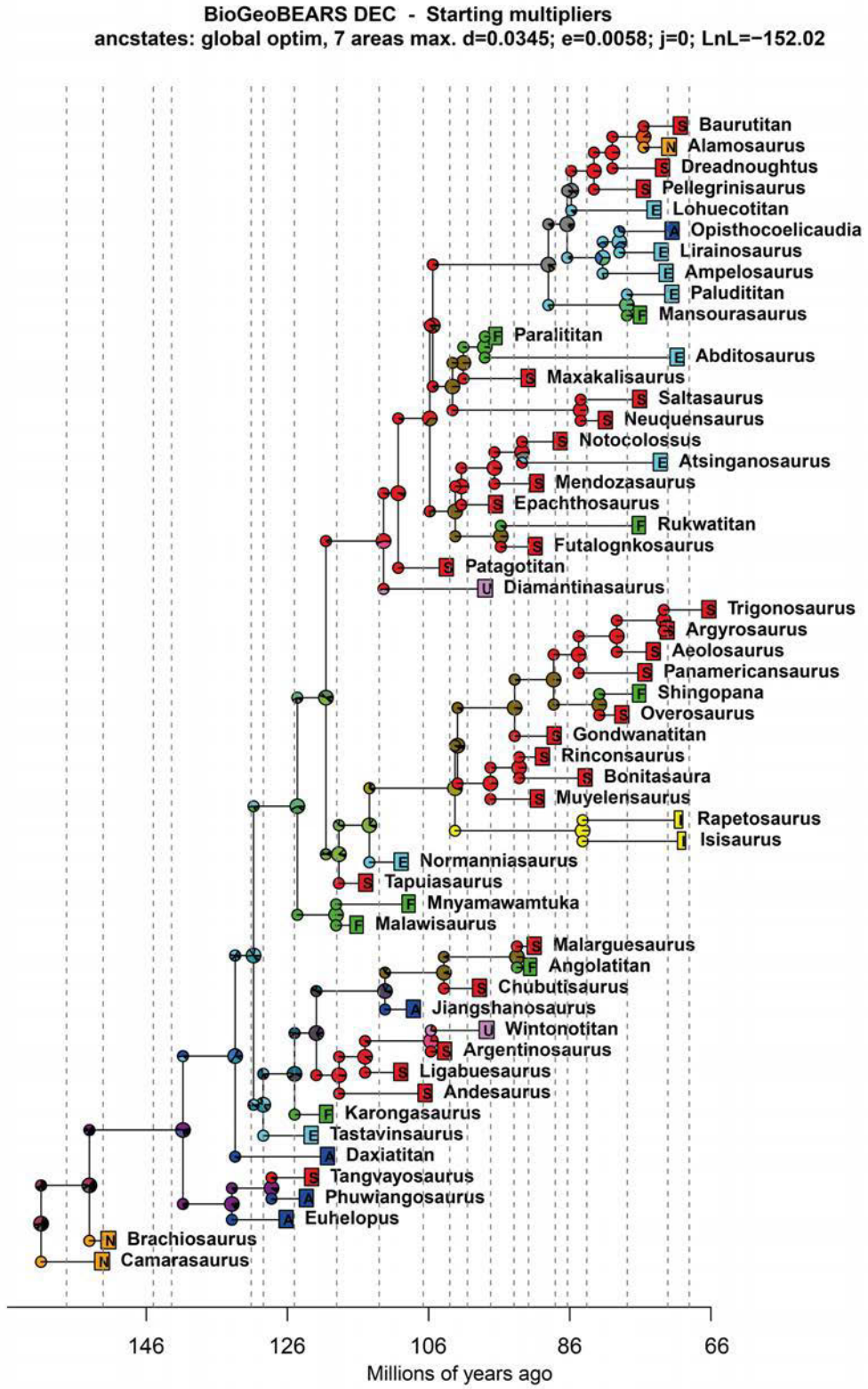

Supplementary Figure 55. **DEC model results on the tip-dated Bayesian phylogenetic analysis using 'starting' distribution multipliers.** Pie charts indicate relative support for ancestral area reconstruction; branch tips indicate taxon area distribution. A: Asia, F: Africa, E: Europe, N: North America, S: South America, I: India. For multiple area ranges colour coding, see Suppl. Figure 54.

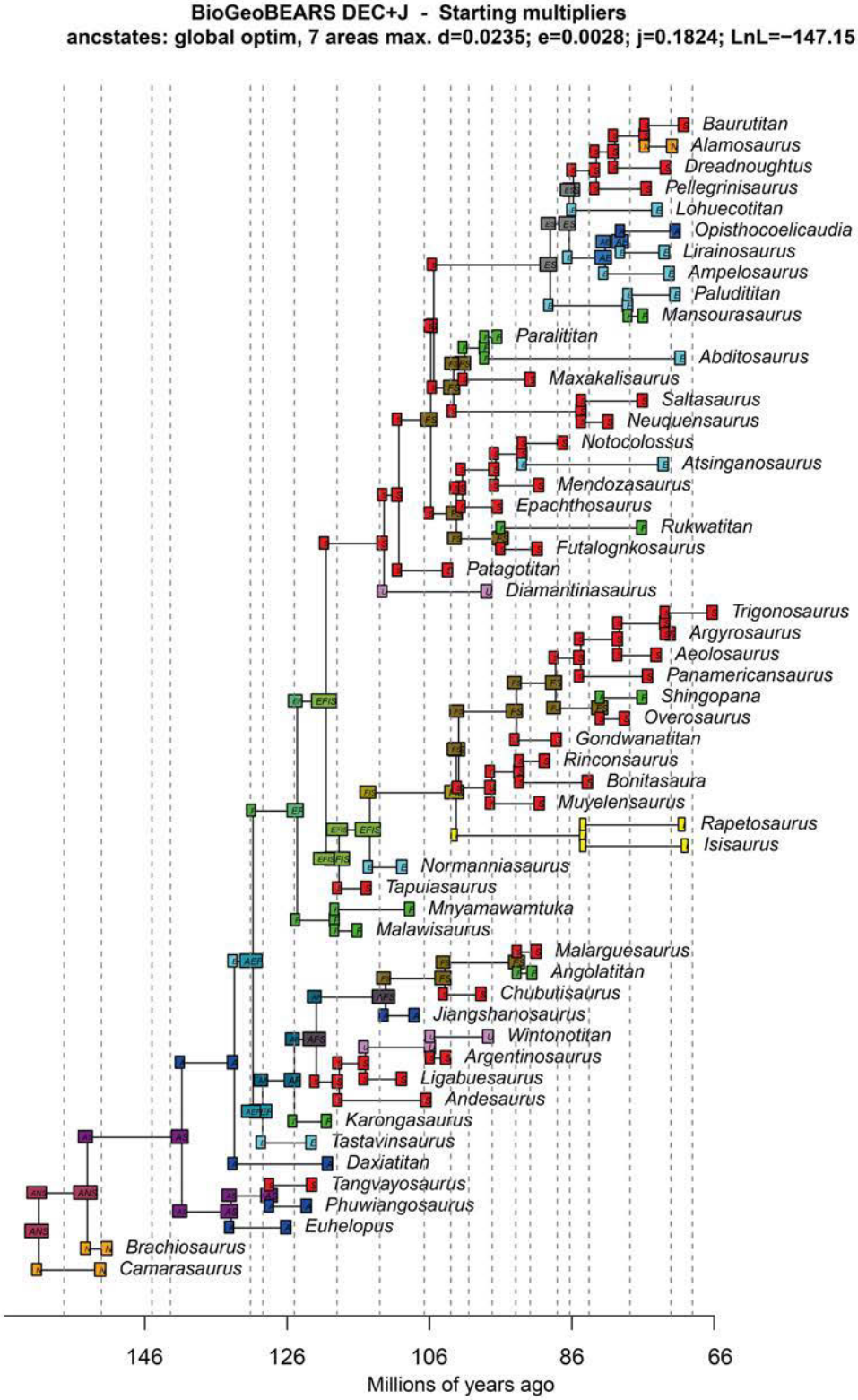

Supplementary Figure 56. **DEC+J model results on the tip-dated Bayesian phylogenetic analysis using 'starting' distribution multipliers.** Node boxes indicate most likely ancestral range reconstruction. A: Asia, F: Africa, E: Europe, N: North America, S: South America, I: India.

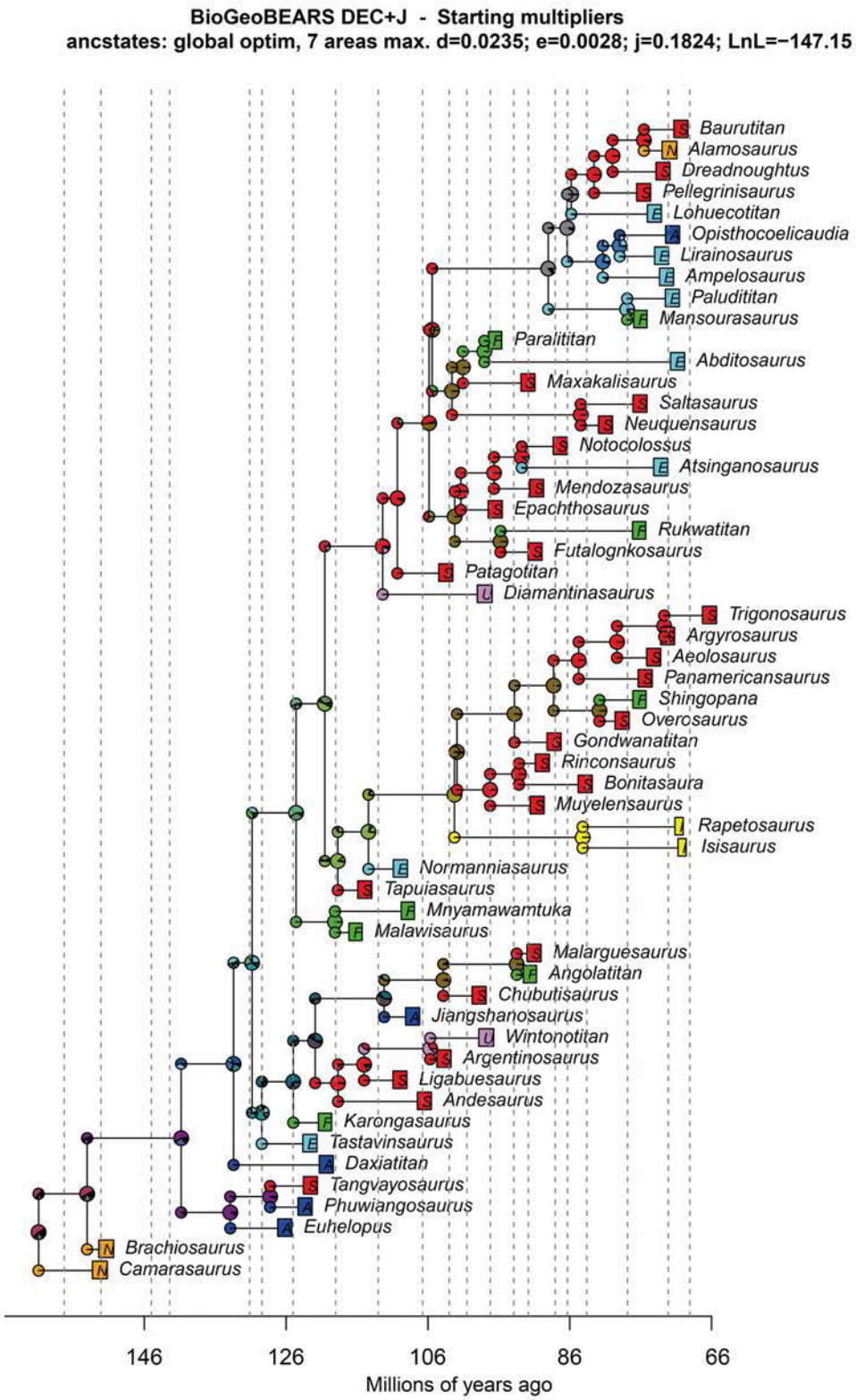

Supplementary Figure 57. **DEC+J model results on the tip-dated Bayesian phylogenetic analysis using 'starting' distribution multipliers.** Pie charts indicate relative support for ancestral area reconstruction; branch tips indicate taxon area distribution. A: Asia, F: Africa, E: Europe, N: North America, S: South America, I: India. For multiple area ranges colour coding, see Suppl. Figure 56.

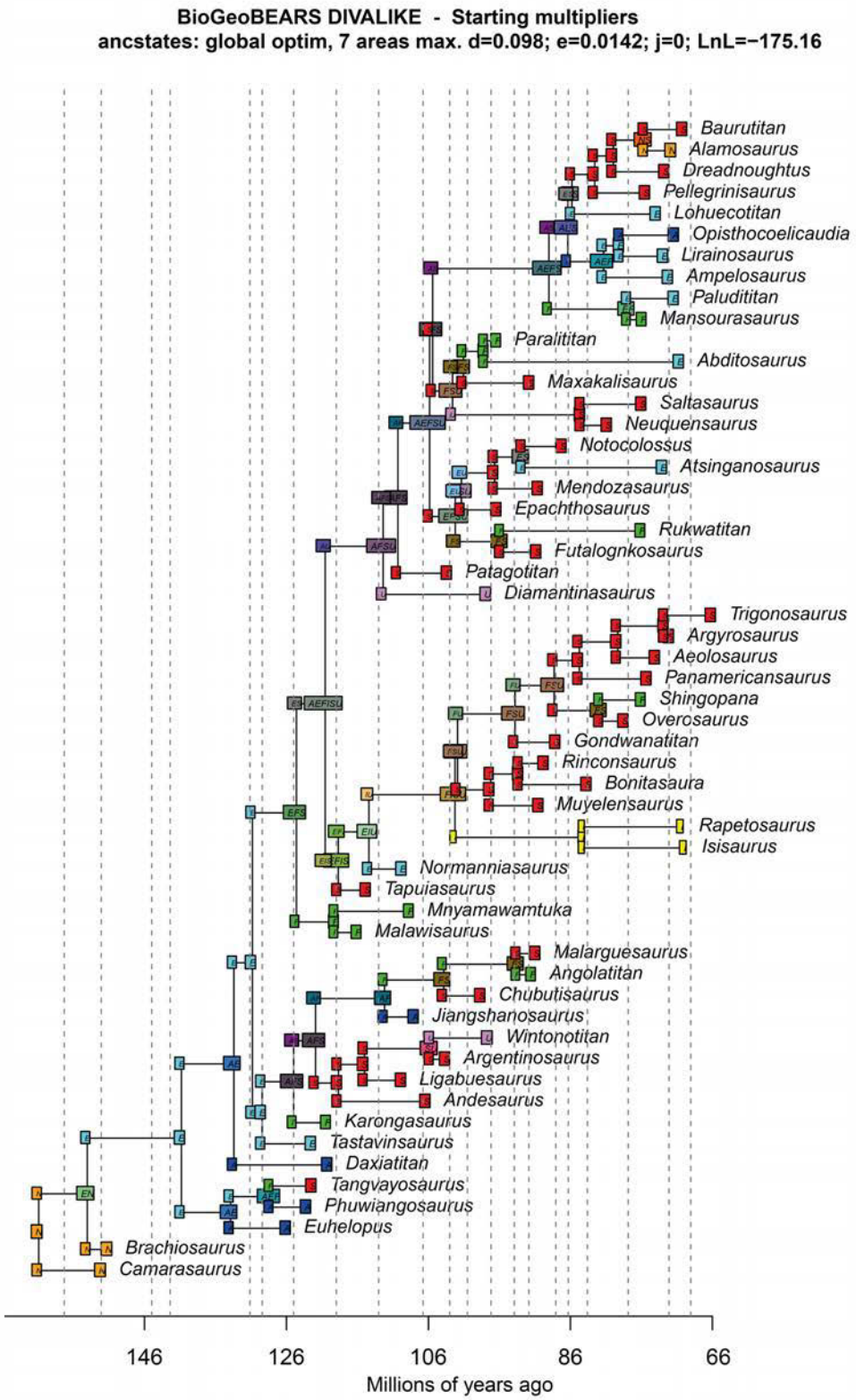

Supplementary Figure 58. **DIVALIKE model results on the tip-dated Bayesian phylogenetic analysis using 'starting' distribution multipliers.** Node boxes indicate most likely ancestral range reconstruction. A: Asia, F: Africa, E: Europe, N: North America, S: South America, I: India.

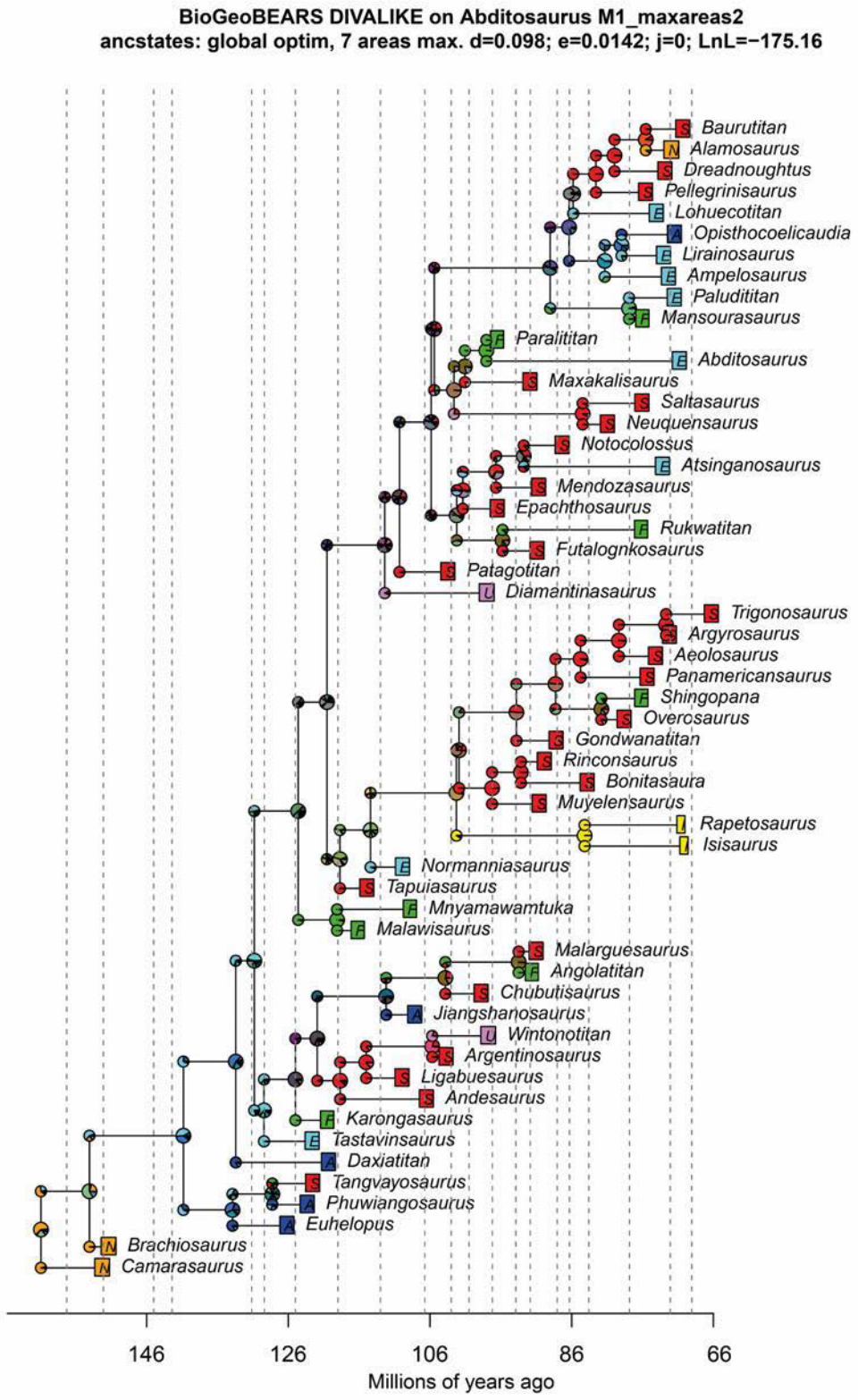

Supplementary Figure 59. **DIVALIKE model results on the tip-dated Bayesian phylogenetic analysis using 'starting' distribution multipliers.** Pie charts indicate relative support for ancestral area reconstruction; branch tips indicate taxon area distribution. A: Asia, F: Africa, E: Europe, N: North America, S: South America, I: India. For multiple area ranges colour coding, see Suppl. Figure 58.

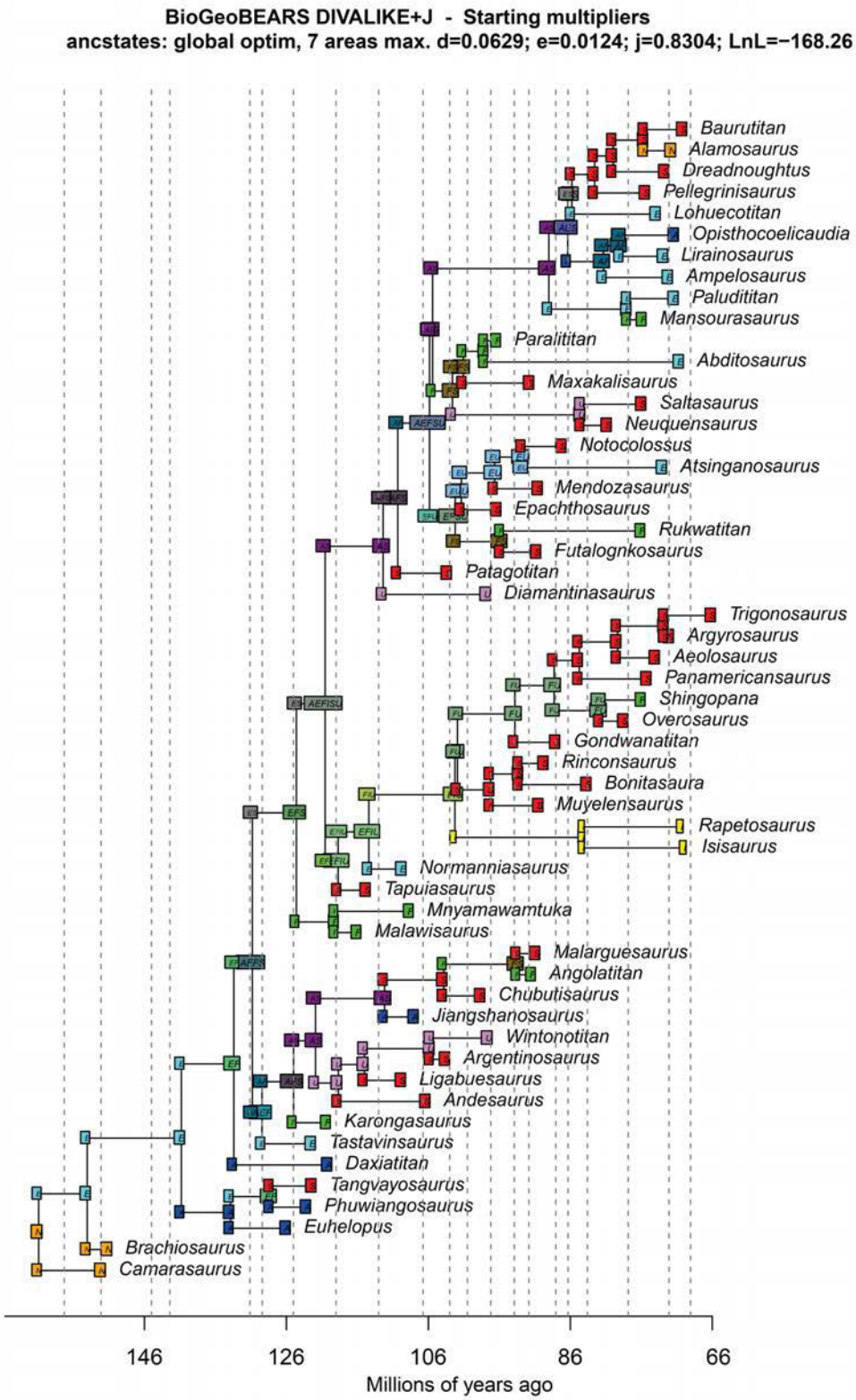

Supplementary Figure 60. **DIVALIKE+J model results on the tip-dated Bayesian phylogenetic analysis using 'starting' distribution multipliers.** Node boxes indicate most likely ancestral range reconstruction. A: Asia, F: Africa, E: Europe, N: North America, S: South America, I: India.

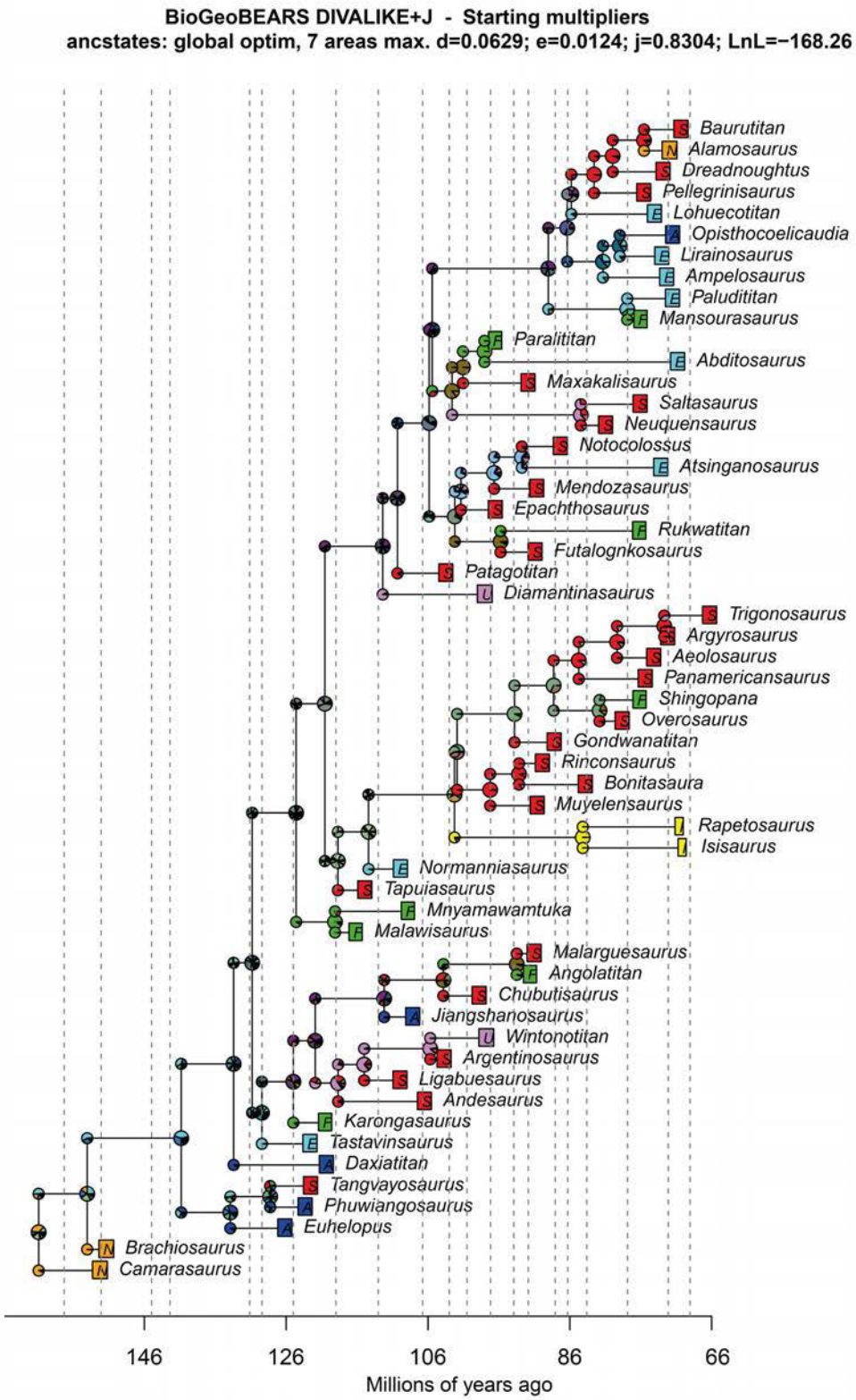

Supplementary Figure 61. **DIVALIKE+J model results on the tip-dated Bayesian phylogenetic analysis using 'starting' distribution multipliers.** Pie charts indicate relative support for ancestral area reconstruction; branch tips indicate taxon area distribution. A: Asia, F: Africa, E: Europe, N: North America, S: South America, I: India. For multiple area ranges colour coding, see Suppl. Figure 60.

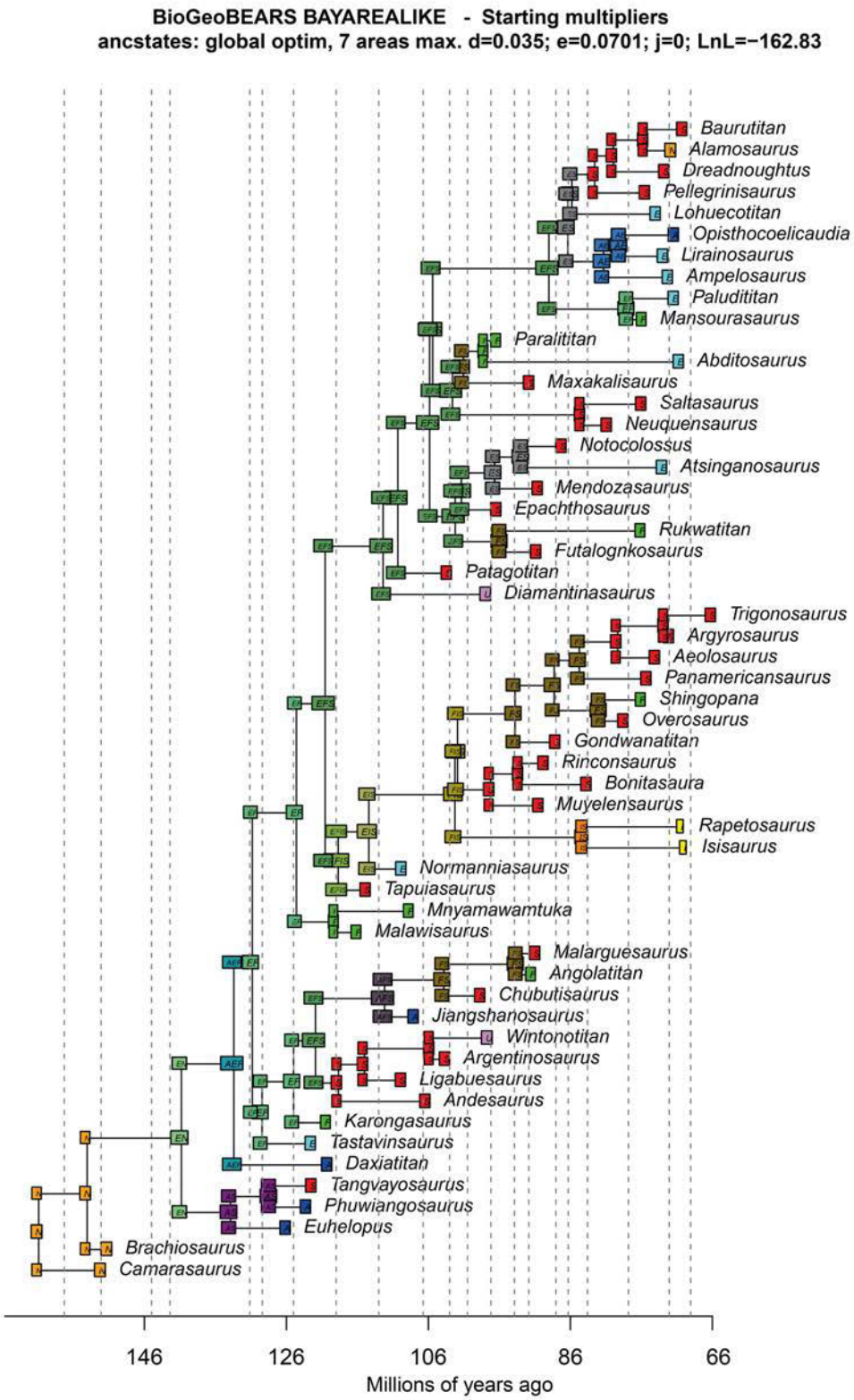

Supplementary Figure 62. **BAYAREALIKE model results on the tip-dated Bayesian phylogenetic analysis using 'starting' distribution multipliers.** Node boxes indicate most likely ancestral range reconstruction. A: Asia, F: Africa, E: Europe, N: North America, S: South America, I: India.

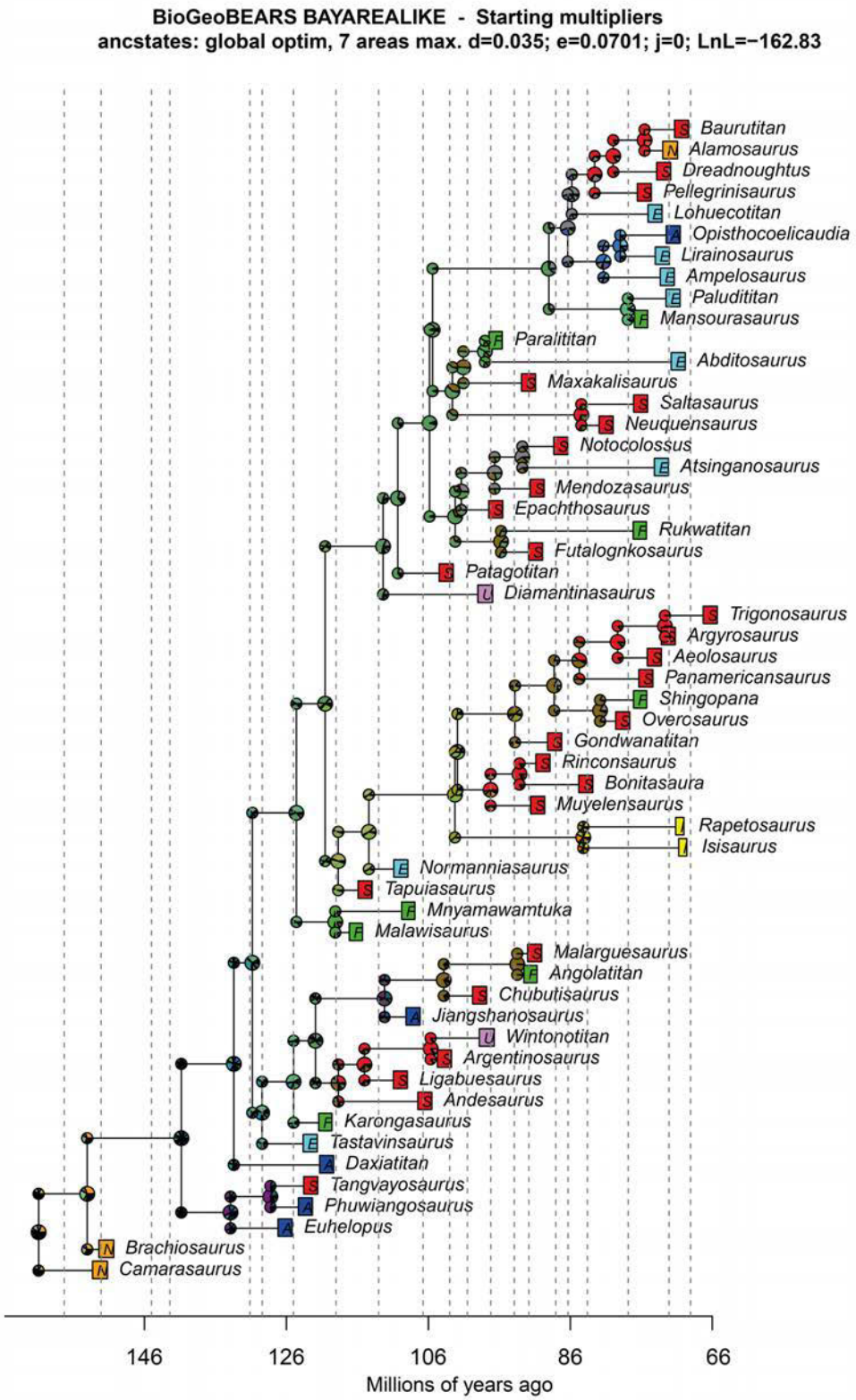

Supplementary Figure 63. **BAYAREALIKE model results on the tip-dated Bayesian phylogenetic analysis using 'starting' distribution multipliers.** Pie charts indicate relative support for ancestral area reconstruction; branch tips indicate taxon area distribution. A: Asia, F: Africa, E: Europe, N: North America, S: South America, I: India. For multiple area ranges colour coding, see Suppl. Figure 62.

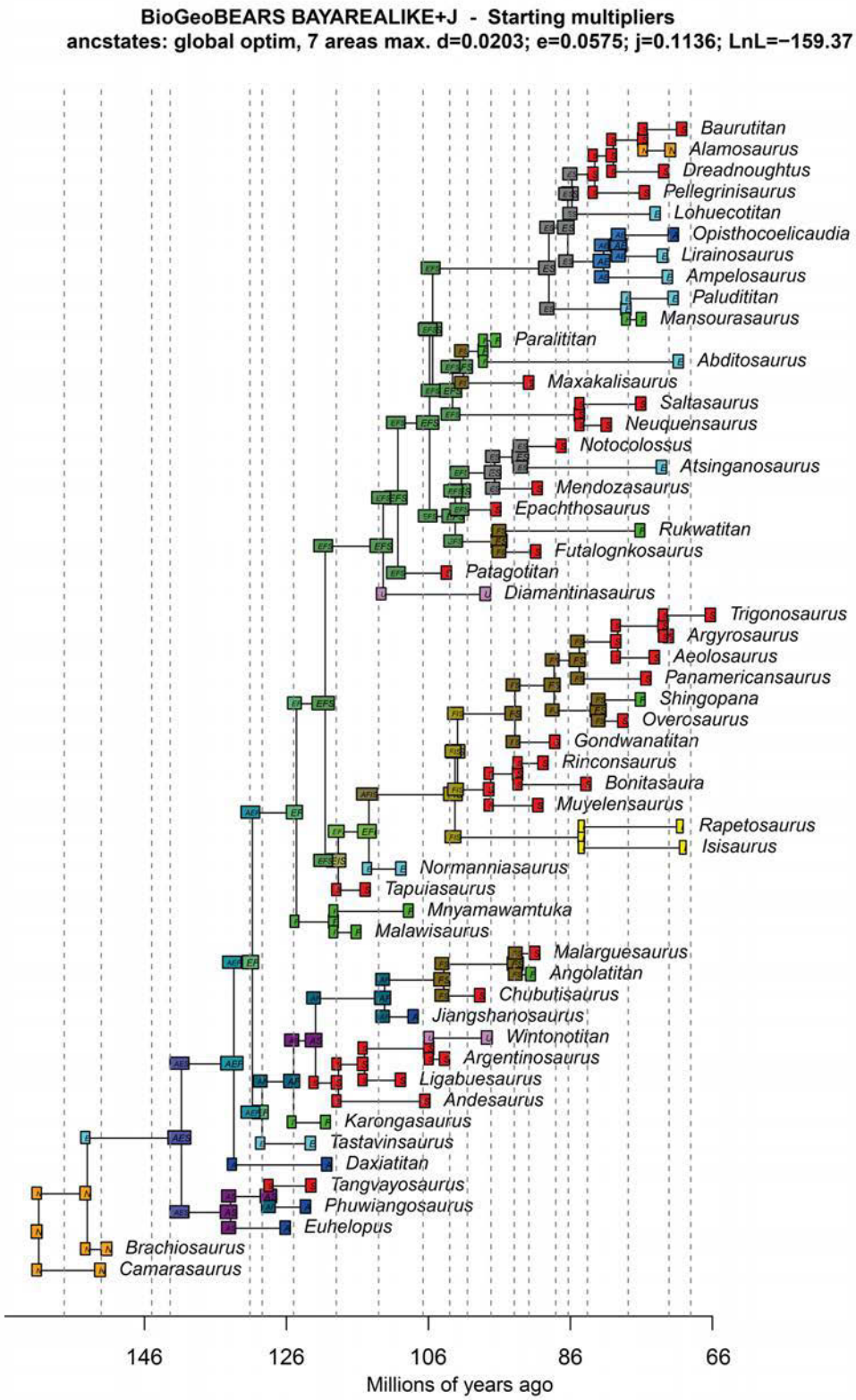

Supplementary Figure 64. **BAYAREALIKE+J model results on the tip-dated Bayesian phylogenetic analysis using 'starting' distribution multipliers.** Node boxes indicate most likely ancestral range reconstruction. A: Asia, F: Africa, E: Europe, N: North America, S: South America, I: India.

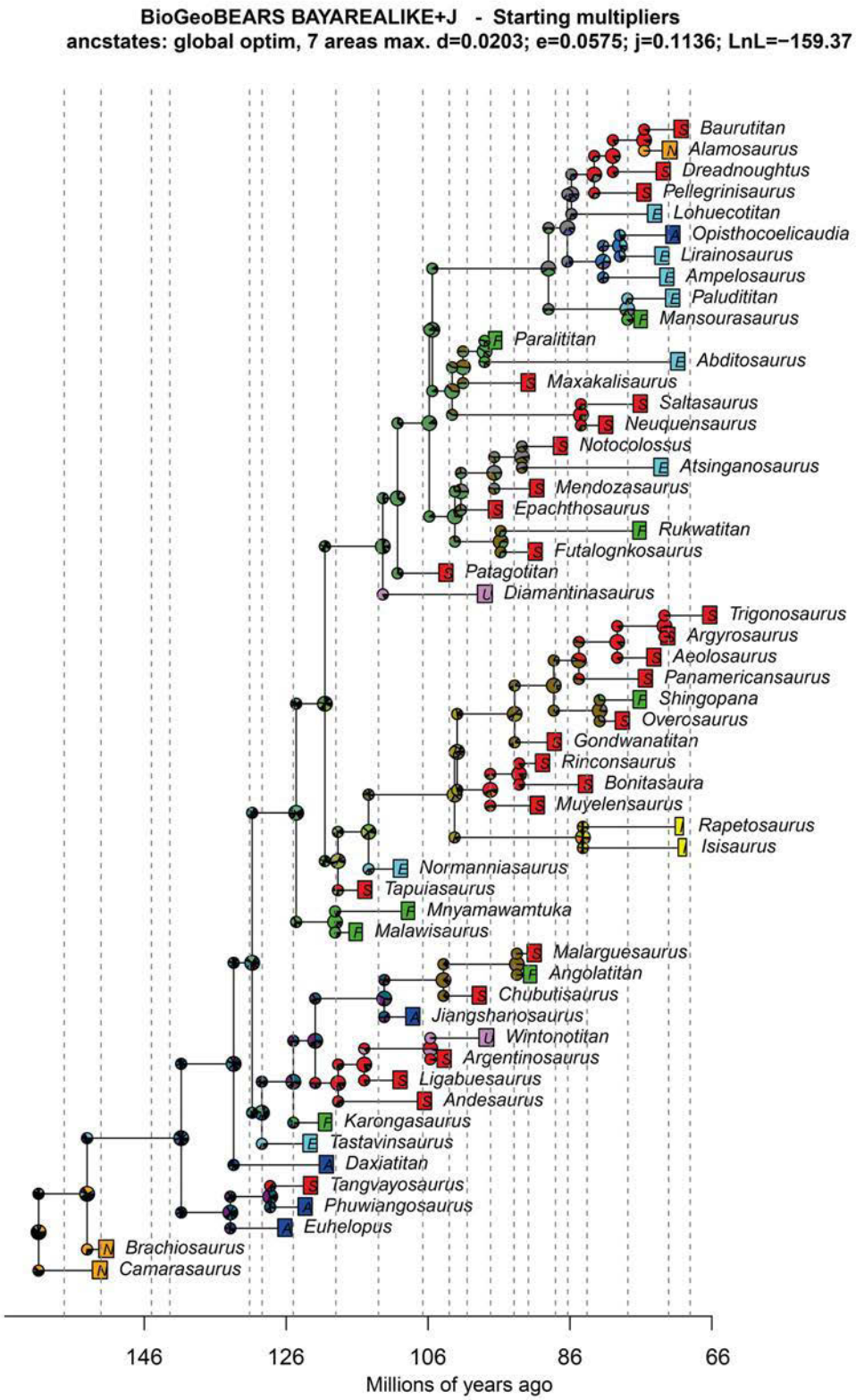

Supplementary Figure 65. **BAYAREALIKE+J model results on the tip-dated Bayesian phylogenetic analysis using 'starting' distribution multipliers.** Pie charts indicate relative support for ancestral area reconstruction; branch tips indicate taxon area distribution. A: Asia, F: Africa, E: Europe, N: North America, S: South America, I: India. For multiple area ranges colour coding, see Suppl. Figure 64.

Prior to the discovery of *Ampelosaurus* and *Lirainosaurus*, Buffetaut[17] and Le Loeuff[18,118] suggested a Gondwanan origin for the latest Cretaceous European titanosaurs. With the increasing number of African and European titanosaur taxa recovered in the last decade[5,6,8,11,16,29,123,170], the hypothesis that Late Cretaceous European titanosaurs are nested within Gondwanan titanosaurian clades is gaining further support. Ezcurra and Agnolín[169] found that, palaeobiogeographically speaking, Europe was more closely related to southern landmasses than to Asiamerica during the Campanian–Maastrichtian, and Gorscak and O'Connor[29] and Dal Sasso et al.[64] highlighted the centralized role of Africa in the dispersal of South American titanosaurs. In this regard, the Gondwanan distribution of the *F. baghensis* oospecies, associated with *Abditosaurus*, adds new evidence for a southern origin. A connection between Europe, Africa, and South America during the Late Cretaceous and a dispersal to Europe from South America through Africa has been suggested by Mannion and Upchurch[171]. More particularly, these authors predicted that the "close relatives of some of the titanosaurs currently endemic to South America should eventually be found in the latest Cretaceous of Africa". Indeed, close relatives of the South American titanosaurs are known in in the latest Cretaceous of Africa[90,123,170], and our results indicate that the sister taxa of the endemic saltasaurins (the *Abditosaurus*-*Maxakalisaurus*-*Paralititan* clade; Fig. 3 and Suppl. Fig. 42–65) are found, in close association with Gondwanan oospecies, for the first time in Europe.

Our results agree with the hypothesis of Díez Díaz et al.[11] regarding the Gondwanan origin of not only one of the distinct lineages (*Paludititan*+*Lohuecotitan*) recognized by the authors in their analysis, but all lineages of European titanosaurs. The present results do not recover *Ampelosaurus*, *Lirainosaurus*, and *Atsinganosaurus* together

and thus do not recognize Lirainosaurinae, the alleged endemic and relictual lineage of Laurasian affinity[11]. Although the topology of *Ampelosaurus* and *Lirainosaurus* is closely related, *Atsinganosaurus* is nested in a South American clade. Indeed, the hypothesis that European titanosaurs were relictual lineages of Laurasian faunas[11,19,20] is not supported in our analysis, as they clearly have a Gondwanan origin followed by several vicariance events (Suppl. Figures 42–65).

Dispersal event

Biogeographic analyses indicate that one migratory wave involving Gondwanan titanosaur clades reached Europe at the end of the Cretaceous. The dispersal was from Africa, as it was, after the break-up of South America and Africa at 100 Ma, the nearest Gondwanan region to the European archipelago during the Late Cretaceous. However, the African and European records are extremely scarce, if not absent, in post-Cenomanian to Campanian times, hindering an understanding of the phylogenetic relationships and the evolution of the titanosaurian clades that inhabited the African landmass, particularly those that were part of the later dispersals to Europe.

The dispersal event from Africa is hypothesized to have led to the arrival of the large-bodied saltasaurines (the *Abditosaurus* lineage and its associated Gondwanan oospecies *Fusioolithus baghensis*) on the Ibero-Armorican Island in the earliest Maastrichtian. The estimated arrival of the *Abditosaurus* lineage falls within the range of marine Campanian–Maastrichtian Boundary Events (CMBE)[3,172] and coincides with the global sea-level drop KMa2[61], a favourable moment for immigrants to enter the archipelago[20]. Arrivals of other dinosaur clades have been documented in the early Maastrichtian; for instance, lambeosaurine hadrosaurids are

hypothesized to have reached western Europe slightly later (ca.70 Ma[3,173]), representing additional evidence of a significant faunal exchange around the CMBE. The time of arrival of the *Abditosaurus* lineage on the Ibero-Armorican Island is additionally supported by the fact that members of this clade are large-bodied and are differentiated from all earlier titanosaur taxa in the region by the absence of life-history traits associated with insular effects (i.e., insular dwarfism). In other words, if members of the *Abditosaurus* lineage had reached the island during pre-Maastrichtian times, they would most likely have reduced their size and evolved insular traits, as seen in late Campanian taxa. In addition, both the FAD of the Gondwanan oospecies *Fusioolithus baghensis* in the region (Fig. 4) and the fusioolithid oospecies from north-western Africa[157,158,174] are reported in early Maastrichtian deposits, thus lending further weight to the hypothesis that the group reached the island no earlier than this. Pereda-Suberbiola et al.[175] also reported a partial hind limb of an indeterminate titanosauriform in the early Maastrichtian of Morocco. Future discoveries will confirm whether this or other closely related lineages (potentially with associated fusioolithid oospecies) reached other regions of the archipelago (e.g., the Haţeg Island), as is suggested by the replacement observed there among titanosaur communities, with large-bodied taxa occurring temporally later than smaller forms[68]. Pending definitive resolution of the phylogenetic position(s) of these large-bodied Romanian taxa[176], we speculate that Maastrichtian titanosaurian newcomers to the Haţeg Island might have a Gondwanan affinity, with a turnover scheme similar to that herein demonstrated for the Ibero-Armorican Island.

<u>The dispersal route</u>

We further point out that the arrival from Africa of the *Abditosaurus* lineage to the Ibero-Armorican Island was favoured by the subaerial emergence of carbonate platforms at the western and southern margins of the Tethyan region during the earliest Maastrichtian. Such emergence would have occurred gradually, during a minor to moderate sea-level fall after the late Campanian highstand[177]. The global eustatic curve indicates a drop in the sea-level (KMa2) in the earliest Maastrichtian (70.6 Ma[61]), a eustatic event that is regionally documented in western European basins[178] and Tunisia[179]. In the central Tethys, the subaerial exposures documented in the Gravovo-Tripoliza carbonate platform (Greece) have been interpreted as a fall in relative sea level in the early Maastrichtian[180, 181]. Northwards, some sectors of the Adriatic–Dinaric Carbonate Platform with exposed and karstified surfaces are interpreted as continental exposures around the Campanian–Maastrichtian boundary[182]; these even preserve some upper Campanian–lower Maastrichtian localities with dinosaur fossils[183]. Similarly, the ancient insular area of what is currently Romania recorded a marine regression[184]. During the KMa2 regressive event (70.6 Ma, early Maastrichtian) that affected the central Tethyan margin and the northern African regions, therefore, various carbonate platforms were subaerially exposed, the Europe-Africa connection was re-established, and the Early Cretaceous migratory routes[19, 62-64, 185, 186] were probably reactivated, making it possible for titanosaur taxa to disperse from north-western Africa to Europe, and more specifically to the Ibero-Armorican Island (Fig. 4). A similar interpretation was proposed by Le Loeuff[18] and adopted by Zarcone et al.[187]. We rule out alternative routes connecting Africa and Europe and functioning as ‘stepping-stones’ for the dispersal of vertebrates, such as the Alboran route[17] because no potential land

connections (i.e., shallow carbonate platforms) nor evidence of emergence have been documented in these areas during early Maastrichtian times.

3. Supplementary tables 1-7

Supplementary Table 1. Estimated body masses (kg) and body lengths (m) of titanosaur individuals from the Ibero-Armorican island. BL, body length; BM, body mass; F, femur; FAPD, femoral anteroposterior diameter at midshaft, in mm; FC, femur minimum midshaft circumference, in mm; FLMD, femoral mediolateral diameter at midshaft, in mm; H, humerus; HC, humerus minimum midshaft circumference, in mm; HC+FC, combined humeral and femoral circumference, in mm; HOS, Histologic Ontogenetic Stage; log, logarithm (base 10). * Estimated value after Ramanujan approximation for ellipse perimeter; ** estimated value after the allometric equation of González Riga et al.[70]. # This paper.

Taxon	Specimen	HOS	Source	FAPD	FLMD	HC	FC	logHC	logFC	HC+FC	logHC+FC	BM	BL
Lirainosaurus	MGUV-17235; F	13	(9)	42	92	191**	218*	2.28101	2.33820	409	2.61158	1189	3.2
astibiae	MGUV-17194; F	13	(9)	44	98	202**	231*	2.30563	2.36396	433	2.63681	1395	3.6
	MGUV-17294; F	13	(9)	41	102	205**	235*	2.31235	2.37099	440	2.64369	1457	3.7
	MCNA 14465; F	indet.	(39)	-	-	210**	241	2.32290	2.38202	451	2.65449	1560	3.9
	MCNA 1817; F	indet.	(39)	-	-	216**	248	2.33479	2.39445	464	2.66667	1685	4.1
	MCNA 7469; F	indet.	(39)	-	-	219**	252	2.34143	2.40140	471	2.67348	1760	4.2
	MCNA 7463; H	indet.	(39)	-	-	221	254**	2.34439	2.40450	475	2.67652	1794	4.3
	MCNA 7462; H	indet.	(39)	-	-	229	263**	2.35984	2.42065	492	2.69234	1983	4.6
	MGUV-16450; F	13	(9)	42	122	237**	273*	2.37491	2.43642	510	2.70779	2186	4.9

	MCNA 3160; F	indet.	(39)	-	-	240**	277	2.38071	2.44248	517	271372	2270	5.0
	MCNA 7465; H	indet.	(39)	-	-	250	289**	2.39794	2.46051	539	2.73138	2538	5.4
	MCNA 7464; H	indet.	(39)	-	-	272	315**	2.43457	2.49882	587	2.76891	3219	6.4
	MCNA 14469; F	indet.	(39)	-	-	302	352	2.48020	2.54654	654	2.81567	4328	7.8
	Mean											**2105**	**5**
Ampelosaurus	C3-1506; H	11	(10)	-	-	195	223**	2.29003	2.34765	418	2.62083	1261	3.4
atacis	C3-1182; F	11	(10)	-	-	220**	253	2.34307	2.40312	473	2.67516	1778	4.3
	C3-708; F	13	(10)	-	-	226**	260	2.35441	2.41497	486	2.68677	1914	4.5
	C3-203; F	12	(10)	-	-	234**	270	2.37008	2.43136	504	2.70283	2119	4.8
	C3-527; F	13	(10)	-	-	243**	280	2.38518	2.44716	523	2.71830	2337	5.1
	C3-175; H	13	(10)	-	-	243	280**	2.38561	2.44761	523	2.71874	2343	5.1
	C3-261; F	12	(10)	-	-	249**	288	2.39688	2.45939	537	2.73029	2521	5.4
	C3-602; H	13	(10)	-	-	250	289**	2.39794	2.46051	539	2.73138	2538	5.4
	C3-238; H	12	(10)	-	-	270	313**	2.43136	2.49546	583	2.76563	3153	6.3
	C3-87; F	Indet.	(15)	40	150	279**	324*	2.44578	2.51054	603	2.78040	3462	6.7
	C3-1482; F	Indet.	(15)	53	147	285**	332*	2.45560	2.52081	617	2.79045	3689	7.0
	C3-143; F	13	(10)	-	-	299**	348	2.47546	2.54158	647	2.81080	4197	7.7
	C3-1239; F	11	(10)	-	-	300**	350	2.47784	2.54407	650	2.81324	4262	7.7
	C3-1189; H	13	(10)	-	-	310	362**	2.49136	2.55822	672	2.82710	4653	8.2
	C3-582; F	13	(10)	-	-	321**	375	2.50648	2.57403	696	2.84260	5132	8.8
	C3-287; F	Indet.	(15)	70	175	344**	403*	2.53609	2.605	746	2.87294	6219	10.0
	C3-20; F	Indet.	(15)	43	216	385**	454*	2.58545	2.65662	839	2.92352	8566	12.5
	C3-78; F	11	(10)	-	-	394**	465	2.59581	2.66745	859	2.93414	9161	13.1

	C3-174; F	12	(10)	-	-	406**	480	2.60899	2.68124	886	2.94765	9979	13.9
	Mean											**4173**	**7.4**
Atsinganosaurus velauciensis	MMS/VBN.09A018;H	14	(11)	-	-	169.4	192.2**	2.22891	2.28372	361.6	2.55821	848	2.6
	MMS/VBN.00.12; H	14	#	-	-	206*	236**	2.31364	2.37233	442	2.64501	1469	3.7
	MMS/VBN.00.12; F	Indet.	(11)	-		206**	236*	2.31393	2.37264	442	2.64531	1472	3.7
	MMS/VBN.09.126; F	14	(11)	-	-	223**	256*	2.34745	2.4077	478.2	2.67965	1830	4.3
	Mean											**1405**	**4**
Garrigatitan meridionalis	MMS/VBN.12.82; H	14	(6)	-	-	230	265**	2.3617	2.42263	495	2.69428	2007	4.6
	MMS/VBN.09A.016; H	12	(6)	-	-	230	265**	2.3617	2.42263	495	2.69428	2007	4.6
	MMS/VBN.00.13; F	13	(6)	-	-	237**	273	2.3747	2.43616	510	2.70753	2183	4.9
	MMS/VBN.09.47; H	14	(6)	-	-	250	289**	2.3979	2.46051	539	2.73138	2538	5.4
												2184	**4.9**
Lohuecotitan pandafilandi	HUE 3018; F	Indet.	(8)	85	140	308**	359*	2.4881	2.55476	666	2.8237	**4554**	**8.1**
Abditosaurus kuehnei	MCD-6987; F + MNCN-79834; H	14	#	-	-	464	540	2.6665	2.74141	1004	3.0017	**14053**	**17.5**

Supplementary Table 2. Taxon list, chronostratigraphic range (in Ma) and palaeobiogeographic range (modified from Gorscak and O'Connor[29]). Upper and lower ranges are based on stages and substages provided by primary literature and based on time scale of Ogg and Hinnov[58]

Taxon	Upper	Lower	Palaeogeographic range	References
Abditosaurus	70.0	71.0	Europe	This work
Aeolosaurus	66.0	83.6	South America	135
Alamosaurus	66.0	72.1	North America	45, 50, 131, 189
Ampelosaurus	71.0	73.0	Europe	4, 109
Andesaurus	96.4	113.0	South America	91, 190
Angolatitan	89.8	91.4	Africa	93
Argentinosaurus	93.9	113.0	South America	23
Argyrosaurus	66.0	83.6	South America	37, 191
Atsinganosaurus	71.6	74.0	Europe	5, 110
Baurutitan	66.0	72.1	South America	188
Bonitasaura	83.6	86.3	South America	106, 192
Brachiosaurus	145.0	157.3	North America	47, 193
Camarasaurus	145.0	157.3	North America	47, 194
Chubutisaurus	93.9	100.5	South America	195, 196
Daxiatitan	113.0	126.3	Asia	197
Diamantinasaurus	93.9	100.5	Australia	136, 198
Dreadnoughtus	66.0	83.6	South America	143
Epachthosaurus	92.9	95.4	South America	92, 199
Euhelopus	113.0	130.8	Asia	58, 200
Futalognkosaurus	86.3	93.9	South America	164, 201
Gondwanatitan	83.6	93.9	South America	30, 96
Isisaurus	66.0	72.1	India-Madagascar	28, 160
Jiangshanosaurus	100.5	113.0	Asia	202
Karongasaurus	113.0	126.3	Africa	203
Ligabuesaurus	100.5	123.4	South America	89
Lirainosaurus	72.0	73.5	Europe	6, 38, 40, 108, 204, 205
Lohuecotitan	69.9	76.4	Europe	8
Malarguesaurus	88.8	91.4	South America	105
Malawisaurus	113.0	126.3	Africa	203, 206, 207
Mansourasaurus	72.1	83.6	Africa	16
Maxakalisaurus	83.6	93.9	South America	97, 120
Mendozasaurus	86.3	88.8	South America	208, 209
Mnyamawamtuka	93.9	126.3	Africa	29
Muyelensaurus	88.8	91.4	South America	27
Neuquensaurus	80.7	83.6	South America	49, 210, 211
Normanniasaurus	107.7	113.0	Europe	88
Notocolossus	85.6	87.9	South America	71
Opisthocoelicaudia	69.9	72.1	Asia	42
Overosaurus	72.1	83.6	South America	26
Paluditiitan	69.9	72.1	Europe	101
Panamericansaurus	69.9	76.4	South America	99

Taxon	Upper	Lower	Palaeogeographic range	References
Paralititan	93.9	100.5	Africa	34
Patagotitan	100.5	107.7	South America	107
Pellegrinisaurus	69.9	83.6	South America	103
Phuwiangosaurus	113.0	130.8	Asia	212, 213, 214
Rapetosaurus	66.0	72.1	India-Madagascar	24, 215, 216
Rinconsaurus	86.3	91.4	South America	95
Rukwatitan	71.4	75	Africa	90, 123
Saltasaurus	69.9	76.4	South America	25, 33, 48, 100, 209
Shingopana	71.4	75	Africa	90, 170
Tangvayosaurus	100.5	126.3	South America	217
Tapuiasaurus	113.0	126.3	South America	218, 219
Tastavinsaurus	123.3	126.3	Europe	104, 220
Trigonosaurus	66	72.1	South America	102
Wintonotitan	93.9	100.5	Australia	197, 221

Supplementary Table 3. Comparation of results of the 'Harsh' and 'Starting' distribution multiplier palaeobiogeographic analyses, for the six different models compared. LnL: Natural logarithm of the likelihood. d: diversification, e: extinction, J: founder speciation. Selected models are highlighted in bold.

Harsh multipliers	LnL	Parameters	d	e	j
DEC	-214.9159	2	0.14152497	0.01261117	0
DEC+J	-113.42654	3	0.02926071	0.00691044	2.99988979
DIVALIKE	-247.046121	2	0.26970775	0.02106558	0
DIVALIKE+J	**-113.291142**	**3**	**0.03387059**	**0.00718592**	**1.99994881**
BAYAREALIKE	-179.098408	2	0.04412644	0.07505801	0
BAYAREALIKE+J	-174.903325	3	0.02806056	0.06139048	0.21092835

Starting multipliers	LnL	Parameters	d	e	j
DEC	-152.018741	2	0.03448649	0.0058278	0
DEC+J	-147.146889	3	0.02345259	0.00277335	0.18235445
DIVALIKE	-175.158326	2	0.09800269	0.01420808	0
DIVALIKE+J	-168.261897	3	0.06291701	0.01237455	0.83037541
BAYAREALIKE	**-162.826338**	**2**	**0.03499269**	**0.07005024**	**0**
BAYAREALIKE+J	-159.370106	3	0.02029749	0.0574896	0.11355085

Supplementary Table 4. Measurements (mm) of cervical and dorsal centra, and corresponding articulated ribs of *Abditosaurus kuehnei*. * Elongation index (cL/ ctW), after Upchurch[222]; Brackets indicate estimated values.

	Anterior cervicals					Mid-cervicals					Posterior cervicals		Anterior dorsals		Mid-dorsals		
	CV3	CV4	CV5	CV6	CV7	CV8	CV9	CV10	CV11	CV12	CV13	CV14	DV1	DV2	DV3	DV4	DV5
Anteroposterior length, centrum (with condyle)	270	-	380	-	-	510	520	500	450	450	390	340	280	295	-	235	220
Transverse width, cotyle	140	-	-	-	-	180	200	255	(280)	(260)	300	300	310	303	250	235	240
Elongation index	1.9	-	-	-	-	2.8	2.6	2	1.6	1.7	1.3	1.1	0.9	0.9	-	1	0.9
Maximum rib length preserved	-	450	1000	540	1080	1290	1340	1280	1350	1120	630	-	890	1040	1180	-	-

Supplementary Table 5. Measurements (mm) of right scapulocoracoid and left sternal plate of *Abditosaurus kuehnei*.

	Scapula (MCD-6724)	**Coracoid (MCD-6742)**	**Sternal plate (MCD-6716)**
Anteroposterior length	1040	390	710
Dorsoventral length	680 (of acromial plate)	295	N/A
Mediolateral length	N/A	N/A	430 (at midheight)

Supplementary Table 6. Measurements (mm) of forelimb bones of *Abditosaurus kuehnei*. Robustness index after Wilson and Upchurch[160]; * Robustness index after Curry Rogers[223]; Brackets indicate estimated values.

	Humerus (MNCN-79834)	**Humerus (MCD-6988)**	**Radius (MCD-6748)**
Proximodistal length	(1045)	(1045)	(720)
Proximal mediolateral length	450	N/A	N/A
Midshaft circumference	464	453	250
Distal mediolateral length	N/A	425	200
Robustness Index	0.33	0.33	0.45*

Supplementary Table 7. Measurements (mm) of hindlimb bones of *Abditosaurus kuehnei*. Robustness index after Wilson and Upchurch[160]; Brackets indicate estimated values.

	Femur	**Tibia**	**Fibula**
	(MCD-6987)	**(MNCN-79837-79838-79848)**	**(MCD-6723)**
Proximodistal length	(1300)	810	810
Proximal anteroposterior length	N/A	310	(200)
Midshaft anteroposterior length	63.4	120	100
Midshaft circumference	540	298	190
Distal anteroposterior length	N/A	810	115
Robustness Index	N/A	0.25	0.16

4. Supplementary Data

Data S1. Parsimony Script.

Script for TNT v1.5, to replicate the parsimony analysis. Calling this script, using the name of the matrix file as an argument will run analyses with both equal and extended implied weights, with different concavity constants.

Data S2. TNT

TNT file including the character scores for the parsimony analyses.

Data S3. MrBayes

Nexus file for MrBayes 3.2.7a, to reproduce the non-clock analyses.

Data S4. BEAST

Script for Beast 2.4.7, based on the script provided by Eric Gorscak, used in Gorscak and O'Connor[29]. Changes to the script include precisions on age ranges according to Supplementary Table 2, and modification of the mcmc parameters.

5. **References for Supplementary Information** (numbering continued from main text)

78. Lapparent, A. F. & Aguirre, E. Présence de Dinosauriens dans le Crétacé supérieur du bassin de Tremp (province de Lérida, Espagne). *CR Somm. Soc. Géol. Fr.* **14**, 261–262 (1956).
79. Martín Jiménez, M. et al. Systematic study of the historical material of Upper Cretaceous reptiles from the Tremp Basin (Catalonia, Spain) housed at the Museo Nacional de Ciencias Naturales (Madrid). *J. Iber. Geol*. **43**, 217–233 (2017).
80. Romer, A. S. Osteology of the Reptiles. University of Chicago Press, Chicago, Illinois, 772 pp (1956).
81. Wilson, J. A. Anatomical nomenclature of fossil vertebrates: standardized terms or 'Lingua franca'?. *J. Vertebr. Paleontol.* **26**, 511–518 (2006).
82. Wilson, J. A. A nomenclature for vertebral laminae in sauropods and other saurischian dinosaurs. *J. Vertebr. Paleontol.* **19**, 639–653 (1999).
83. Wilson, J. A., D'Emic, M. D., Ikejiri, T., Moacdieh, E. M. & Whitlock, J. A. A nomenclature for vertebral fossae in sauropods and other saurischian dinosaurs. *PLoS ONE* **6**, e17114 (2011).
84. Tschopp, E., Mateus, O. & Benson, B. J. A specimen-level phylogenetic analysis and taxonomic revision of Diplodocidae (Dinosauria, Sauropoda). *PeerJ* **3**, e857 (2015).
85. Schneider, C. A., Rasband, W. S. & Eliceiri, K. W. NIH Image to ImageJ: 25 years of image analysis. *Nat. Methods* **9**, 671–675 (2012).
86. Ramanujan, S. Ramanujan's Collected Works, Chelsea, New York, (1962).

87. Bouckaert, R. et al. BEAST 2: A Software Platform for Bayesian Evolutionary Analysis. *PLoS Comput. Biol*. **10**, e1003537 (2014).

88. Le Loeuff, J., Suteethorn, S. & Buffetaut, E. A new sauropod dinosaur from the Albian of Le Havre (Normandy, France). *Oryctos* **10**, 23–30 (2013).

89. Bonaparte, J. F., González Riga, B. J. & Apesteguía, S. *Ligabuesaurus leanzai* gen. et sp. nov. (Dinosauria, Sauropoda), a new titanosaur from the Lohan Cura Formation (Aptian, Lower Cretaceous) of Neuquén, Patagonia, Argentina. *Cretaceous Res*. **27**, 364–376 (2006).

90. Widlansky, S. J., Clyde, W. C., O'Connor, P. M., Roberts, E. M. & Stevens, N. J. Paleomagnetism of the Cretaceous Galula Formation and implications for vertebrate evolution. *J. African Earth Sci.* **139**, 403–420 (2018).

91. Mannion, P. D. & Calvo, J. O. Anatomy of the basal titanosaur (Dinosauria, Sauropoda) *Andesaurus delgadoi* from the mid–Cretaceous (Albian–early Cenomanian) Río Limay Formation, Neuquén Province, Argentina: implications for titanosaur systematics. *Zool. J. Linn. Soc.* **163**,155–181 (2011).

92. Martínez, R., Gimenez, O., Rodriguez, J., Luna, M. & Lamanna, M. An articulated specimen of the basal titanosaurian (Dinosauria: Sauropoda) *Epachthosaurus sciuttoi* from the early Late Cretaceous Bajo Barreal Formation of Chubut Province, Argentina. *J. Vertebr. Paleontol.* **24**,107–120 (2004).

93. Mateus, O. et al. *Angolatitan adamastor*, a new sauropod dinosaur and the first record from Angola. *Anais Da Academia Brasileira De Ciencias* **83**, 221–233 (2011).

94. González Riga, B. J., Mannion, P. D., Poropat, S. F., Ortiz David, L. D. & Coria, J. P. Osteology of the Late Cretaceous Argentinean sauropod dinosaur *Mendozasaurus neguyelap*: implications for basal titanosaur relationships, *Zool. J. Linn. Soc.* **184**, 136–181 (2018).

95. Calvo, J. O. & González Riga, B. J. *Rinconsaurus caudamirus* gen. et sp. nov., a new titanosaurid (Dinosauria, Sauropoda) from the Late Cretaceous of Patagonia, Argentina. *Rev. Geol. Chile* **30**, 333–353 (2003).

96. Novas, F. E. in *The Age of Dinosaurs in South America* (ed Farlow, J) 1–452 (Indiana University Press, Bloomington & Indianapolis, 2009).

97. França, M. A. G., de A. Marsola, J. C., Riff, D., Hsiou, A. S. & Langer, M.C. New lower jaw and teeth referred to *Maxakalisaurus topai* (Titanosauria: Aeolosaurini) and their implications for the phylogeny of titanosaurid sauropods. *PeerJ* **4**, e2054 (2016).

98. Salgado, L., Apesteguía, S. & Heredia, S. E. A new specimen of *Neuquensaurus australis*, a Late Cretaceous saltasaurine titanosaur from north Patagonia. *J. Vertebr. Paleontol*. **25**, 623–634 (2005).

99. Calvo, J. O. & Porfiri, J. D. *Panamericansaurus schroederi* gen. nov. sp. nov. Un nuevo Sauropoda (Titanosauridae-Aeolosaurini) de la Provincia del Neuquén, Cretácico Superior de Patagonia, Argentina. *Braz. Geogr. J. Geosci. Hum. Res. Med.* **1**, 100–115 (2010).

100. Bonaparte, J. F. & Powell, J. E. A continental assemblage of tetrapods from the Upper Cretaceous beds of El Brete, northwestern Argentina (Sauropoda–Coelurosauria– Carnosauria– Aves). *Mém. Soc. géol. Fr.* **139**, 19–28 (1980).

101. Csiki, Z., Codrea, V., Jipa–Murzea, C. & Godefroit, P. A partial titanosaur (Sauropoda, Dinosauria) skeleton from the Maastrichtian of Nalat–Vad, Hateg Basin, Romania. *Neues Jahrb Geol Palaontol Abh* **258**, 297–324 (2010).

102. Campos, D. de A., Kellner, A. W. A., Bertini, R. J. & Santucci, R. M. On a titanosaurid (Dinosauria, Sauropoda) vertebral column from the Bauru Group, Late Cretaceous of Brazil. *Arq. Mus. Nac. Rio de Janeiro* **63**, 565–593 (2005).

103. Salgado, L. *Pellegrinisaurus powelli* nov. gen. et. sp. (Sauropoda, Titanosauridae) from the upper Cretaceous of Lago Pellegrini, Northwestern Patagonia, Argentina. *Ameghiniana* **33**, 355–365 (1996).

104. Canudo, J. I., Royo-Torres, R. & Cuenca-Bescós, G. A new sauropod *Tastavinsaurus sanzi* gen. et sp nov from the Early Cretaceous (Aptian) of Spain. *J. Vertebr. Paleontol*. 28:712–731 (2008).

105. González Riga, B. J., Previtera, E. & Pirrone, C. A. *Malarguesaurus florenciae* gen. et sp. nov., a new titanosauriform (Dinosauria, Sauropoda) from the Upper Cretaceous of Mendoza, Argentina. *Cretaceous Res*. **30**, 135–148 (2009).

106. Apesteguía, S. *Bonitasaura salgadoi* gen. et sp. nov.: a beaked sauropod from the Late Cretaceous of Patagonia. *Sci. Nat.* **91**, 493–497 (2004).

107. Carballido, J. L. et al. A new giant titanosaur sheds light on body mass evolution among sauropod dinosaurs. *Proc R Soc Lond B Biol Sci* **284**, 20171219 (2017).

108. Corral, J. C. et al. Magnetostratigraphy and lithostratigraphy of the Laño vertebrate site: implications in the uppermost Cretaceous chronostratigraphy of the Basque-Cantabrian Region. *Cretaceous Res*. **57**, 473–489 (2016).

109. Fondevilla, V. et al. Magnetostratigraphy of the Maastrichtian continental record in the Upper Aude Valley (northern Pyrenees, France): Placing age constraints on the succession of dinosaur-bearing sites. *Cretaceous Res*. **57**, 457–472 (2016).

110. Cincotta, A. et al. Integrated paleoenvironmental reconstruction and taphonomy of a unique Upper Cretaceous vertebrate-bearing locality (Velaux, southeastern France). *PLOS ONE* **10**, e0134231 (2015).

111. Poropat, S. F. et al. New Australian sauropods shed light on Cretaceous dinosaur palaeobiogeography. *Sci. Rep.* **6**, 34467 (2016).

112. Ree, R. H. & Sanmartín, I. Conceptual and statistical problems with the DEC+ J model of founder-event speciation and its comparison with DEC via model selection. *J. Biogeogr.* ***45***, 741–749 (2018).

113. Matzke, N. Statistical comparison of DEC and DEC+J Is identical to comparison of two class submodels and is therefore valid. *OSF Preprints* (27 Apr. 2021, web).

114. Kielan-Jaworowska, Z. In pursuit of early mammals. Indiana University Press, Indiana, 254 pp (2013).

115. Kielan-Jaworowska, Z., Cifelli, R. L., & Luo, Z-X. Mammals from the Age of Dinosaurs: Origins, Evolution, and Structure. Columbia University Press, New York, 630 pp. (2004).

116. Talens, J. Descubrimiento de dinosaurios en Tremp (Lleida). *Estud. Geol.* **11**, 86 (1955).

117. Talens, J. Exploraciones sobre los dinosaurios de la Cuenca de Tremp (Lérida)". *Estud. Geol.* **11**, 456 (1955).

118. Le Loeuff, J. European titanosaurids. Rev. *Paléobiol*. **7**, 104–117 (1993).

119. Santafé, J. V., Casanovas, M. L. & Llompart, C. in *Els Dinosaures i el seu entorn geològic*. Diputació de Lleida, Lleida, 69 pp (1997).

120. Kellner, A. W. A. et al. On a new titanosaur sauropod from the Bauru Group, Late Cretaceous of Brazil. *Boletim Do Museu Nacional* **74**,1–31 (2006).

121. Tykoski, R. S. & Fiorillo, A. R. An articulated cervical series of *Alamosaurus sanjuanensis* Gilmore, 1922 (Dinosauria, Sauropoda) from Texas: new perspective on the relationships of North America's last giant sauropod. *J. Syst. Palaeontol.* **15**, 339–364 (2017).

122. Silva Junior, J. G., Marinho, T. S., Martinelli, A. G. & Langer, M. C. Osteology and systematics of *Uberabatitan ribeiroi* (Dinosauria; Sauropoda): a Late Cretaceous titanosaur from Minas Gerais, Brazil. *Zootaxa* **4577**, 401–438 (2019).

123. Gorscak, E., O'Connor, P. M., Stevens, N. J. & Roberts, E. M. The basal titanosaurian *Rukwatitan bisepultus* (Dinosauria, Sauropoda) from the middle Cretaceous Galula Formation, Rukwa Rift Basin, southwestern Tanzania. *J. Vertebr. Paleontol.* **34**, 1133–1154 (2014).

124. Salgado, L. & Coria, R.A. *Barrosasaurus casamiquelai* gen. et sp. nov., a new titanosaur (Dinosauria, Sauropoda) from the Anacleto Formation (Late

Cretaceous: early Campanian) of Sierra Barrosa (Neuquén, Argentina). *Zootaxa* **2222**, 1–16 (2009).

125. Díez Díaz, V., Pereda Suberbiola, X. & Sanz, J. L. The axial skeleton of the titanosaur *Lirainosaurus astibiae* (Dinosauria: Sauropoda) from the latest Cretaceous of Spain. *Cretaceous Res*. **43**, 145–160 (2013).

126. Filippi, L. S. & Garrido, A. *Pitekunsaurus macayai* gen. et sp. nov., nuevo titanosaurio (Saurischia, Sauropoda) del Cretácico Superior de la Cuenca Neuquina, Argentina. *Ameghiniana* **45**, 575–590 (2008).

127. Voegele, K. K., Lamanna, M. C. & Lacovara K. J. Osteology of the dorsal vertebrae of the giant titanosaurian sauropod dinosaur *Dreadnoughtus schrani* from the Late Cretaceous of Argentina. *Acta Palaeontol. Pol.* **62**, 667–681 (2017).

128. Otero, A., Gallina, P. A., Canale, J. I. & Haluza, A. Sauropod haemal arches: morphotypes, new classification and phylogenetic aspects. *Hist Biol* **24**, 243–256 (2011).

129. Wilson J. A. Sauropod dinosaur phylogeny: critique and cladistic analysis. *Zool. J. Linn. Soc.* **136**, 217–276 (2002).

130. Santucci, R. M. & de Arruda–Campos, A. C. A new sauropod (Macronaria, Titanosauria) from the Adamantina Formation, Bauru Group, Upper Cretaceous of Brazil and the phylogenetic relationships of Aeolosaurini. *Zootaxa* **3085**,1–33 (2011).

131. D'Emic, M. D., Wilson, J. A. & Williamson, T. E. A sauropod dinosaur pes from the latest Cretaceous of North America and the validity of *Alamosaurus sanjuanensis* (Sauropoda: Titanosauria). *J. Vertebr. Paleontol*. **31**, 1072–1079 (2011).

132. Otero, A. Forelimb musculature and osteological correlates in Sauropodomorpha (Dinosauria, Saurischia). PLoS ONE **13**, e0198988 (2018).

133. Fronimos, J. A & Lehman, T. M. New specimens of a titanosaur sauropod from the Maastrichtian of Big Bend National Park, Texas. *J. Vertebr. Paleontol*. **34**, 883–899 (2014).

134. Wilson, J. A., Barrett, P. M. & Carrano, M. T. An associated partial skeleton of *Jainosaurus* cf. *septentrionalis* (Dinosauria: Sauropoda) from the Late Cretaceous of Chhota Simla, central India. *Palaeontology* **54**, 981–998 (2011).

135. Salgado, L., Coria, R. A. & Coria, J. O. Presencia del género *Aeolosaurus* (Sauropoda, Titanosauridae) en la Formación Los Alamitos, Cretácico superior de la Província de Río Negro, Argentina. *Geociencias* **2**, 44–49 (1997).

136. Poropat, S. F. et al. Revision of the sauropod dinosaur *Diamantinasaurus matildae* Hocknull et al. 2009 from the mid-Cretaceous of Australia: implications for Gondwanan titanosauriform dispersal. *Gondwana Res.* **27**, 995–1033 (2015).

137. Salgado, L., Gallina, P.A. & Carabajal, P. Redescription of *Bonatitan reigi* (Sauropoda: Titanosauria), from the Campanian–Maastrichtian of the Río Negro Province (Argentina). *Hist Biol* **27**, 525–548 (2015).

138. Klein, N. & Sander, P. M. Ontogenetic stages in the long bone histology of sauropod dinosaurs. *Paleobiology* **34**, 247–263 (2008).

139. Woodward, H. N., Horner, J. R. & Farlow, J. O. Quantification of intraskeletal histovariability in *Alligator mississippiensis* and implications for vertebrate osteohistology. *PeerJ* **2**, e422 (2014).

140. Sander, P. M. Long bone histology of the Tendaguru sauropods: implications for growth and biology. *Paleobiology* **26**, 466–488 (2000).

141. Stein, K. et al. Small body size and extreme cortical remodeling indicate phyletic dwarfism in *Magyarosaurus dacus* (Sauropoda: Titanosauria). Proc. Natl. Acad. Sci. *USA*, **107**, 9258–9263 (2010).

142. Woodward, H. N. & T. M. Lehman, T. M. Bone histology and microanatomy of *Alamosaurus sanjuanensis* (Sauropoda: Titanosauria) from the Maastrichtian of Big Bend National Park, Texas. *J. Vertebr. Paleontol*. **29**, 807–821 (2009).

143. Lacovara, K. J. et al. A gigantic, exceptionally complete titanosaurian sauropod dinosaur from Southern Patagonia, Argentina. *Sci. Rep.* **4**, 6196 (2014).

144. Gallina, P. A. Histología ósea del titanosaurio *Bonitasaura salgadoi* (Dinosauria: Sauropoda) del Cretácico superior de Patagonia. *Ameghiniana* **49**, 289–302 (2012).

145. Curry Rogers, K. & Kulik, Z. Osteohistology of *Rapetosaurus krausei* (Sauropoda: Titanosauria) from the Upper Cretaceous of Madagascar. *J. Vertebr. Paleontol*. **38**, 1–24 (2018).

146. Dercourt, J. et al. (eds) in *Atlas Peri-Tethys Palaeogeographical Maps*. 269 pp (CCGM/CGMW, París, 2000).

147. Pérez-Pueyo, M. et al. The tetrapod fossil record from the uppermost Maastrichtian of the Ibero-Armorican Island: An integrative review based on the outcrops of the Western Tremp Syncline (Aragón, Huesca Province, NE Spain). *Geosciences* **11**, 162 (2021).

148. Vianey-Liaud, M., Mallan, M. P., Buscail, O. & Montgelard, C. in Dinosaur eggs and babies (eds Carpenter, K., Hirsch, K.F. & Horner, J.R.) 151–183 (Cambridge University Press, Cambridge, 1994).

149. Vianey-Liaud, M., Khosla, A. & Garcia, G. Relationships between European and Indian dinosaur eggshells of the oofamily Megaloolithidae. *J. Vertebr. Paleontol.* **23**, 575–585 (2003).

150. Sellés, A. G. et al. Dinosaur eggs in the Upper Cretaceous of the Coll de Nargó area, Lleida Province, south-Central Pyrenees, Spain: oodiversity, biostratigraphy and their implications. *Cretaceous Res.* **40**, 10–20 (2013).

151. Codrea, V. et al. Dinosaur egg nests, mammals, and other vertebrates from a new Maastrichtian site of the Hateg Basin (Romania). *C. R. Palevol* **1**, 173–180 (2002).

152. Dhiman, H., Prasad, G. V. R. & Goswami, A. Parataxonomy and palaeobiogeographic significance of dinosaur eggshell fragments from the Upper Cretaceous strata of the Cauvery Basin, South India. *Hist*. *Biol*. **31**, 1310–1322 (2019).

153. Kapur, V. V. & Khosla, A. Late Cretaceous terrestrial biota from India with special references to vertebrates and their implications for biogeographic connections. *New Mex Mus Nat Hist Sci Bull* **71**, 161–172 (2016).

154. Khosla, A. Paleobiogeographical inferences of Indian Late Cretaceous vertebrates with special reference to dinosaurs. *Hist. Biol.*, doi.org/10.1080/08912963.2019.1702657 (2019).

155. Fernández, M. S. & Khosla, A. Parataxonomic review of the Upper Cretaceous dinosaur eggshells belonging to the oofamily Megaloolithidae from India and Argentina. *Hist*. *Biol*. **27**, 158–180 (2015).

156. Fernández, M. S. Important contributions of the South American record to the understanding of dinosaur reproduction. *New Mex Mus Nat Hist Sci Bull* **71**, 91–105 (2016).

157. Garcia, G. et al. First record of dinosaur eggshells and teeth from the North-West African Maastrichtian (Morocco). *Palaeovertebrata* **32**, 59–69 (2003).

158. Vianey-Liaud, M. & Garcia, G. Diversity among North African dinosaur eggshells. *Palaeovertebrata* **32**, 171–188 (2003).

159. Goloboff, P. A. Extended implied weighting. *Cladistics* **30**, 260–272 (2014).

160. Wilson, J. A. & Upchurch, P. A revision of *Titanosaurus* Lydekker (Dinosauria–Sauropoda), the first dinosaur genus with a 'Gondwanan' distribution. *J. Syst. Palaeontol.***1**, 125–160 (2003).

161. Franco-Rosas, A. C., Salgado, L., Rosas, C. F. & de Souza Carvalho, I. Nuevos materiales de titanosaurios (Sauropoda) en el Cretácico superior de Mato Grosso, Brasil. *Rev. Bras. de Paleontol* **7**, 329–336 (2004).

162. Goloboff, P. A., Torres, A. & Arias, J. S. Weighted parsimony outperforms other methods of phylogenetic inference under models appropriate for morphology. *Cladistics* **34**, 407–37 (2017).

163. Simões, T. R. et al. The origin of squamates revealed by a middle Triassic lizard from the Italian Alps. *Nature* **557**, 706–709 (2018).

164. Calvo, J. O., Porfiri, J. D., González Riga, B. J. & Kellner, A. W. Anatomy of *Futalognkosaurus dukei* Calvo, Porfiri, González Riga & Kellner, 2007 (Dinosauria, Titanosauridae) from the Neuquén Group (Late

Cretaceous), Patagonia, Argentina. *Arquivos Do Museu Nacional, Rio De Janeiro* **65**, 511–526 (2007).

165. Scotese, C. R. A continental drift flipbook. *J. Geol.* **112**, 729–741 (2004).

166. Torsvik, T. H., Rousse, S., Labails, C. & Smethurst, M. A. A new scheme for the opening of the South Atlantic Ocean and the dissection of an Aptian salt basin. *Geophys. J. Int.* **177**, 1315–1333 (2009).

167. Seton, M. et al. Global continental and ocean basin reconstructions since 200 Ma. *Earth-Sci. Rev.* **113**, 212–270 (2012).

168. Fanti, F. in *Earth and Life: Global Biodiversity, Extinction Intervals and Biogeographic Perturbations Through Time* (eds Talent, J. A.) 883–911 (Springer Science, 2012).

169. Ezcurra, M. D. & Agnolín, F. L. A new global palaeobiogeographical model for the Late Mesozoic and Early Tertiary. *Syst. Biol.* **61**, 553–566 (2012).

170. Gorscak, E., O'Connor, P. M., Roberts, E. M. & Stevens, N. J. The second titanosaurian (Dinosauria: Sauropoda) from the middle Cretaceous Galula Formation, southwestern Tanzania, with remarks on African titanosaurian diversity. *J. Vertebr. Paleontol.* **30**, e1343250–23 (2017).

171. Mannion, P. D. & Upchurch, P. A re-evaluation of the ‘mid-Cretaceous sauropod hiatus’ and the impact of uneven sampling of the fossil record on patterns of regional dinosaur extinction. *Palaeogeogr. Palaeoclimatol. Palaeoecol.* **299**, 529–540 (2011).

172. Voigt, S., Gale, A. S., Jung, C. & Jenkyns, H. C. Global correlation of Upper Campanian- Maastrichtian successions using carbon-isotope

stratigraphy: development of a new Maastrichtian timescale. *Newsl. Stratigr.* **45**, 25–53 (2012).

173. Conti, S. et al. The oldest lambeosaurine dinosaur from Europe: insights into the arrival of Tsintaosaurini. *Cretaceous Res*. **107**, 104286 (2020).

174. Chassagne-Manoukian, M. et al. Dating the “red beds” of the Eastern Moroccan High Plateaus: Evidence from late Late Cretaceous charophytes and dinosaur eggshells. *Geobios* **46**, 371–379 (2013).

175. Pereda Suberbiola, X., Bardet, N., Iarochène, M., Bouya, B. & Amaghzaz, M. The first record of a sauropod dinosaur from the Late Cretaceous phosphates of Morocco. *J. Afr. Earth Sci.* **40**, 81–88 (2004).

176. Mannion, P. D. et al. Dwarfs among giants: resolving the systematics of the titanosaurian sauropod dinosaurs from the latest Cretaceous of Romania. *Abstracts of the Annual Meeting of the Society of Vertebrate Paleontolog*y **79**, 148A (2019).

177. Masse, J. P., Philip J., Camoin G. in *The Tethys Ocean* (eds Nairn, A. E. M., Ricou, L. E., Vrielynck, B., Dercourt, J.) 215–235 (Springer, Boston, 1995).

178. Hardenbol, J. et al. Mesozoic and Cenozoic sequence chronostratigraphic framework of European Basins. *SEPM Special Publication*, **60**, 3–13 (1998).

179. Li, L., Keller, G., Adatte, G. & Stinnesbeck, W. Late Cretaceous sea-level changes in Tunisia: a multi-disciplinary approach. *Geol. Soc. Lond*. **157**, 447–458 (2000).

180. Bernier, P. & Fleury, J-J. La plate-forme carbonatée de Gavrovo-Tripolitza (Grèce): évolution des conditions de sédimentation au cours du Mesozoïque. *Géologie Méditerranéenne* **7**, 247–259 (1980).

181. Landrein, P., Loreau, J.-P. & Fleury, J.-J. Émersion généralisée intra-maastrichtienne de la plate-forme de Gavrovo-Tripolitza (Grèce): effets sur les populations de foraminifères Rhapydionininae. *Bull. Soc. géol. Fr.* **172**, 85–98 (2001).

182. Jez, J. & Otoničar, B. Late Cretaceous geodynamics of the northern sector of the Adriatic Carbonate Platform (W Slovenia). *Newsl Stratigr*. **51**, 381–410 (2018).

183. Dalla Vecchia, F. M. *Tethyshadros insularis*, a new hadrosauroid dinosaur (Ornithischia) from the Upper Cretaceous of Italy. *J. Vertebr. Paleontol*. **29**, 1100–1116 (2009).

184. Vremir, M. et al. Petresti-Arini - An important but ephemeral Upper Cretaceous continental vertebrate site in the southwestern Transylvanian Basin, Romania. *Cretaceous Res.* **49**, 13–38 (2014).

185. Bosellini, A. Dinosaurs “re-write” the geodynamics of the eastern Mediterranean and the paleogeography of the Apulia Platform. *Earth Sci Rev* **59**, 211–234 (2001).

186. Dalla Vecchia, F. M. in Thunder-Lizards: The Sauropodomorphs dinosaurs (eds Tidwell, V. & Carpenter, K.) 395–429 (Indiana University Press, Indiana, 2005).

187. Zarcone, G. et al. A possible bridge between Adria and Africa: new palaeobiogeographic and stratigraphic constraints on the Mesozoic

palaeogeography of the Central Mediterranean area. *Earth Science Reviews* **103**, 154–162 (2010).

188. Kellner, A. W. A., Campos, D. A. & Trotta, M. N. F. Description of a titanosaurid caudal series from the Bauru Group, Late Cretaceous of Brazil. *Arquivos do Museu Nacional, Rio de Janeiro* **63**, 529–564 (2005).

189. Gilmore, C. W. Discovery of a sauropod dinosaur from the Ojo Alamo Formation of New Mexico. *Smithsonian Miscellaneous Collections* **81**,1–9 (1922).

190. Calvo, J. O. & Bonaparte, J. F. *Andesaurus delgadoi*, gen. et sp. nov. (Saurischia–Sauropoda), dinosaurio Titanosauridae de la Formacíon Río Limay (Albiano–Cenomaniano), Neuquén, Argentina. *Ameghiniana* **28**, 303–310 (1991).

191. Lydekker, R. The dinosaurs of Patagonia. *Anales del Museo de la Plata, Sección de Paleontología* **2**, 1–14 (1893).

192. Gallina, P. A. & Apesteguía, S. Postcranial anatomy of *Bonitasaura salgadoi* (Sauropoda, Titanosauria) from the Late Cretaceous of Patagonia. *J. Vertebr. Paleontol*. **35**, e924957 (2015).

193. Riggs, E. S. *Brachiosaurus altithorax*, the largest known dinosaur. *Am. J. Sci.* **15**, 299–306 (1903).

194. Cope, E. D. On a gigantic saurian from the Dakota epoch of Colorado. *Paleontol. Bull.* **25**, 5–10 (1877).

195. del Corro, G. Un nuevo saurópodo del Cretácico *Chubutisaurus insignis* gen. et sp. nov. (Saurischia–Chubutisauridae nov.) del Cretácico Superior (Chubutiano), Chubut, Argentina. *Actas I Congreso Argentino de Paleontología y Bioestratigrafía* **2**, 229–240 (1975).

196. Carballido, J. L., Pol, D., Cerda, I. & Salgado, L. The osteology of *Chubutisaurus insignis* del Corro, 1975 (Dinosauria: Neosauropoda) from the “middle” Cretaceous of Central Patagonia, Argentina. *J. Vertebr. Paleontol*. **31**, 93–110 (2011).

197. You, H., Li, D., Zhou, L. & Ji, Q. *Daxiatitan binglingi*: a giant sauropod dinosaur from the Early Cretaceous of China. *Gansu Geology* **17**, 1–12 (2008).

198. Hocknull, S. A. et al. New mid–Cretaceous (latest Albian) dinosaurs from Winton, Queensland, Australia. *PLoS ONE* **4**, e6190 (2009).

199. Powell, J. E. *Epachthosaurus sciuttoi* (gen. et sp. nov.) un dinosaurio saurópodo del Cretácico de Patagonia (Provincia de Chubut, Argentina). *V Congreso Argentino de Paleontología y Bioestratigrafía, Tucumán, Actas* **1**:123–128 (1990).

200. Wiman, C. Die Kreide–Dinosaurier aus Shantung. *Palaeontologia Sinica* **6**, 1–67 (1929).

201. Calvo, J. O., Porfiri, J. D., González Riga, B. J. & Kellner, A. W. A. A new Cretaceous terrestrial ecosystem from Gondwana with the description of a new sauropod dinosaur. *Anais Da Academia Brasileira De Ciencias* **79**, 529–541 (2007).

202. Tang, F., Kang, X. M., Jin, X. S., Wei, F. & Wu, W. T. A new sauropod dinosaur of Cretaceous from Jiangshan, Zhejiang Province. *Vertebrata PalAsiatica* **39**, 277–282 (2001).

203. Gomani, E. M. Sauropod dinosaurs from the Early Cretaceous of Malawi, Africa. *Palaeontol. Electron*. **8**,1 (2005).

204. Díez Díaz, V., Pereda-Suberbiola, X. & Sanz, J. L. Juvenile and adult teeth of the titanosaurian dinosaur *Lirainosaurus* (Sauropoda) from the Late Cretaceous of Iberia. *Geobios* **45**, 265–274 (2012).

205. Díez Díaz, V., Pereda Suberbiola, X. & Sanz, J. L. Braincase anatomy of the titanosaurian sauropod *Lirainosaurus astibiae* from the Late Cretaceous of the Iberian Peninsula. *Acta Palaeontol. Pol.* **56**, 521–533 (2011).

206. Haughton, S. H. On some reptilian remains from the dinosaur beds of Nyasaland. *Transactions of the Royal Society of South Africa* **16**, 67–75 (1928).

207. Jacobs, L., Winkler, D. A., Downs, W. R. & Gomani, E. M. New material of an Early Cretaceous titanosaurid sauropod dinosaur from Malawi. *Palaeontology* **36**, 523–534 (1993).

208. González Riga, B. J. A new titanosaur (Dinosauria, Sauropoda) from the Upper Cretaceous of Mendoza province, Argentina. *Ameghiniana* **40**, 155–172 (2003).

209. González Riga, B. J. New fossil remains of *Mendozasaurus neguyelap* (Sauropoda, Titanosauria) from the Late Cretaceous of Mendoza, Argentina. *Ameghiniana* **42**, 535–548 (2005).

210. Powell, J. E. Revisión de los titanosáuridos de América del Sur. Unpublished PhD dissertation, Universidad Nacional de Tucumán, Argentina, 340 pp (1986).

211. D'Emic, M. D. & Wilson, J. A. New remains attributable to the holotype of the sauropod dinosaur *Neuquensaurus australis*, with implications for saltasaurine systematics. *Acta Palaeontol. Pol.* **56**, 61–73 (2011).

212. Martin, V., Buffetaut, E. & Suteethorn, V. A new genus of sauropod dinosaur from the Sao Khua Formation (Late Jurassic or Early Cretaceous) of northeastern Thailand. *C. R. Acad. Sci.* **319**, 1085–1092 (1994).

213. Suteethorn S. et al. 2009. A new skeleton of *Phuwiangosaurus sirindhornae* (Dinosauria, Sauropoda) from NE Thailand. *Special Publication of the Geological Society of London* **315**, 189–215 (2009).

214. Suteethorn, S., Le Loeuff, J., Buffetaut, E. & Suteethorn, V. Description of topotypes of *Phuwiangosaurus sirindhornae*, a sauropod from the Sao Khua Formation (Early Cretaceous) of Thailand, and their phylogenetic implications. *Neues Jahrb Geol Palaontol Abh***. 256**, 109–121 (2010).

215. Curry Rogers, K. A. & Forster, C. A. The last of the dinosaur titans: a new sauropod from Madagascar. *Nature* **412**, 530–534 (2001).

216. Curry Rogers, K. & Forster, C. A. The skull of *Rapetosaurus krausei* (Sauropoda: Titanosauria) from the Late Cretaceous of Madagascar. *J. Vertebr. Paleontol*. **24**, 121–144 (2004).

217. Allain, R. et al. Un nouveau genre de dinosaure sauropode de la formation des Grès supérieurs (Aptien–Albien) du Laos. *Earth Planet. Sci. Lett.* **329**, 609–616 (1999).

218. Zaher H. et al. A complete skull of an Early Cretaceous sauropod and the evolution of advanced titanosaurians. *PLoS ONE* **6**, e16663 (2011).

219. Wilson, J. A., Pol, D., Carvalho, A. B. & Zaher, H. The skull of the titanosaur *Tapuiasaurus macedoi* (Dinosauria: Sauropoda), a basal titanosaur from the Lower Cretaceous of Brazil. *Zool. J. Linn. Soc.* **178**, 611–662 (2016).

220. Royo-Torres, R. et al. High European sauropod dinosaur diversity during Jurassic-Cretaceous transition in Riodeva (Teruel, Spain). *Palaeontology* **52**, 1009–1027 (2009).

221. Poropat, S. F. et al. Reassessment of the non-titanosaurian somphospondylan *Wintonotitan wattsi* (Dinosauria: Sauropoda: Titanosauriformes) from the mid-Cretaceous Winton Formation, Queensland, Australia. *Papers in Palaeontology* **1**, 59–106 (2015).

222. Upchurch, P. The phylogenetic relationships of sauropod dinosaurs. *Zool. J. Linn. Soc.* **124**, 43–103 (1998).

223. Curry Rogers, K. in The Sauropods: Evolution and Paleobiology (eds Curry Rogers, K. & Wilson, J. A.) 50–103 (Univ. California Press, Berkeley, 2005).